NOTICE

The quality of this microform is heavily dependent upon the quality of the original thesis submitted for microfilming. Every effort has been made to ensure the highest quality of reproduction possible.

If pages are missing, contact the university which granted the degree.

Some pages may have indistinct print especially if the original pages were typed with a poor typewriter ribbon or if the university sent us an inferior photocopy.

Reproduction in full or in part of this microform is governed by the Canadian Copyright Act, R.S.C. 1970, c. C-30, and subsequent amendments.

AVIS

La qualité de cette microforme dépend grandement de la qualité de la thèse soumise au microfilmage. Nous avons tout fait pour assurer une qualité supérieure de reproduction.

S'il manque des pages, veuillez communiquer avec l'université qui a conféré le grade.

La qualité d'impression de certaines pages peut laisser à désirer, surtout si les pages originales ont été dactylographiées à l'aide d'un ruban usé ou si l'université nous a fait parvenir une photocopie de qualité inférieure.

La reproduction, même partielle, de cette microforme est soumise à la Loi canadienne sur le droit d'auteur, SRC 1970, c. C-30, et ses amendements subséquents.

MELT TREATMENT EFFECTS ON POROSITY AND IMPACT STRENGTH IN HYPOEUTECTIC ALUMINUM SILICON ALLOY

by

WITTAYA LA-ORCHAN

A Thesis submitted to the Faculty of Graduate Studies and Research
in partial fulfillment of the requirements for the degree of
Master of Engineering

Department of Mining and Metallurgical Engineering
McGill University, Montreal
June 1991

ISBN 0-315-72252-5

ABSTRACT

The effects of the three factors (modification, grain refinement, and hydrogen level) on the amount of porosity, impact strength, and performance of the reduced pressure test in A356 alloy have been studied. It was found that grain refinement, acting singly and in combination with modification, reduces the porosity by inducing mass feeding. However, this beneficial effect may not be found at all cooling rates and casting sizes. There is less total shrinkage in Sr-alloyed samples than in those which are non Sr-alloyed. The reason for this is supposed to be a difference in the liquid density which may be higher in Sr-alloyed samples. Modification has the strongest effect on improving the impact strength of A356 alloy. Hydrogen reduces it slightly. On the other hand, grain refinement, acting singly or in combination with modification, was not found to improve the impact strength of the alloy. To obtain optimum impact strength, it is recommended that a combination of modification and degassing to about 0.1 ml.H_2/100 g. Al. be used. An excellent linear relationship between density and hydrogen level exists for all combinations of melt treatment processes when the reduced pressure test is used. Three methods of predicting the true hydrogen level are proposed, and calculated hydrogen levels agree reasonably well with measured melt hydrogen within the error range of $\pm$0.05-0.1 ml./100 g. Al.

RÉSUMÉ

Les effects de trois facteurs (modification, affinage du grain et le niveau d'hydrogène) sur la quantité de porosité, la résilience et la performance de l'essai sous vide, pour l'alliage A356 ont été étudiés. Il a été trouvé que l'affinage du grain, agissant seul ou en combinaison avec la modification, réduit la porosité en améliorant l'alimentation en métal. Cependant, cet effet bénéfique peut ne pas être obtenu pour toutes les vitesses de refroidissement et toutes les tailles de moulage. Il y a moins de contraction totale dans les échantillons avec du strontium que dans ceux sans Sr. On suppose que ceci est dû à la différence en densité liquide, qui peut être plus élevée dans les échantillons contenant du strontium. C'est la modification qui a le plus d'effet sur la résilience de l'alliage: en améliorant cette dernière. L'hydrogène la réduit légérement. Par contre, l'affinage du grain seul, ou en combinaison avec la modification, n'a pas d'effet sur la résilience de l'alliage. Pour obtenir une résilience optimale, il est recommandé de combiner la modification et un dégazage à un niveau approximatif de 0.1 ml.H_2/ 100 g. Al. utilisé. Pour l'essai sous vide, une relation linéaire excellente, entre la densité et le niveau d'hydrogène, existe pour toutes les combinaisons utilisées pour traiter les coulées. Trois méthodes pour prédire le niveau d'hydrogène réel sont proposées, et les valeurs calculées correspondent raisonnablement à celles mesurées dans la coulée avec une marge d'erreur de $\pm$0.05-0.1 ml./100 g. Al.

ACKNOWLEDGEMENTS

The author wishes to express his deep gratitude to his thesis supervisor, Professor J.E. Gruzleski, for his patience, encouragement, and valuable guidance during this project.

The author gratefully acknowledge the financial support from the Canadian International Development Agency and the Royal Thai Navy.

Thanks are due to Dr. H. Mulazimoglu and F. Paray for their technical collaboration; and to N. Handiak for his help during the preparation of this thesis.

Finally, the author would like to thank his wife, Ratree, for her love, patience and support through all these years.

TABLE OF CONTENTS

LIST OF TABLES

LIST OF FIGURES

FIGURES PAGES

FIGURES PAGES

Chapter 1
Introduction

Since this work deals with hypoeutectic Al-Si casting alloys, the importance of these materials will be discussed first. This will be followed by a discussion of the problems concerning these alloys, and finally the aims of this work will be outlined.

1.1 Hypoeutectic Al-Si Alloys.

Aluminum casting alloys are used extensively in many applications because of their excellent strength to weight ratio and corrosion resistance. Among these, aluminum-silicon alloys are found to be the most important, primarily because of their excellent casting characteristics. The silicon constituent greatly improves fluidity, volumetric shrinkage, and hot cracking resistance [1-3]. The binary system of Al-Si exhibits a simple eutectic phase diagram, as shown in Fig. 1.1, which makes these alloys suited for high volume production.

A wide range of commercial compositions has been developed in the Al-Si family, but the most preferred group are the hypoeutectic alloys some of which are listed in Table 1.1.

The popularity of these alloys comes from the various combinations of physical and mechanical properties which are mostly affected by silicon and some alloying elements. Al-Si alloys can be considered as composite materials consisting of hard particles of silicon embedded in ductile matrix of aluminum. The tensile strength of the Si and Al are of the order of 1520 and 546 MPa., respectively. The amount of silicon, as well as its shape and distribution, are therefore the important factors that determine

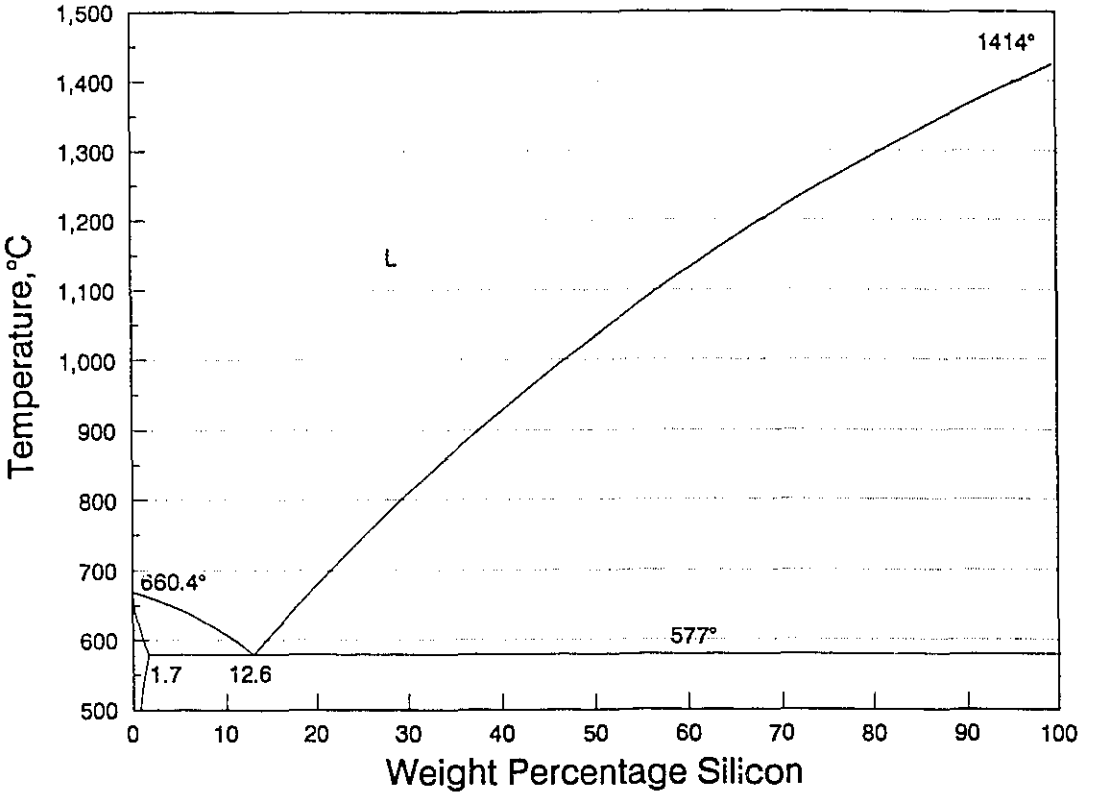

Figure 1.1 Phase diagram of a binary Al-Si alloy.

the mechanical properties of these alloys. Moreover, the alloys are heat-treatable, with the strength in the heat-treated condition controlled by two elements, Mg and Cu.

Other advantages of these alloys are their weldability, machinability, and pressure tightness. The alloys are, therefore, attractive for many applications including several in the transport industries. Sand, die, and permanent mold castings of these alloys are critically important in engine construction;engine blocks, intake manifolds, crankcases, carburators, transmission housings etc. In the shipbuilding industry, they are commonly used for a large variety of applications such as hatch covers, windows, air ports, ventilation equipment and fuel tanks.

There are, however, two major disadvantages of hypoeutectic alloys. The first one

Table 1.1 Chemical compositions of typical hypoeutectic Al-Si Casting Alloys [1].

Alloy AA No.*	Chemical Composition**, wt. %						Type of Casting***
	Si	Fe	Cu	Mg	Zn	Other	
355	5.0	<0.6	1.25	<0.5	<0.35		S,P
A355	5.0	<0.2	1.25	<0.5	<0.10		S,P
443	5.25	<0.8	<0.6	<0.05	<0.5		S,P
A443	5.25	<0.8	<0.3	<0.05	<0.5		S
356	7.0	<0.6	<0.25	<0.35	<0.35		S,P
A356	7.0	<0.2	<0.20	<0.35	<0.10		S,P
357	7.0	<0.15	<0.05	0.55	<0.05		S,P
A357	7.0	<0.20	<0.20	0.55	<0.10	0.05 Be	S,P
444	7.0	<0.6	<0.25	<1.0	<0.35		S,P
A444	7.0	<0.6	<0.10	<0.05	<0.10		S,P
332	9.5	<1.2	3.0	1.0	1.0	0.4 Mn	P

* AA : Aluminum Association.
** Remainder : Aluminum and unlisted impurities.
*** S : Sand casting; P : Permanent mold casting.

is the sharp edges of the coarse acicular silicon phase which occurs in the microstructure. These cause crack initiation and propagation resulting in poor mechanical properties. Another disadvantage is their notably long freezing range which leads to feeding difficulties in the interdendritic region resulting in increased porosity. These disadvantages can, however, be overcome by applying proper melt treatment processes.

1.2 Origin of the Problems.

In the aluminum casting industry, there are three melt treatment processes commonly employed to control the porosity and mechanical properties; namely, modification, grain refinement, and degassing. Each process has its own advantages and disadvantages. To obtain optimum casting quality, these processes are normally used in

combination: however, the interaction between these processes and their effects are not clearly understood.

Through the modification process, the acicular silicon can be transformed to a fibrous shape resulting in noticeable improvement in elongation and strength. The convenient way to modify the silicon phase is by adding a small amount of certain alloying elements to the alloy. Na and Sr are among those elements that are commercially used. In recent years, Sr has been preferred because of its permanent effect. It has, however, one serious disadvantage in that it increases the porosity level of the cast alloy. It has been reported that Sr-modified alloys are more prone to porosity than untreated alloys [4-7]. Consequently, it has been suggested that this porosity problem could be minimized by the combination of modification with the two other melt treatment processes, grain refinement and degassing.

Porosity caused by dissolved gas can undoubtedly be minimized by degassing. Hydrogen, the only gas that causes porosity in aluminum, can be purged out by bubbling inert gas into the melt. The inert gas is introduced through a lance into the molten metal in such a manner that a uniform dispersion of tiny gas bubbles is produced. When a gas is bubbled through a melt, dissolved hydrogen in the melt diffuses into the stream of bubbles and rises up to the melt surface.

Unlike degassing, there are some doubts as to the effectiveness of grain refinement in casting alloys. The purpose of this technique is to reduce the grain size. This can be accomplished by several methods. Among these methods, the addition of grain refining elements is most favoured because of its simplicity. Grain refiners such as Al-Ti and Al-Ti-B are added to a melt to enhance nucleation and control grain size in castings. However, this process does not reduce hydrogen in the melt, but only aims to disperse and reduce the porosity size. It is possible that the total amount of porosity might be the same as in the un-grain refined case. The first aim of this thesis is therefore to study the effect of grain refinement, acting singly and in combination with modification, on the amount of porosity in a hypoeutectic alloy.

The mechanical properties of cast Al-Si alloys are strongly influenced by two

parameters; silicon morphology and porosity. Modified silicon is generally known to improve the mechanical properties, but porosity accompanying this process can cause the properties to deteriorate. Degassing is commonly used to combat porosity and it is generally accepted that grain refinement can also reduce porosity effects.

The beneficial effect of grain refinement is to reduce the porosity size which in turn improves mechanical properties. This may be true in the case of a large amount of porosity, but under normal casting conditions, the pores caused by modification are relatively small. Grain refinement may not have a significant effect on reducing the pore size and in turn may not necessarily improve mechanical properties. Moreover, grain size reduction in hypoeutectic Al-Si alloys does not have significant effects on mechanical properties [8-9], but rather is found to reduce the ductility of the alloy [10]. Nevertheless, published work on the effects on mechanical properties of grain refinement when used in combination with modification is quite scarce, particularly at different levels of hydrogen.

Many investigators [9-13] have studied the effects of melt treatment on mechanical properties. Most of these investigations employed the tensile test, and their results are rather scattered resulting in interpretation difficulties. The impact test is used in this work since it was found that this test is extremely sensitive to silicon morphology [14]. In addition, published experimental data using this test are scarce. The second aim of this work is therefore to study the effects of grain refinement, acting singly and in combination with modification, on the impact properties of the alloy.

Another area of research dealt with in this thesis is the possibility of quantifying the amount of hydrogen in the melt by the Reduced Pressure Test. This technique has an advantage over other hydrogen measuring methods because of its simplicity and low cost. The basic concept of this technique is to solidify a sample of the melt in a reduced pressure chamber. The volume occupied by the gas porosity is magnified by the reduced pressure, resulting in a visibly porous sample if the hydrogen level is sufficiently high as shown in Fig. 1.2. The samples so solidified are evaluated either by observation for bubble emission during solidification, by sectioning the solidified sample and examining

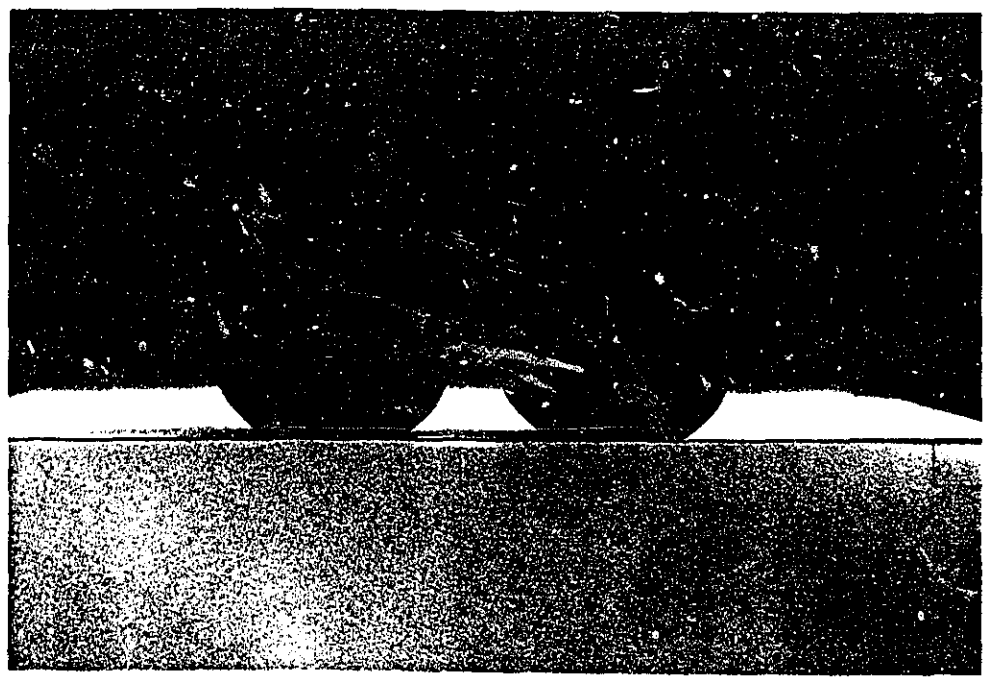

Figure 1.2 Effect of solidification pressure on the degree of porosity, sample on the right solidified at 76 mm. Hg.; on the left at atmospheric pressure.

for porosity, or by determining the density of the solidified sample. This makes the test quite popular and widely used by hundreds of foundries worldwide. However, the test is only semiquantitative. Development of this technique to a fully quantitative level would be a major breakthrough in simple and inexpensive control of melt quality.

Several investigators [15-20] have considered the problem of a quantitative reduced pressured test. The principle involved is to measure the density of the reduced pressure sample, and from this to calculate the volume of pores in the sample. It is then assumed that these pore are filled with hydrogen gas. Thus the volume of hydrogen equals the pore volume of the sample, and the amount of hydrogen can then be calculated by applying Gas Laws.

Prior to the calculation step, it is necessary to have a good relationship between the density of the sample and the amount of hydrogen dissolved in the melt. Several attempts to do this have been reported [15-21], but good correlations were not found in every system.

A simple Gas Law calculation yields hydrogen values much less than the actual hydrogen in the melt. This has led to the idea of a correction factor as proposed by Rosenthal and Lipson [15].

This factor is obtained by solidifying similar samples from the same melt with the same hydrogen concentration at atmospheric pressure and under reduced pressure. The hydrogen concentrations are then calculated from the density, and the correction factor is determined as:

$$C.F. = \frac{[\,H_C\,]_A}{[\,H_C\,]_R} \tag{1.1}$$

where

C.F. = correction factor

$[H_C]_A$ = calculated hydrogen level from atmospheric pressure sample

$[H_C]_R$ = calculated hydrogen level from reduced pressure sample.

There do not appear to have been many studies in which the calculated hydrogen level from the test is compared to the actual melt hydrogen measured by some independent means. Recently, Mulazimoglu, Handiak, and Gruzleski [21] have found a good relationship between density and hydrogen content in untreated and Sr-modified A356 alloy. They were also able to correct the calculated hydrogen levels from reduced pressure samples to obtain a reasonable agreement with the Telegas hydrogen.

The success of this approach offers hope that the reduced pressure test could be calibrated in such a way as to make it quantitative. These experiments were, however, rather limited in that only a few untreated and modified samples within a narrow range of hydrogen levels, about 0.07-0.2 ml./100 gm. Al., were studied.

The third, and final, aim of this work is therefore to study the relationship between density and hydrogen content over a wider range of hydrogen, as well as the effect of various combinations of melt treatment on this relationship. If good correlation is found, the concept of a correction factor will be applied to these results in order to gain a better understanding of the physical significance of the correction factor.

1.3 The Aims of This Work.

In summary, this thesis deals with the interaction between grain refinement, modification and dissolved hydrogen. The three main aims are as follows:

1) To determine the effects of grain refinement, acting singly or in combination with modification, on porosity in hypoeutectic Al-Si casting alloys.

2) To determine the effects of grain refinement, modification and hydrogen level on the impact strength of a cast Al-Si alloy.

3) To develop a realistic correction factor for the reduced pressure test and so to make this test truly quantitative.

Chapter 2

Theoretical Background and Literature Review

Since this work aims to study the porosity, impact strength, and quantification of the reduced pressure test, theoretical background concerning these subjects will be discussed in this chapter. A literature review of the previous work will be added as appropriate.

2.1 Types of Porosity.

Porosity is the most common defect found in metal castings. There are two major effects which contribute to the formation of porosity in solidifying metals: shrinkage resulting from the volume decrease in going from liquid to solid, and gas evolution resulting from the decrease in gas solubility in solid metal compared to the liquid. These phenomena may occur separately or, as is more often the case, simultaneously, interacting with each other to develop porosity in solidifying metals.

2.1.1 Shrinkage Porosity

Volumetric shrinkage is a primary and permanent source of porosity formation in solidifying castings. The volumetric change in aluminum casting alloys can be up to 3.5-8% upon transforming from the liquid to solid state, depending on the magnitude of the difference between the liquid and solid densities. Shrinkage can develop on both the macro and micro scale. Macroshrinkage can be found as slumping and contraction, and piping in a riser as shown schematically in Fig.2.1.

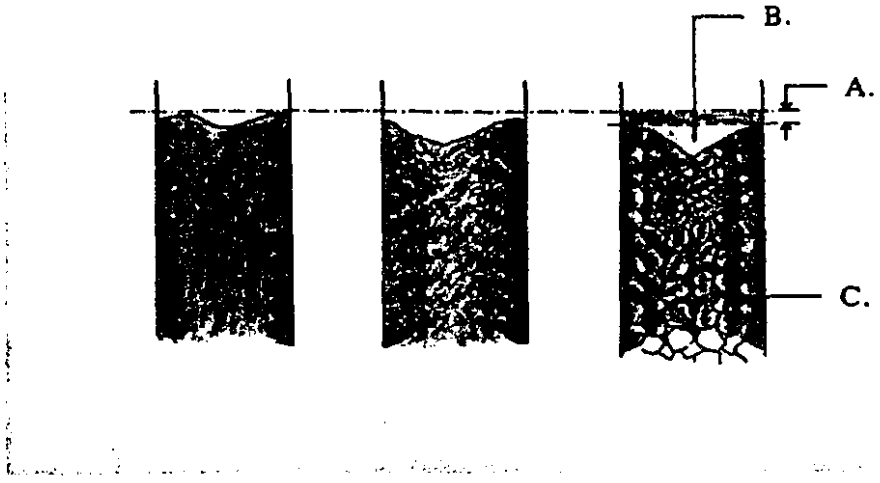

Figure 2.1 Macro and microshrinkage in the casting.
A = Slumping and contraction volume, B = Pipe volume, C = Microporosity.

After liquid metal has filled the mold to a certain level, solidification takes place at the mold wall toward the center of the mold. Once the solid forms, contraction due to the phase change occurs followed by slumping, which is collapse cause by low strength in the semi-solid state. This process stops when the solid formed has enough strength to prevent further slumping as shown in region A. of Fig. 2.1.c. From this point, further shrinkage occurs to the end of solidification, and results in pipe formation as shown in region B. of Fig. 2.1.c. Risering systems are normally designed to confine the shrinkage porosity to the upper portion of risers. In the case that risers are unable to provide the required metal feeding, local porosity will form in the casting in the last regions to solidify.

Shrinkage porosity also occurs as an extremely fine form of dispersed porosity called "microshrinkage" or "microporosity". This type of porosity is normally found in the interdendritic regions of alloys with large differences between liquidus and solidus temperatures. Liquid metal feeding in the dendritic solidification zone plays a key role

in formation of this type of porosity. Another region where this type of shrinkage can be found is at the grain boundaries. Liquid metal trapped among grains shrinks upon solidification resulting in porosity at the grain boundary. Microporosity is shown in region C. of Fig. 2.1.c.

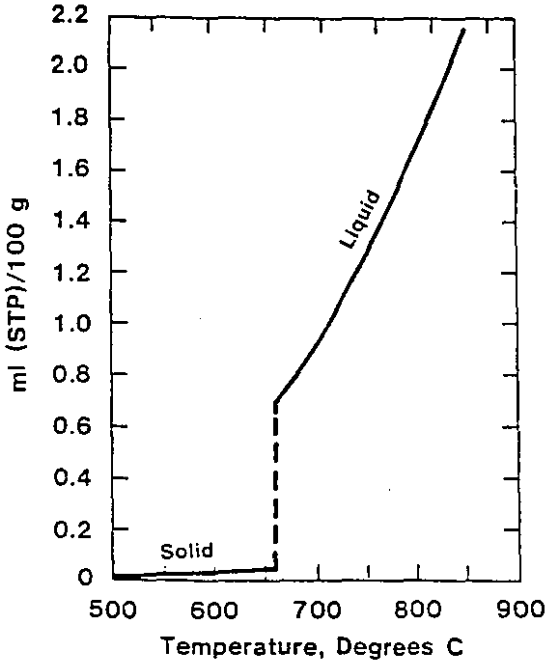

Figure 2.2 Solubility of hydrogen in pure aluminum. [22]

2.1.2. Gas Porosity

Gas evolution can also contribute to the formation of porosity. Hydrogen is the only gas capable of dissolving to a significant extent in liquid aluminum. Although the amount of gas dissolved in aluminum is small compared with many other metals, problems arise because of the large difference in solubility at the melting point. This is illustrated in Fig.2.2., for pure aluminum where the ratio of solubility in the liquid to that in the solid at the freezing point is 20:1. This dramatic decrease in solubility results in gas evolution on solidification. The solute gas rejected from the solid phase accumulates in front of the liquid-solid interface, and when a certain concentration is reached, molecular gas may be evolved.

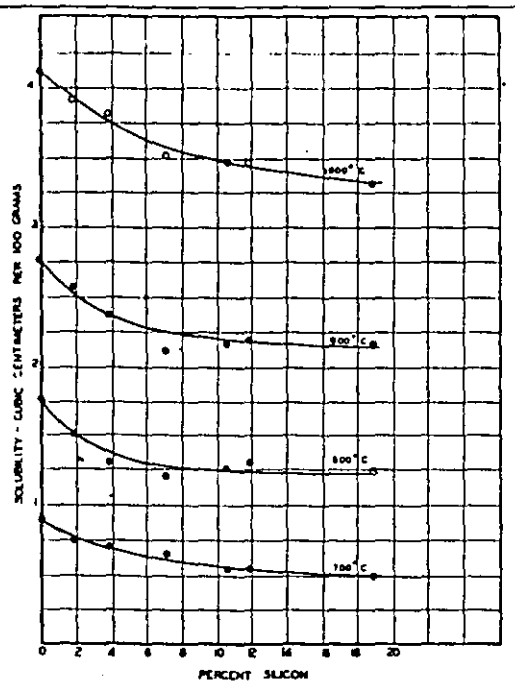

Figure 2.3 Effect of silicon content and temperature upon the solubility of hydrogen in liquid aluminum at atmospheric pressure [22].

The formation of this "gas porosity" occurs not only because of the change in solubility on phase transformation, but also because the liquid phase is continuously enriched in the gaseous component as the solid forms. The accumulation of solute elements is also another factor that influences gas porosity since the solubility of gases in liquid metals changes as the amount of solute increases. Opie and Grant [23] have shown that increasing Si and reducing temperature in aluminum significantly reduce the solubility of hydrogen in the melt, as shown in Fig. 2.3.

Nucleation of a gas bubble is required before growth of gas porosity can occur. Homogeneous nucleation is quite unlikely for gas porosity since it requires very high energy. Shahani and Fredriksson [24] have shown that for the formation of gas porosity in aluminum alloys, gas pressures of at least 35000 atm. are required. Gas porosity thus forms heterogeneously with the aid of some foreign nucleus such as inclusions, an existing gas bubble, or even the solid metal itself which is abundant during the solidification process. However, when shrinkage porosity forms, the large energy requirements for nucleation of a gas bubble can be overcome.

Under normal casting conditions, gas porosity occurs in a fine form in the interdendritic region and along grain boundaries. It is thus impossible to completely separate porosity caused by shrinkage or dissolved gas. The term microporosity used in this thesis will refer to microvoids caused by a combination of these two effects.

2.1.3. Tatur Test.

Macro and microporosity are rarely quantified; however, when they are, the Tatur test is the most commonly used technique. The test utilizes a copper mold with a special shape. When liquid metal in the mold solidifies, the shape of the mold enhances the formation of microporosity, pipe, and slumping and contraction with the pattern as shown

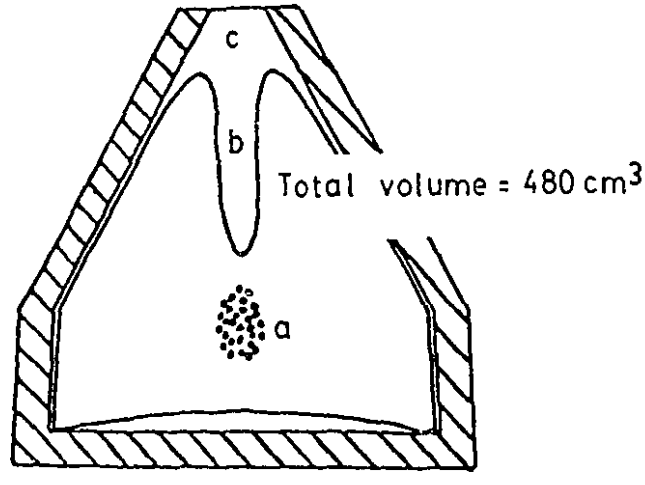

a = microporosity, b = pipe volume, c = slumping and contraction volume.

Figure 2.4 Schematic representation of shrinkage pattern in Tatur test samples.

in Fig. 2.4. The volumes of these various types of shrinkage can be quantified as will be discussed in Chapter 3. These volumes, which are interchangeable within a constant volume of the mold during solidification, are affected by many parameters, ie. alloying elements, gas content in the melt, melt treatment process; modification, and grain refinement. By maintaining all other parameters constant, except for the gas content, or modification and grain refinement, a comparison of the distribution between macro and microporosity as affected by these parameters can be obtained.

Previous work [7,25-26] using the results of the Tatur test as affected by these melt treatments has shown that it is possible to use this test in a comparative fashion. Charbonnier et al [25] have reported Tatur test results on A-S7G (Al-7%Si) alloy comparing unmodified and Na-modified samples to show that the modified alloy has up to 50% more microporosity than the unmodified alloy. Recently, Argo and Gruzleski [7] have used this test to identify differences in the distribution of macro and microporosity in Sr-modified and unmodified alloy. Their results have shown that modification leads to a redistribution of porosity on solidification, from pipe into microporosity, appearing thereby to increase the microporosity. At almost the same time, Morimoto et al [26] have reported their Tatur test results as affected by gas content showing that the gas content also has remarkable effects on the distribution between pipe volume and porosity. So far, no work has been reported using this test to determine the effects of grain refinement, and the combination of grain refinement and modification.

2.1.4. Formation of Microporosity

In the absence of hydrogen in the melt, the formation of microporosity caused by volumetric shrinkage is dependent on the percent of shrinkage due to the phase change and the feeding mechanism. Shrinkage due to the phase change is generally known to be dependent on the difference between liquid and solid densities, but feeding depends on many parameters. The role of feeding will be discussed here first. In the presence of hydrogen, the formation of gas porosity is complicated by many parameters. However,

the factors which affect the formation of this porosity depend mainly on the external pressure exerted on the gas bubble, and the pressure inside the bubble developed from hydrogen dissolved in the melt. These pressures will be discussed after examination of the role of feeding.

2.1.4.1. The Role of Feeding.

There are two important feeding mechanisms which occur during solidification processing. The first mechanism is liquid feeding which occurs at any stage until the end of solidification. The second is mass feeding which occurs only in the mushy zone. Microporosity is caused by the limitations of these feeding mechanisms.

Mass feeding occurs during the early stages of solidification until crystals are no longer free to move. In the initial stages of freezing, the primary crystals are free to move to some extent in the mixture of solid and liquid, and shrinkage caused by the phase change is compensated by a fall of these crystals to the level of the fluid. Mass feeding is believed to compensate for roughly about two-thirds of the total liquid-to-solid shrinkage of the alloy [27]. Unfortunately, there is no experimental evidence to account for this statement. This phenomenon has been neglected by many researchers who work on porosity modelling. Mass feeding stops when the primary crystals become so large that they interlock with each other.

Liquid feeding at the early stage of solidification does not have a strong effect on porosity formation since the flow resistance is small. However, when a network of dendritic structure forms in the mushy zone, liquid feeding through this network, which is known as interdendritic feeding, is considered to be most important in the creation of microporosity. When the volume contraction occurs during solidification, liquid must flow from the riser through the dendritic network to compensate for this contraction. This results in a pressure difference between the riser and points within the casting. When this pressure difference becomes sufficiently large, a cavity forms. In short, when resistance to fluid flow within the casting become sufficiently large, the pressure within the casting

drops to a level at which a void will nucleate. This is most simply illustrated by the relation for pressure drop during flow through porous media in equation 2.1 [28]:

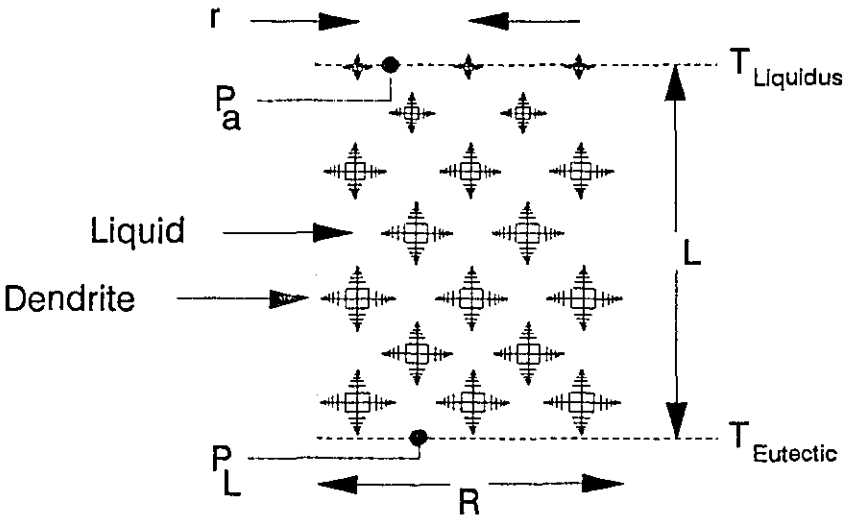

Figure 2.5 Schematic representation of mushy zone and parameters in equation 2.1.

$$P_a - P_L = \frac{32\mu\beta'\lambda^2 L^2}{r^4}\left(\frac{t^2}{\pi R^2 n}\right) \qquad (2.1)$$

where,

P_a = ambient pressure,

P_L = pressure at L, see Fig. 2.5,

$\beta' = \beta/(1-\beta)$

β = solidification contraction (solid density minus liquid density divided by solid density) at the solidification temperature,

μ = metal viscosity,

L = length of mushy zone,

t = "tortuosity" factor to account for the fact that the liquid flow channels are not straight and smooth; effective flow channel length, tL, with $t \geq 1$,

n = number of channels per unit area,

R = radius of cylindrical casting,

r = radius of liquid channel,

λ = heat flow constant = $k'(T_m-T_o)\rho_s H\sqrt{\pi\alpha'}$,

k' = mold thermal conductivity,

Tm = melting point of metal,

To = ambient temperature,

ρ_s = solid metal density,

H = heat of fusion of metal,

α' = thermal diffusivity of mold.

From this equation, it can be deduced that different melt treatments affect the flow of liquid in the interdendritic region in different ways. Modification is generally known to suppress the eutectic temperature by about 5-10°C [29]. This results in increasing the mushy zone length, L. A larger pressure difference in modified alloy is then expected, and microporosity may form easier in modified alloy than in untreated alloy. Experimental evidence of more porosity in modified alloys has been reported by many researchers [4-7].

Grain refinement reduces the radius of liquid channel, r, and increases the number of flow channels, n, since many crystals form in the mushy zone. This should result in an increased pressure difference in the interdendritic region and so interdendritic feeding with grain refinement should be more difficult. Thus, porosity should in theory form more easily in grain refined alloys than in untreated and perhaps even modified alloy. There are a few published works [30-31] on the effect of grain refinement on the amount of porosity, and their results are in contradiction with this interdendritic feeding concept. Among these is a paper by Drossel, Mai, and Liesenberg [30] who have found that the addition of a titanium-boron master alloy at a level of 0.02 % titanium increases casting densities by 0.02-0.04 $g.cm^{-3}$. This may indicate that grain refinement introduces another factor that dominates the effect of interdendritic feeding during the formation of microporosity.

Modification and grain refinement used together will combine the negative effects of these two processes. The mushy zone will be longer and the radius of liquid channels smaller while the number of flow channels will increase. It is thus reasonable to expect that there should be more porosity in this case. Reported work on the effect of these two melt treatments in combination is scarce. Quite recently, Wang, Shivkumar, and Apelian [32] have studied this effect and found that the amount of porosity in the alloy treated by the combination of grain refinement and modification is lower than in modified alloy but higher than in grain refined alloy.

Another important factor found recently to affect interdendritic feeding is capillary pressure [33]. This pressure occurs when the free surface of the riser solidifies to form a mushy zone. Once this mushy zone forms the interdendritic flow rate decreases dramatically. The apparent permeability at this stage was found to be two orders of magnitude smaller than the inherent permeability at the earlier stage when capillary pressure was absent.

2.1.4.2. Pressure of Hydrogen in the Melt.

The formation of gas porosity requires a considerable amount of energy for both nucleation and bubble stability in the liquid. Nucleation may be facilitated since there is often a considerable amount of shrinkage porosity to aid in the nucleation of gas bubbles in the melt. The energy required to stabilize the bubble is also significant. Consider a gas bubble in liquid metal. This bubble must have an internal gas pressure to counterbalance the external forces which can act to collapse the bubble, as shown in Fig. 2.6. These external forces are: the pressure exerted by the atmosphere, the metallostatic head pressure, and the pressure due to surface tension. As solidification proceeds, this bubble is also subjected to shrinkage pressure. This is a negative pressure which enhances the formation of the bubble; hence the equation for bubble stability becomes,

$$P_g + P_s = P_{atm} + P_H + P_{st} \qquad (2.2)$$

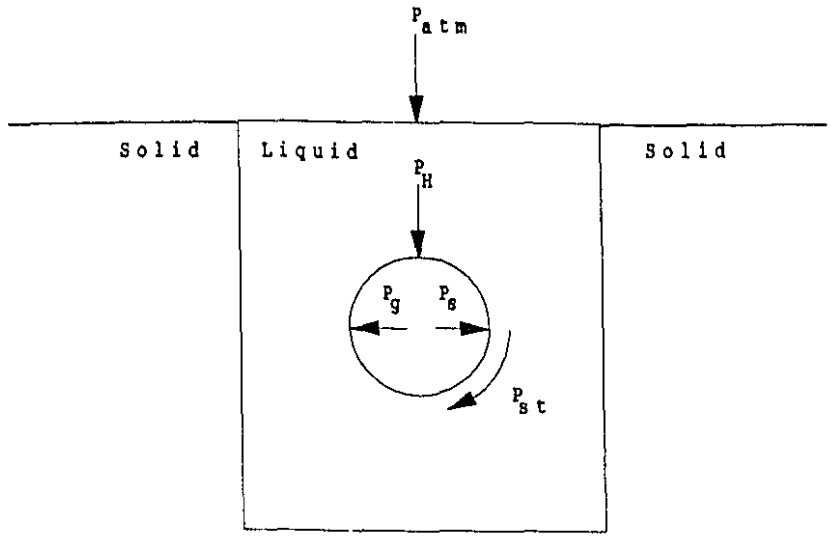

Figure 2.6 Various types of pressure acting on gas bubble.

where,

P_g = gas pressure,

P_s = shrinkage pressure,

P_{atm} = ambient pressure,

P_H = metallostatic head pressure,

P_{st} = pressure due to surface tension = $2\sigma/r$, for spherical bubble,

σ = the gas-liquid surface tension,

r = radius of the bubble.

For a given casting shape, most of these pressure terms will be constant except for the shrinkage pressure, P_s, and the pressure due to surface tension, P_{st}, which could be affected by the melt treatment process. Shrinkage pressure relates directly to the interdendritic feeding mechanism. Melt treatment will thus affect this pressure in the same manner as described previously.

Pressure due to surface tension is important particularly at small bubble radius. A melt treatment which reduces the surface tension should lead to increased porosity.

This is one hypothesis that is used to explain the porosity problem in modified alloys [34]; however, there are no physical measurements of surface tension as affected by melt treatments such as modification.

The internal gas pressure can be calculated from Sievert's Law (equation 2.3) which assumes thermodynamic equilibrium between the molecular gas in the bubble and the diatomic hydrogen dissolved in the melt.

$$P_g = \left(\frac{C_H}{S}\right)^2 \tag{2.3}$$

where,

P_g = equilibrium partial pressure of the dissolved gas,

C_H = amount of hydrogen dissolved in the melt,

S = solubility constant of the melt.

The gas pressure in the bubble can then be assumed to be equal to P_g from this equation. In order to form a gas bubble, the internal gas pressure must be equal to or greater than the external pressure.

From equation 2.3, it is seen that the gas pressure is proportional to the square of the amount of gas dissolved in the melt, C_H. This means that gas pressure rises rapidly as hydrogen in the melt increases. As solidification proceeds, rejected hydrogen which accumulates in the melt results in increasing gas pressure. To reach a particular pressure to form a bubble, a certain period of solidification time is required. The initial amount of hydrogen dissolved in the melt thus plays a key role in this matter. The higher the gas level dissolved in the melt, the faster the gas pressure rises, and the more rapidly porosity can form and grow.

Another factor that controls the gas pressure is the solubility constant of the melt, S. As shown in equation 2.3, gas pressure increases as solubility of hydrogen decreases. Opie and Grant [22] determined the solubility of hydrogen in Al-Si melts for $0 < \text{wt.pct.Si} < 16$ and for $973 < T < 1273$ K. They found that the solubility of hydrogen decreased when temperature dropped, and the amount of silicon in the melt increased,

as given in the equation:

$$\log_{10} S = -\frac{A}{T} + B \tag{2.4}$$

where,

S = solubility constant of the melt,

A and B are parameters that depend on the concentration of silicon in the alloy.

Yeum and Poirier [35] have analyzed the values of A and B given by Opie and Grant [22] and expressed these values in terms of the concentrations of the alloy elements as:

$$A = a_0 + a_1 C_i^{\frac{1}{2}} + a_2 C_i + a_3 C_i^{\frac{3}{2}} \tag{2.5}$$

and

$$B = b_0 + b_1 C_i^{\frac{1}{2}} + b_2 C_i + b_3 C_i^{\frac{3}{2}} \tag{2.6}$$

where,

C_i = wt.% of silicon in the melt,

a_x and b_x are coefficients given in Appendix 4.2.

As solidification proceeds, the temperature drops and the solubility of hydrogen in the melt is reduced dramatically. This results in increased gas pressure, and so gas porosity is expected to form at the later stages of solidification.

It is possible that various melt treatment processes could affect the solubility of hydrogen in the melt. A melt treatment process that reduces the solubility of hydrogen should lead to an increase in porosity. There is, however, no experimental work on the effect of melt treatment on the solubility of hydrogen in aluminum-silicon melts.

2.1.5. The Effects of Melt Treatment on Microporosity Formation.

In summary, microporosity forms easily when the following conditions are satisfied;

1. poor mass feeding,
2. difficulties in interdendritic feeding,
3. low nucleation energy,
4. low external pressure, ie. atmospheric pressure, and pressure due to surface tension,
5. high hydrogen pressure, ie. high gas content, low gas solubility in the solid ($k_0 << 1$).

There is no complete understanding of the effects of modification or grain refinement on these factors. However, the last four conditions are thought to be influenced by modification. Modification suppresses the eutectic temperature resulting in increases in the mushy zone length which in turn increase difficulties in interdendritic feeding. Modification may introduce inclusions into the melt resulting in enhanced pore nucleation. It has also been reported that modification may reduce surface tension of the melt. Fang and Granger [34] have used their porosity model to predict the porosity in a modified alloy, and found that surface tension in a modified alloy must be reduced by 50% in order to match their calculated and experimental results. The final factor that may be affected by modification is the solubility of hydrogen in the melt, but there is no experimental evidence to support this hypothesis.

Most experimental evidence indicates that grain refinement reduces microporosity [30-31]. Grain refinement may therefore act in the opposite manner to modification. Although, there is a difficulty with interdendritic feeding in the presence of grain refinement, it may improve other factors, for example mass feeding.

2.2. Instrumented Impact Testing.

Most of the reported mechanical properties of cast aluminum-silicon alloys originate from tensile testing. Considerable scatter is usually observed in the results because this test is very sensitive to porosity in the test sample. Furthermore, the test results are not a strong function of silicon morphology. Since this work deals with the variation of porosity and silicon morphology, a test much more sensitive to these was used. Instrumented impact testing was employed in this thesis since the test has been found to be extremely sensitive to silicon morphology [14,36], and data on impact properties is relatively scarce in these alloys.

The test apparatus consists of the standard hammer equipped with electronic components used to record load and energy as a function of time. The load acting on the impact specimen is recorded by a strain gage. The triggering system is used to turn on the recording system in order to coordinate the load-time, and energy-time trace. The velocity system is used to measure the velocity of the hammer before, during, and after the impact which in turn gives information on the energy due to the change in kinetic energy of the hammer. These two systems work by mean of an opto-electronic device which can trace the load acting on the specimen in time scales of the order of milliseconds.

A typical load, energy and time curve obtained from this test is shown in Fig. 2.7. The y-axis represents load (upper curve) and energy (lower curve) and the x-axis records time. The load-time curve shows different stages of deformation. The initial rise corresponds to the elastic regime, P_0-P_y. At higher loads, prior to P_{max}, the specimen deforms plastically while after P_{max} the load decay is indicative of controlled crack propagation.

The energy curve shows the amount of apparent energy, E_a, which is a direct integration of the load-time signal based on the assumed constant velocity, as a function of recording time. The more accurate energy value, E_t, is found by

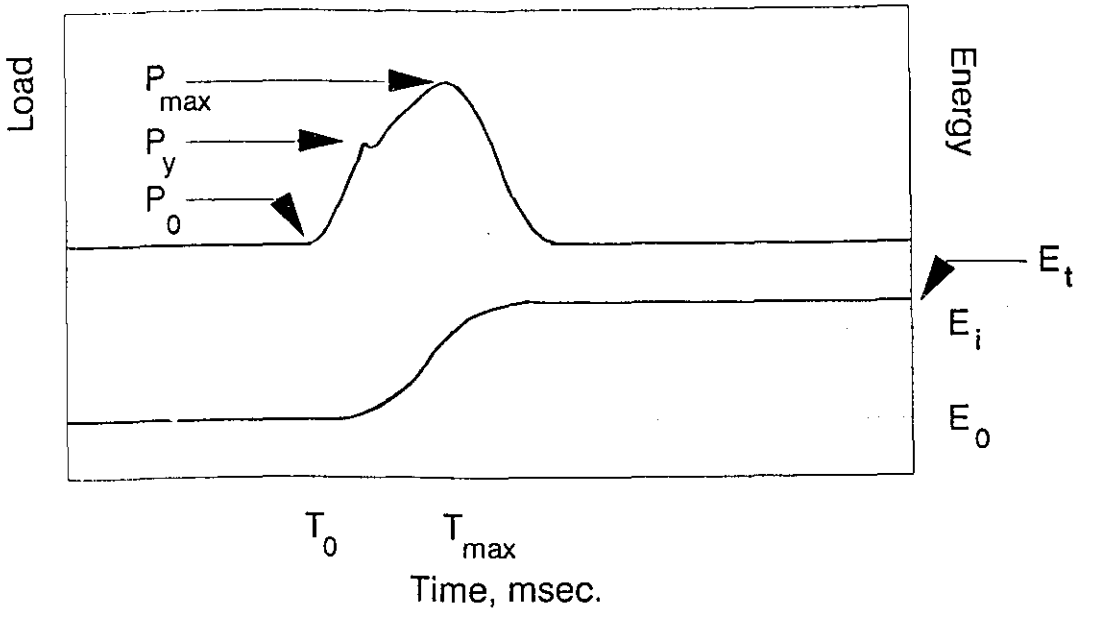

Figure 2.7 Typical load-time, and energy-time curves as obtained from instrumented impact testing.

$$E_t - E_a \left(1 - \frac{E_a}{4\,E_0} \right) \tag{2.7}$$

The absorbed energy can be separated into two stages. The first stage is the stage where the energy is required for crack initiation, E_i, which is the energy at T_{max}. The second stage is the stage of crack propagation energy, E_p, which is the difference between the total energy and the crack initiation energy.

Work on the effect of melt treatment on impact strength is scarce. Among these is a study by Closset [14] who investigated the unnotched impact strength of Sr-modified and unmodified alloy and found that the impact strength of the modified alloy was significantly higher than that of unmodified alloy as shown in Fig. 2.8. Similar work was also reported by Komatsu, Nakamura, and Yamamoto [36]. They employed instrumented impact testing on Na-modified and unmodified alloy with different stages of heat treatment, and found that not only the impact strength, but also the maximum load and propagation energy, were significantly affected by silicon morphology.

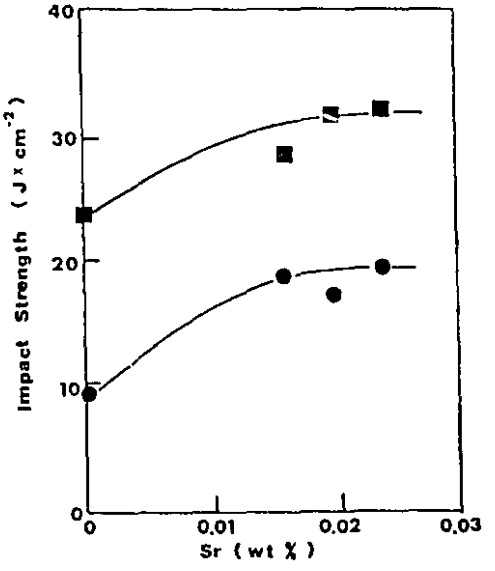

Figure 2.8 Impact strength of as-cast and heat treated A356.2 Alloy: ●=as cast,■=heat treated [14].

2.3. Quantification of the Reduced Pressure Test.

The idea of quantifying gas content from the density of a solidified sample was originally described by Ohira and Kondic [37]. They measured the density of a well-fed atmospherically-solidified test piece and related this density to the gas content of the melt. Their simple idea was to calculate the volume of the pores in the sample from its density. It was then assumed that these pores are all filled with hydrogen gas. Thus the volume of hydrogen equals the pore volume of the sample, and the hydrogen content can then be calculated by applying the Gas Laws and assuming that gas pressure is equal to pressure during solidification as shown below:

$$(H_c) - K\left(\frac{1}{D_a} - \frac{1}{D_{th}} \right) \qquad (2.8)$$

where,

H_c = calculated hydrogen level, ml./100 g. Al.,

D_s = density of the sample, g./cc.,

D_{th} = theoretical density, g./cc.,

K is a gas law constant which corrects the hydrogen volume from the solidification temperature and pressure to standard temperature and pressure (STP). Thus:

$$K = \frac{T_1}{T_2} \times 100 \tag{2.9}$$

where,

T_1 = 273 K

T_2 = solidus temperature of the alloy in degrees Kelvin.

Although they have shown that their results are very close to the actual gas content of the melt, this test does not lend itself particularly well to the foundry floor because the density of the sample solidified under atmospheric pressure is not very sensitive to hydrogen level. Very high precision is required for density measurement from this sample.

This led to the idea of quantifying gas content by the reduced pressure test sample originally proposed by Rosenthal and Lipson [15]. They showed that the reduced pressure solidification of a sample resulted in magnification of the effect of dissolved gas on the density of the test sample, and in this way reduces the accuracy requirement of the density measurement. The only change in the calculation of the hydrogen content is the gas law constant, K, which has to be modified as shown:

$$K = \frac{P_2}{P_1} \times \frac{T_1}{T_2} \times 100 \tag{2.10}$$

where,

P_1 = 760 mm. Hg.

P_2 = pressure in the test chamber during solidification.

However, there are several problems accompanying the calculation of hydrogen content from the reduced pressure test sample. Sulinski and Lipson [16] have pointed out that this simple calculation is unlikely to lead to a correct value for the hydrogen concentration since it assumes that:

i) no hydrogen is retained in solid solution in the alloy.

ii) all hydrogen originally present in the liquid forms pores in the solid and none is pumped out of the system during the test.

iii) the gas forms at the solidus temperature of the alloy and at a pressure equal to the chamber pressure.

iv) the theoretical density of the alloy is known accurately.

There is much evidence to suggest that only the second assumption leads to significant errors. Ransley and Neufeld [22] have determined that the equilibrium solid solubility of hydrogen in aluminum is small, approximately 0.012 ml./100 g. Al. at 0.1 atm. Since the gas in solid solution does not produce unsoundness in the casting, its presence is not really a factor in the test. Variations in alloy chemistry within specification limits result in differences in theoretical density. This would be a source of error when used as the basis for the gas content calculation. Under reduced pressure solidification at 0.1 atm., this error is reduced by a factor of ten, and can be regarded as negligible. That gas forms at a pressure equal to the chamber pressure is another assumption that should not lead to any large error. The pressure inside a gas bubble, as shown in equation 2.2, should be equal to the sum of the chamber pressure, metallostatic pressure, and surface tension pressure minus the shrinkage pressure. Metallostatic pressure is negligible since reduced pressure samples are small. The gas pressure increase as the surface tension pressure increases. This pressure becomes significant only at a very small radius of the bubble. However, most pores in reduced pressure samples have large radii, and so the surface tension pressure term is negligible, and can be ignored. There

are of course some pores in the sample that have small radii. The gas pressure in these could well be above the chamber pressure due to the surface energy term; however, these pores are too small to significantly affect the sample density, and so will not lead to any large error in the calculation of hydrogen content.

The single assumption that may lead to serious error is that all the hydrogen in the melt forms pores in the solid. Since the test is conducted in a partially vacuum condition and the diffusion coefficient of hydrogen is very high, it is likely that hydrogen may be lost into the pumping system. The hydrogen which remains in the melt thus forms a smaller pore volume, and the hydrogen content calculated from the reduced pressure test should be less than the actual melt hydrogen. This effect was found by Rosenthal and Lipson [15]. They have reported that the amount of hydrogen loss was dependent on the amount of hydrogen initially dissolved in the melt and the holding period. A melt that initially contained high hydrogen tended to lose hydrogen to the system faster than a melt with low hydrogen. The hydrogen in the melt was also found to decrease as the holding time in the chamber increased. The hydrogen loss rate was also dependent on the ratio of free surface area of the melt to its volume [38] which was determined by the crucible size and shape.

In the same paper, Rosenthal and Lipson [15] introduced a correction factor to correct the calculated hydrogen from the reduced pressure test as discussed in Chapter 1. It is interesting to note here that this correction factor is based on the assumption that the calculated hydrogen content from the sample solidified under atmospheric pressure yields an accurate value for the hydrogen in the melt.

An accurate $[H_c]_A$ will only be measured if the crucible is designed properly in such a way that volume shrinkage is well fed by liquid metal, so that porosity is formed solely by gas in the melt. This idea led to the concept of a risered constant volume test. Sulinski and Lipson [16] developed a well-fed constant volume crucible as shown schematically in Fig. 2.9. By using this crucible, they claimed that their results are reproducible with a standard deviation of only 0.002 cc./100 g. Al. However, their crucible size is relatively large and this complicates the test procedure.

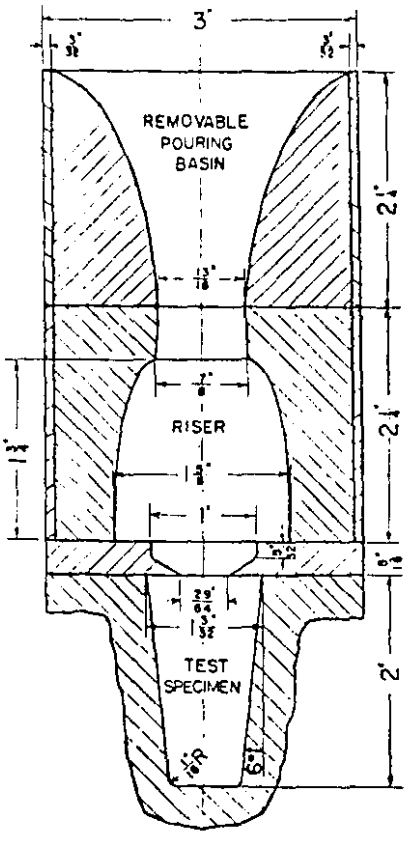

Figure 2.9 Constant volume mold developed by Sulinski and Lipson [16].

Another factor that may lead to an error in quantification of the test is the presence of inclusions. Inclusions in the melt reduce the nucleation energy required by gas bubbles thus enhancing the formation of porosity. At the same hydrogen level, samples rich in inclusions may have a lower density than ones with fewer inclusions. This phenomenon may lead to a lack of correlation between the densities of the sample and the hydrogen content in the melt as reported by Hess and his co-workers [19-20]. Brondyke and Hess [19] compared several methods of measuring hydrogen in the melt including the reduced pressure test and the solid-extraction method. By comparing the amount of hydrogen determined by solid-extraction and the density of reduced pressure test samples in 2014 alloy, they found that there was no correlation between hydrogen

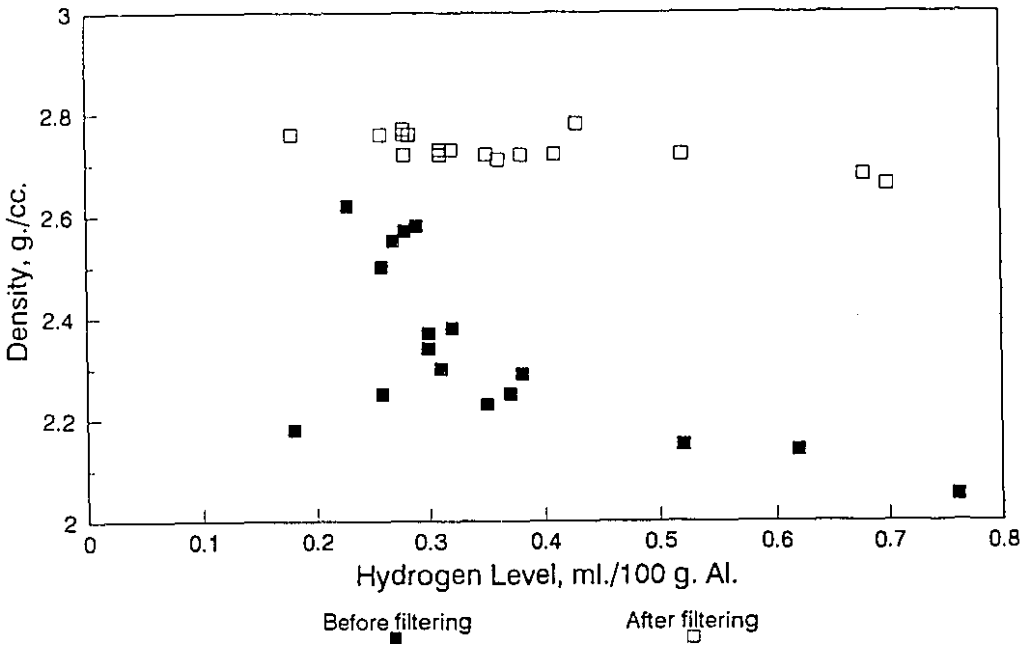

Figure 2.10 The effect of inclusions on the correlation of density and hydrogen content in the reduced pressure test [19].

content and the sample density, as shown in Fig. 2.10. However, when filtration was applied, they found that the correlation was improved. They then concluded that inclusions play a key role in this matter. It is interesting to note here that this work was carried out at hydrogen levels between 0.3-0.7 ml./100 g. Al., which is not representative of normal casting conditions. Moreover, at these hydrogen levels, the internal gas pressure rises up and exceeds the external pressure rapidly. Gas bubbles then form easily if nucleation sites are available, and the presence of inclusions should have a significant effect on the formation of porosity.

It may be concluded at this point that it should be possible to quantify the gas content from the reduced pressure sample density provided three important pieces of information are present;

i) the hydrogen loss into the system,

ii) the effect of inclusions on the density-hydrogen content correlation of the test,

iii) accurate value of $[H_C]_A$ in which shrinkage does not play a role.

Recently, Mulazimoglu, Handiak, and Gruzleski [21] studied the correlation

between density and hydrogen level measured by the most reliable modern technique which is the Telegas instrument. Their results have shown good correlation between density and hydrogen in Sr-modified and unmodified alloy. At the same time, they applied the quantification method as proposed by Rosenthal and Lipson [15], and found a reasonable agreement with the experimental results.

However, these experiments were limited in that only a few samples were studied within a narrow range of hydrogen levels. Crucible design, and the effect of inclusions were not considered. No authors have considered the nature of the correction factor used in hydrogen level determination in any detail. Clearly, it is the key to correct quantification of the hydrogen concentration. A study of the correction factor forms an important part of the present work.

Chapter 3

Experimental Procedures

3.1 Material and Melt Treatment Procedures.

A356 alloy was used since it is the most important alloy in this group. This alloy has an optimum combination of casting characteristics, and physical and mechanical properties, and so is widely used in industry. The composition of the A356 alloy used is shown in Table 3.1.

Table 3.1 Chemical composition of A356 alloy.

Elements	Wt.%
Si	7.00
Mg	0.32
Fe	0.15
Cu	0.03
Mn	0.02
Zn	0.02
Ti	0.07
Al	Balance

About 10 kg. of alloy was melted in a silicon carbide crucible in a gas-fired furnace. Various hydrogen levels were obtained by the degassing and regassing process. The melt was degassed below 0.1 ml./100 gm. Al. by bubbling prepurified argon gas into the melt using a perforated graphite tube. The regassing process was carried out by stirring the melt with a graphite rod or by slowly inserting moistened paper into the melt.

To modify the silicon phase, 90% Sr-10% Al master alloy was added to obtain 0.02 wt% Sr before degassing. The melt was held for at least 30 minutes to allow complete dissolution of the master alloy.

Grain refinement was obtained using either of two different types of commercial alloy-5Ti-1B-Al and 2.5Ti-2.5B-Al. The master alloys were added before degassing, and the amount of titanium was kept at 0.17 wt.% in the melt. The aim was to bring the alloy to the composition where these two grain refiners yield optimum performance, which is roughly about 0.1 wt.% Ti [39]. An excess of 0.07 wt.% Ti was added to compensate for fading which occured during the experiment. Two grain refiner alloys were used because it was desired to determine if there is a difference in their effects particularly when coupled with modification. The difference between these two grain refiners is their active nucleant type when dissolved in the melt. The 5Ti-1B-Al is reported to contain TiB_2, whereas the 2.5Ti-2.5B-Al contains a solid solution of AlB_2 and TiB_2 [40]. For the combination of modification and grain refinement, Sr and Ti master alloys were added at the same time before degassing the melt.

Hydrogen levels in the melt were measured by a recirculating gas technique whose reliability has been established [20,41]. The TELEGAS™ instrument was used in conjunction with newly developed A*l*SCAN™ probes. This method had been shown in an independent study to yield accurate results, and has the advantage that the probe life is longer than that of the ceramic probe of the TELEGAS™ instrument.

3.2 Porosity Quantification.

The amount of porosity in a sample can be quantified by the relation:

$$\% \ Porosity = \frac{Theoretical \ Density - Apparent \ Density}{Theoretical \ Density} \times 100 \ \% \qquad (3.1)$$

Theoretical density can be obtained by calculation, whereas apparent density can be quantified by density measurement. Theoretical density was calculated by a technique developed by Kundle and Willey [42]. A sample calculation is shown in Table 3.2.

Table 3.2 Sample calculation of the theoretical density.

Elements	1/density,cc.g.$^{-1}$	Weight,g.	Volume,cc.
Si	0.4292	7.00	3.0044
Mg	0.5522	0.32	0.1767
Fe	0.1271	0.15	0.0191
Cu	0.1116	0.03	0.0033
Mn	0.1346	0.02	0.0027
Zn	0.1401	0.02	0.0028
Ti	0.2219	0.07	0.0155
Al	0.3705	92.39	34.2305
Total		100.0	37.455
Theoretical density = 100/37.455 = 2.670 g./cc.			

It is clearly seen that the theoretical density is dependent on the amount of alloying elements which were assumed to be constant in this experiment. However, it was found that the amount of alloying elements varied within ± 3 % of the assumed values. This variation results in a maximum error of only ±5 % in the theoretical density. For the alloy that was treated by Sr and Ti, the theoretical densities were calculated to the values shown in Table 3.3.

Table 3.3 Theoretical densities of the alloys treated by various melt treatments.

Melt Treatment Processes	Theoretical Densities (g./cc.)
Untreated	2.670
Modified	2.670
Grain Refined : 2.5Ti-2.5B	2.670
Grain Refined : 2.5Ti-2.5B and Modified	2.670
Grain Refined : 5Ti-1B	2.671
Grain Refined : 5Ti-1B and Modified	2.671

The apparent density in this work was measured by the Archimedes principle of weighing the sample in air and water. Once the mass of the sample measured in air and water was known, the apparent density was calculated by applying the equation:

$$Apparent\ Density = \frac{Mass\ in\ air}{Mass\ in\ air - Mass\ in\ water} \times Density\ of\ water \qquad (3.2)$$

The density of water, at the measuring temperature, was taken from published values [43]. For all in-water measurements, a minor amount of Teepol 610™ was added to a distilled water bath to reduce the surface tension between the sample surface and water.

To ensure accurate measurement, the apparatus was tested by evaluating the density of cold rolled pure aluminum and comparing the result with the known value [43]. It was found that the measured density agreed to within 1 % of the published value.

3.3 Tatur Test.

The Tatur test was used in this work since the test yields information not only on the microporosity, but also on the amount of macroporosity (pipe volume, and the slumping and contraction volume) in the casting. The test consists of a copper mold whose dimensions are shown in Fig.3.1 a.

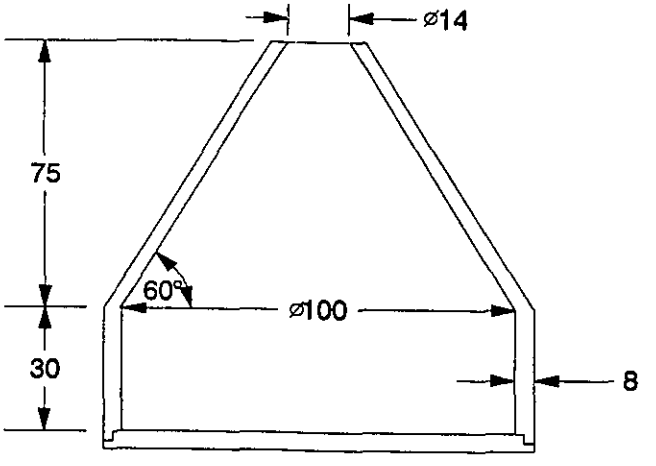

Fig. 3.1a. Dimensions of Tatur test mold.

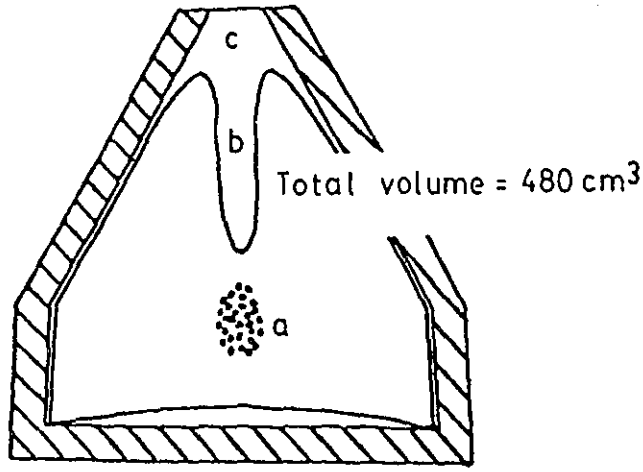

a = microporosity, b = pipe volume, c = slumping and contraction volume.

Fig. 3.1b. Shrinkage patterns in the Tatur mold.

Figure 3.1 Dimensions and shrinkage patterns in the Tatur mold.

The mold was preheated on a hot plate to obtain 175°C at the bottom of the mold prior to filling with the molten metal. Molten alloy was added to the mold by a hand-pouring technique. This technique may easily introduce human error, which results in variation of experimental data from time to time or between different operators. Once the mold was filled, liquid aluminum solidified from the sides of the mold toward the center. The last part to solidify is the liquid that is initially in the pipe volume area which tends to shrink toward the mold center. The porosity and shrinkage distribution pattern after solidification are shown in Fig.3.1 b. These specified volumes can be calculated by applying the following equations :

$$V_c = \frac{(M_A - M_w)}{D_w} \tag{3.3}$$

$$D_A = \frac{M_A}{V_c} \tag{3.4}$$

$$V_{por} = \frac{(D_{th} - D_A)\, V_c}{D_{th}} \tag{3.5}$$

$$V_{sc} = 480 - V_p - V_c \tag{3.6}$$

$$V_{ts} = V_p + V_{sc} + V_{ms} \tag{3.7}$$

where,

V_c = casting volume (cm^3)

M_A = casting weight in air (g.)

M_w = casting weight in distilled water (g.)

D_w = density of distilled water ($g.cm.^{-3}$)

D_A = casting apparent density ($g.cm.^{-3}$)

V_{por} = volume of porosity (ml.)

D_{th} = theoretical density of A356 alloy ($g.cm^{-3}$)

V_{sc} = volume of slumping and contraction (ml.)

V_p = volume of pipe (ml.)

V_{ts} = volume of total shrinkage (ml.)

The parameters which can be directly quantified from the Tatur sample are pipe volume and apparent density. Pipe volume was quantified by measuring the weight of sand that completely filled the pipe. The volume was then calculated from the density of the sand. The apparent density was evaluated by the method previously described. It is also interesting to note here that these two parameters are important since they affect the rest of the calculations made from Tatur test data. This point will be discussed later in Chapter 4.

3.4 Impact Test.

The impact test specimens were obtained from the sand casting pattern as shown in Fig. 3.2. Ten samples were obtained in each casting, and each of them was machined

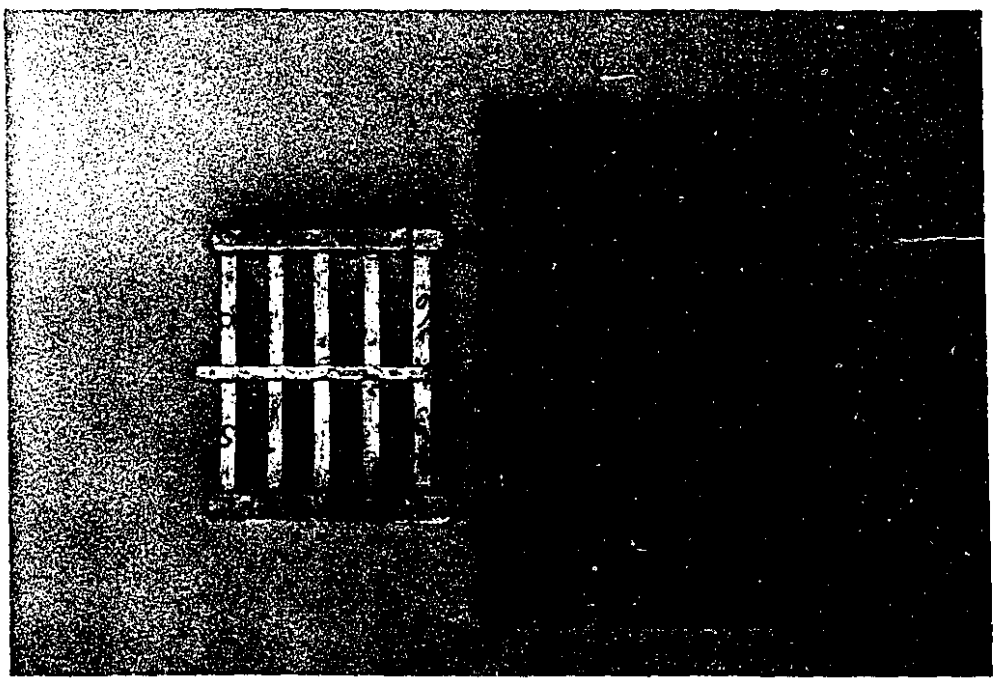

Figure 3.2 Sand casting pattern of the impact test.

and polished to the standard size (10 x 10 x 55 mm.) without notches. The test was carried out on a standard instrumented impact test apparatus. The results of the tests were provided in the form of a visual record of the applied load and apparent energy absorbed during fracture in impact. The load, energy and time could then be quantified.

3.5 Reduced Pressure Test.

The reduced pressure test system used in this experiment, like other systems widely used on the foundry floor, consisted of a vacuum pump, a reduced pressure

chamber, crucible, pressure gauge, timer, and a valve to adjust the pressure. A schematic of the reduced pressured test system is shown in Fig. 3.3. The chamber pressure used

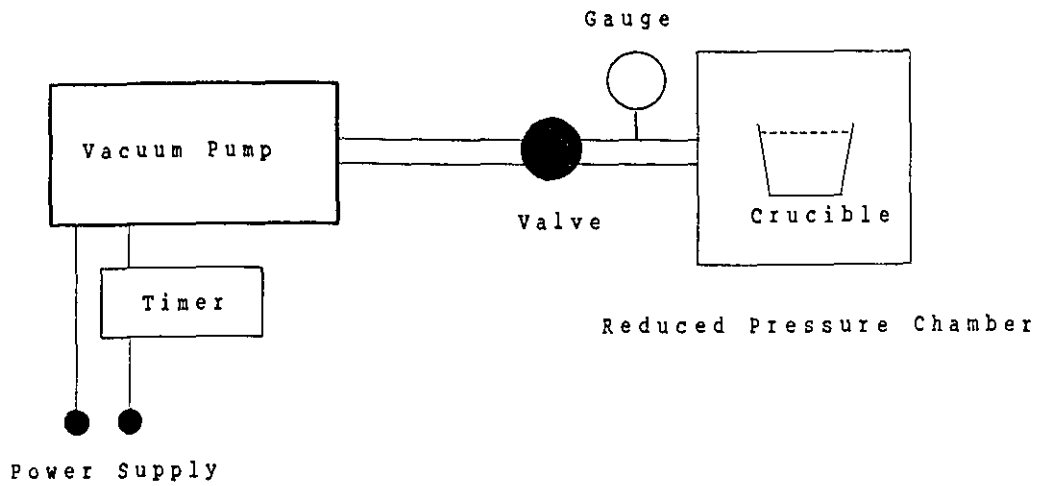

Figure 3.3 A schematic diagram of the reduced pressure test apparatus.

in this experiment was 0.1 atm. (76 mm. or 27 in. of Hg). The crucible used was a standard 100 ml. capacity iron cup normally used in the reduced pressure test as shown in Fig. 3.4. An iron oxide mold wash was used to coat the inside surface of the crucible.

Immediately after the hydrogen concentration was measured by Telegas, about 200 g. of the metal from the melt was poured into two preheated crucibles. One crucible was placed in the reduced pressure chamber, whereas the other was left to solidify at atmospheric pressure. The sample in the chamber was allowed to solidify for 5 minutes at the test pressure. The sample density was determined by the Archimedes principle as previously described.

3.6. Grain Size Measurement.

Grain size measurement was done by the line interception method. The sample was etched by Reagant reagent, whose composition is given in Table 3.4, and then placed

Figure 3.4 Steel crucible for reduced pressure test.

placed on the microscope using polarized light to allow grain boundary detection. One of the eyepieces in the microscope contained a vernier scale of known length, and the number of grains along this line was counted at five random locations on the sample. Known values were then compared with the grain size given in ASTM E112.

Table 3.4 Chemical composition of Poulton's reagent.

HCl(c)	60 %
HNO_3(c)	30 %
HF(48%)	5 %
H_2O	5 %

3.7. Modification Rating.

Modification rating was measured to quantify the level of modification in Sr-modified alloys. The samples were examined by photomicrograph and the rating was calculated from the proportion of the sample surface which had a particular class of modification as described by Apelian, Sigworth, and Whaler [12].

Chapter 4
Porosity in the Tatur Test

For aluminum casting alloys macro and microshrinkage are valuable data since they are the important factors that determine riser size and defects in castings. By employing the Tatur test, macro and microshrinkage and the effects of melt treatments on these parameters can be studied. The results of this test will be presented in this chapter.

4.1. Dispersion of the Results.

Before presenting these results, it is important to note that the experimental data obtained from this test are quite scattered. This scattering is mainly in the pipe volume which is one of two data that can be directly measured from the test. A typical data set is shown in Fig. 4.1.

Only five data points were obtained for each hydrogen level at a specific melt treatment, and their coefficients of correlation, R^2, are only 20-30 %. These data points were, statistically, not enough to reach the 95 % confidence level. To achieve such confidence, at least 17 data points per hydrogen level have to be obtained. Experimentation at this level was beyond the economic resources available for this project. The following results are therefore only the *trends* derived from the regression analysis.

Since the test yields many pieces of information, these results will be presented separately as follows:

i) microporosity,

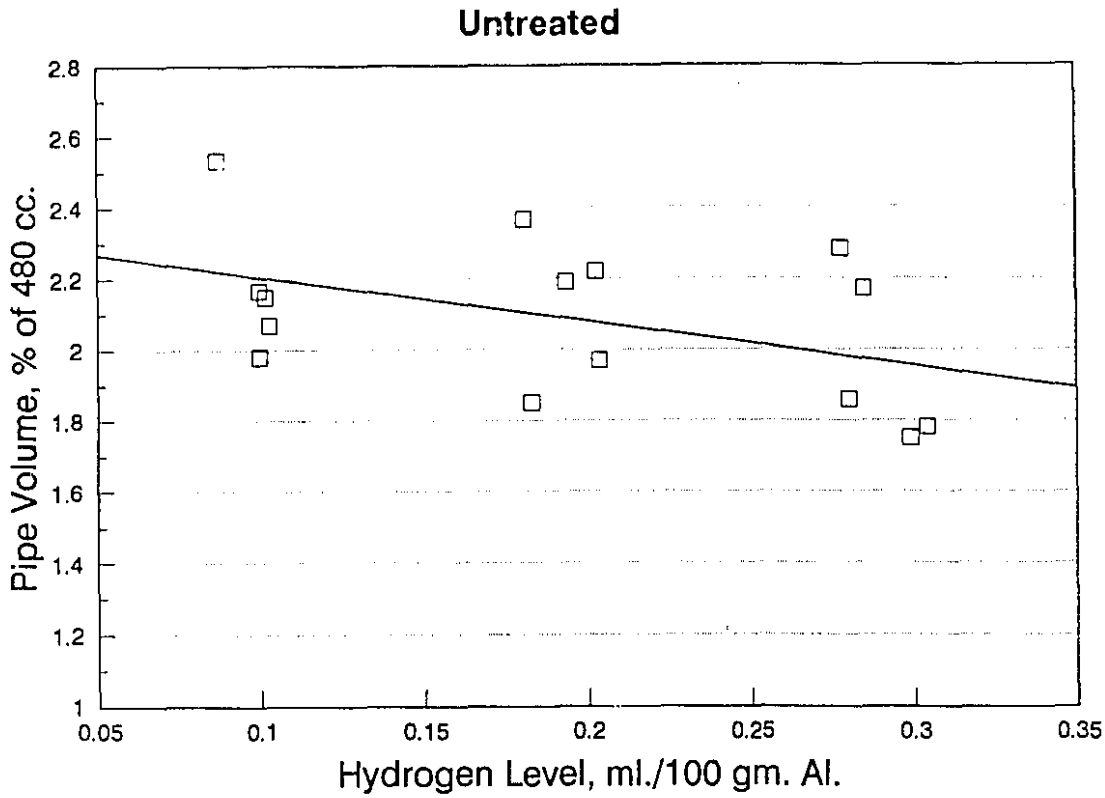

Figure 4.1 Data scattering of the pipe volume as obtained from the Tatur test.

ii) pipe volume,

iii) slumping and contraction, and

iv) total shrinkage.

4.2 Microporosity.

The effects of the various melt treatments on microporosity are shown in Fig. 4.2. It is obvious that the amount of porosity is a strong function of hydrogen level. When the melt was degassed from 0.2 to 0.1 ml./100 gm. Al., porosity decreased substantially, between 85-250 %. As hydrogen in the melt increased to 0.3 ml./100 g. Al., porosity increased by 45-70 %, depending on the melt treatment process used.

No significant differences in porosity were found for the various melt treatment

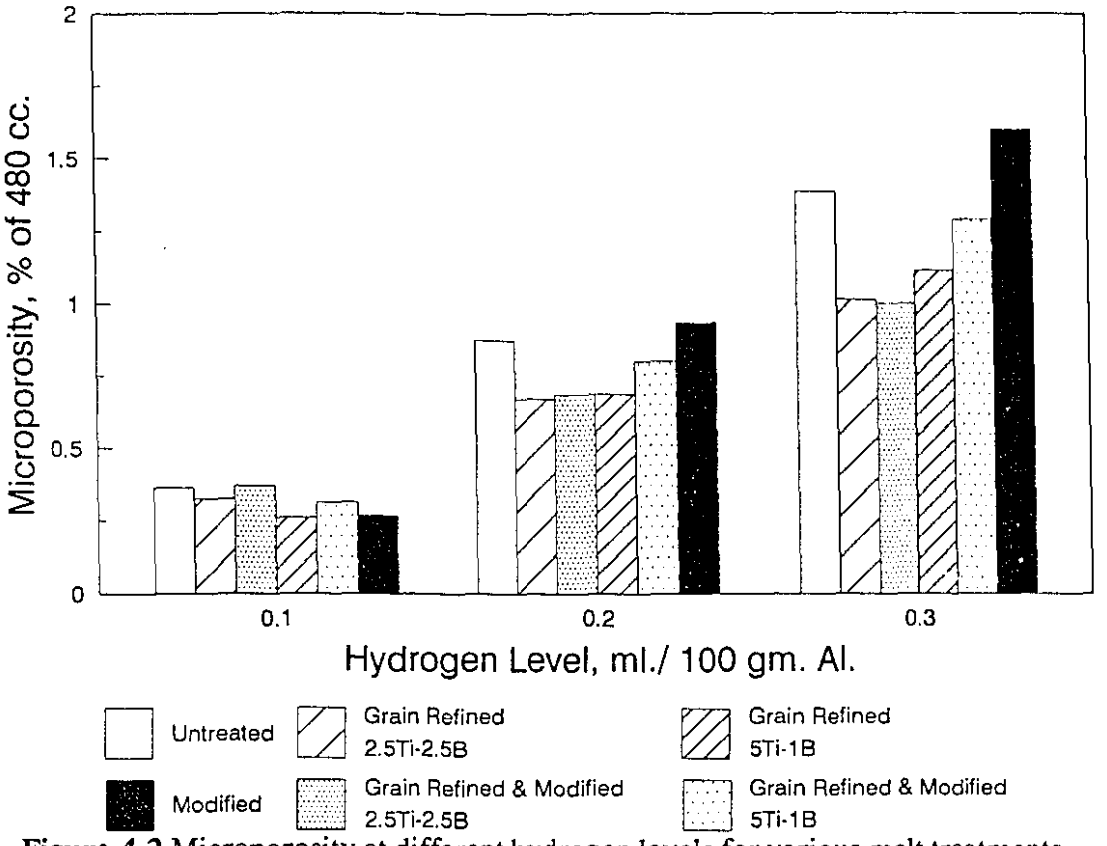

Figure 4.2 Microporosity at different hydrogen levels for various melt treatments.

conditions after the melt was degassed to 0.1 ml./100 g. Al. Degassing is clearly the best way to reduce porosity in the modified alloy since porosity is reduced by 250%, as hydrogen is reduced from 0.2 to 0.1 ml./100 g. Al. The level of porosity at 0.1 ml./100 g. Al. as well as the percent of porosity reduction when alloys were degassed from 0.2 to 0.1 ml./100 g. Al. are summarized in Table 4.1. The use of grain refinement along with modification does not substantially reduce porosity. No beneficial effects of grain refinement are clearly seen at this hydrogen level.

Among all of these combinations, at 0.3 ml./100 g. Al., the modified alloy exhibited the most serious porosity problem, follow by the untreated alloy. The porosity level in the modified alloy was 7.7 ml. while the untreated alloy had porosity of about 6.6 ml. The grain sizes in these two alloys were relatively large, 323 μm. in both untreated and modified alloy. For the alloy that had been grain refined, the grain sizes

Table 4.1 The effects of the combination of degassing and other melt treatments on porosity.

Melt Treatment Processes	Porosity after degassing to 0.1 ml./100 g.Al. (ml.)	% porosity reduction from 0.2 to 0.1 ml./100 g. Al.
Untreated	1.7	142
Modified	1.3	252
Grain refined 2.5Ti-2.5B	1.6	106
Grain refined 2.5Ti-2.5B and Modified	1.8	86
Grain refined 5Ti-1B	1.2	165
Grain refined 5Ti-1B and Modified	1.5	157

were roughly 200 μm., and porosity was noticeably reduced. Grain refinement reduced porosity by about 22 % from the untreated case; however, there was no significant difference between the two types of grain refinement as to their effects on the amount of porosity. Thus the negative effect of modification on porosity in this case can be minimized by incorporating grain refinement. The amount of porosity in the modified alloy was reduced by 38 % and 20 % respectively when applying 2.5 Ti-2.5B and 5Ti-1B grain refiner. The amount of porosity in the grain refined and modified samples was less than in the untreated ones.

At 0.2 ml./100 g. Al., similar phenomena also occured; however, the beneficial effects of grain refinement were less evident than in the previous case. Grain refinement reduced the negative effect of modification on porosity by about 28 % and 14 % with 2.5 Ti-2.5B and 5ti-1B respectively. Compared to the untreated case, the combination of grain refinement and modification reduced porosity by only 22 % and 7 %. At these hydrogen levels, beneficial effects of grain refinement do exist, but it must be appreciated that 0.2-0.3 ml./100 g.Al. of hydrogen is relatively high for a normal casting operation.

4.3 Slumping and Contraction Volume.

These experimental results are shown in Fig. 4.3. Slumping and contraction

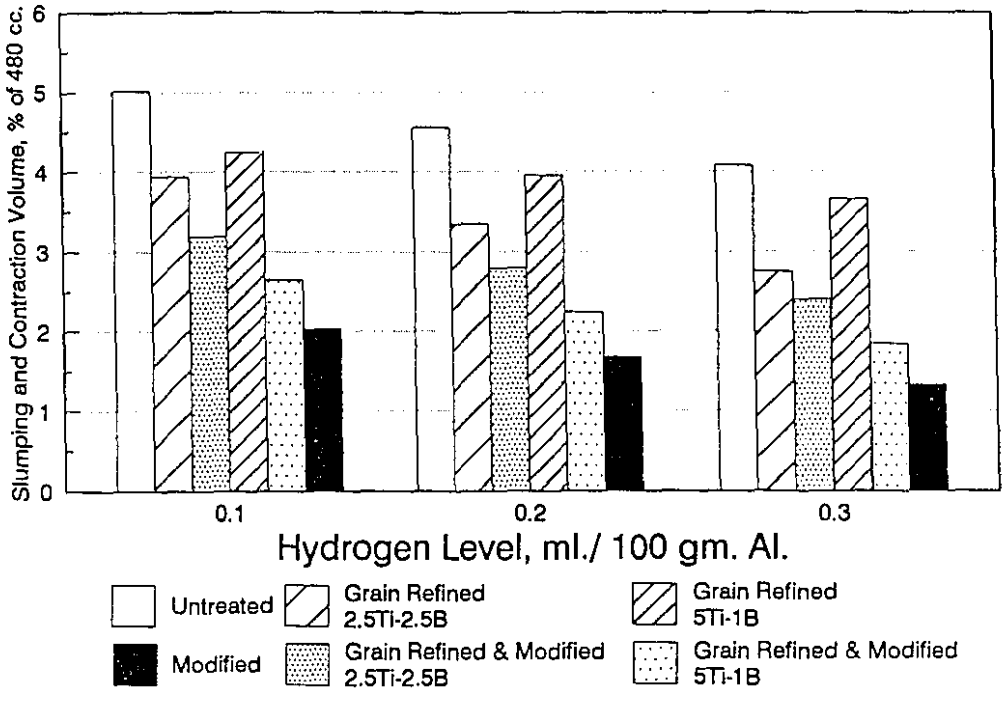

Figure 4.3 Slumping and contraction volume at different hydrogen levels for various melt treatments.

volume is dependent on the melt treatment process. Untreated alloy exhibited the most severe slumping problem, followed by the grain refined alloy, at about 5 %, and 4 % of the mold volume, respectively. Among these processes, the modified alloy yielded the least slumping volume, only 2 % of the mold volume. Modification also helped to reduce slumping when used in combination with grain refinement. Slumping in grain refined alloy was reduced to about 3 % when modification was used.

Another factor that governs slumping is porosity or hydrogen levels. As hydrogen increases, the slumping volume is slightly reduced, the exact amount being dependent on the amount of porosity in the sample.

4.3 Pipe Volume.

The effects of melt treatments on pipe volumes are similar to those observed on the slumping and contraction volumes (Fig. 4.4). Pipe volumes in the grain refined alloy

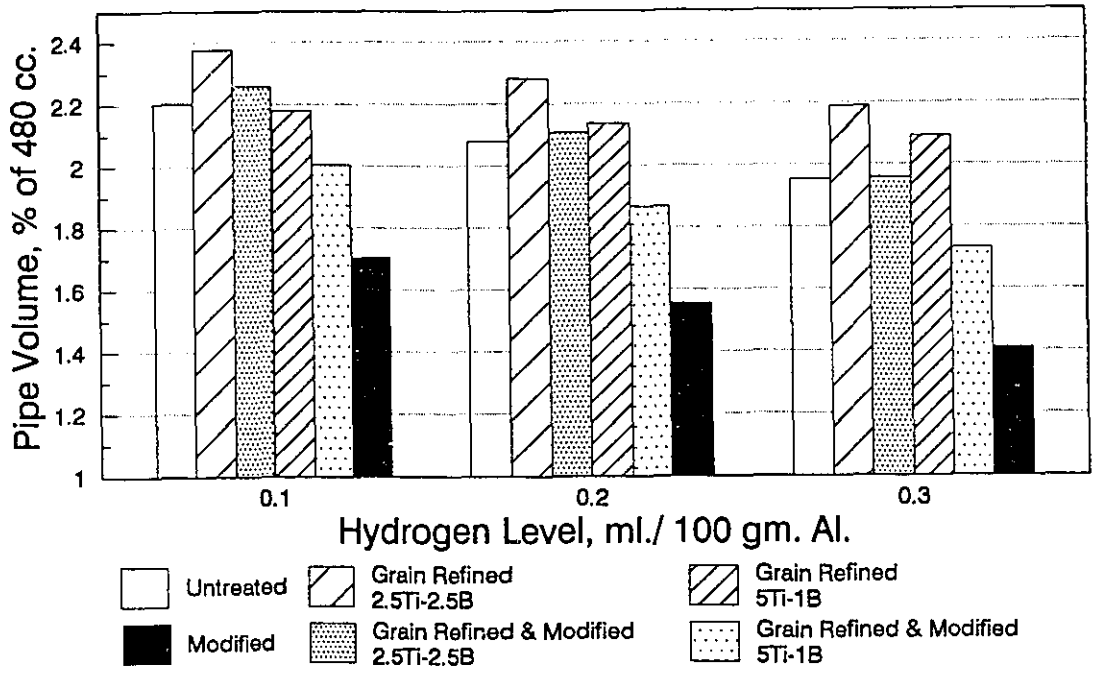

Figure 4.4 Pipe volume at different hydrogen levels for various melt treatments.

were the highest, followed by the untreated alloy. Pipe volumes in grain refined alloy were about 2.3 % of the mold volume. Modification significantly reduced the pipe volume in the alloy. The pipe volume in the modified alloy was about 20 % less than that in the untreated alloy. A combination of modification and grain refinement also slightly reduced pipe volume.

Pipe volume was also dependent on hydrogen level, but the degree of dependence was less than in the case of slumping and contraction. As hydrogen increased from 0.1 to 0.3 ml./100 g. Al., pipe volume was reduced by only 4-17 % whereas slumping reduced from 15 to 35 %.

4.5 Total Shrinkage.

Total shrinkage is the sum of porosity, pipe volume, and slumping and contraction volume. As seen in Fig. 4.5., it depends on the specific melt treatment used, but is unaffected by the melt hydrogen level.

Both grain refinement and modification had a notable influence on the total shrinkage which was a minimum in the modified alloy (4 %) and a maximum in the

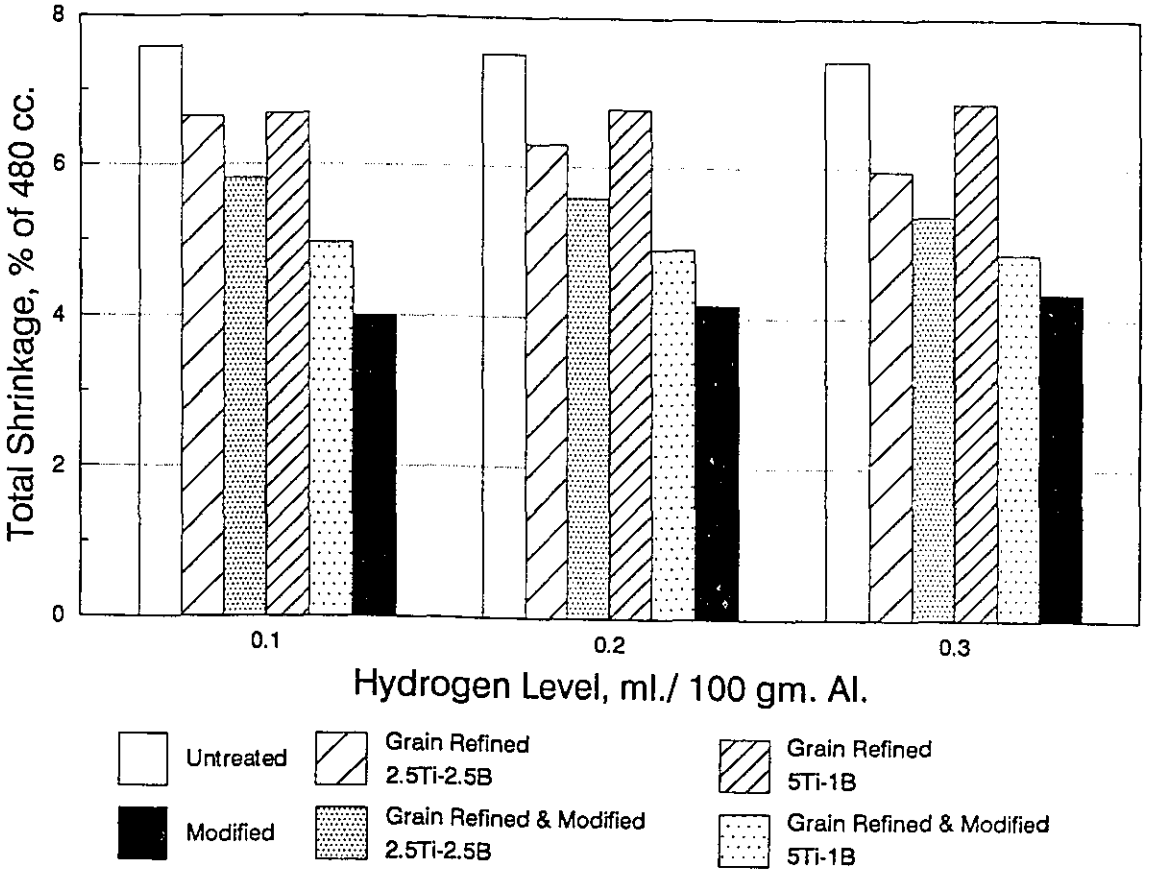

Figure 4.5 Total shrinkage at different hydrogen levels for various melt treatments.

untreated alloy at about 7.5 % of the Tatur mold volume. Grain refinement reduced the total shrinkage to 6.5 %. The total shrinkages in samples treated by the combination of grain refinement and modification lay between the volumes observed when these two processes were used singly.

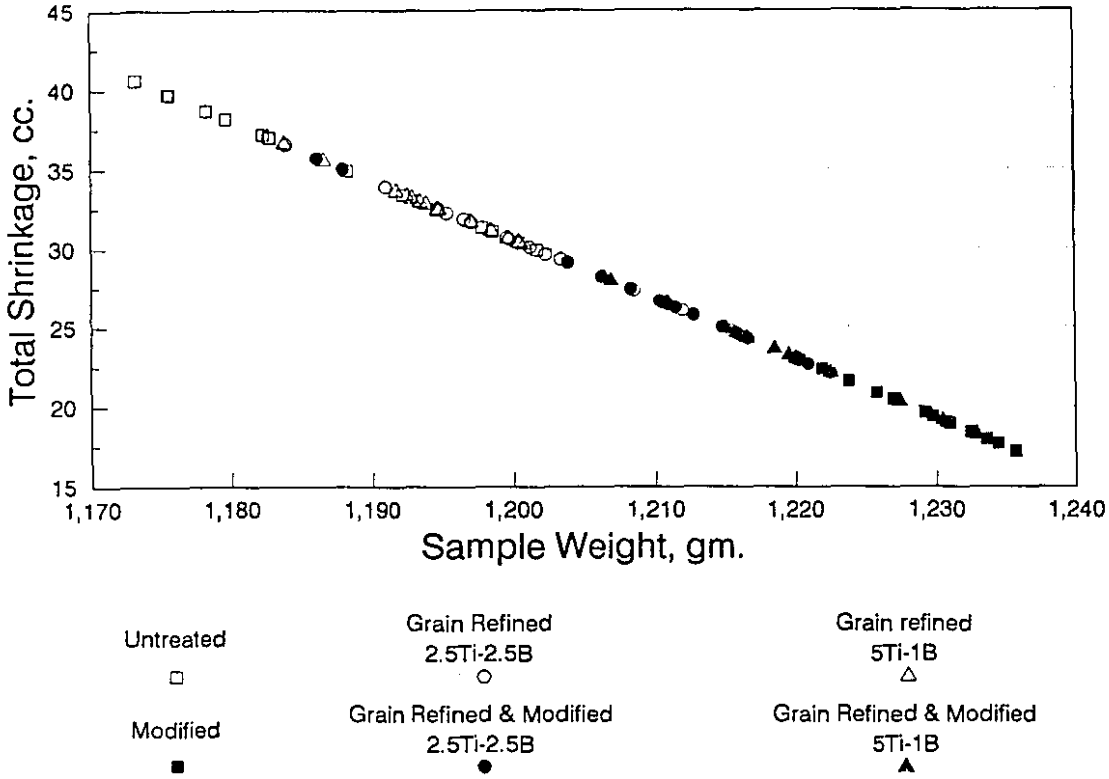

Figure 4.6 The relationship between total shrinkage and sample weight of various melt treatment processes.

The major factor that controls the amount of total shrinkage was found to be the casting weight which varied depending on the melt treatment. Possible reasons for this are discussed in the next section. Fig. 4.6 summarises the relationship between total shrinkage and sample weight obtained from various melt treatment processes. It is obvious that heavier samples posses less total shrinkage than do the lighter ones. Also shown in this figure is that the Sr-alloyed samples (solid points) yield less total shrinkage than non Sr-alloyed samples (open points). In this work, average sample weights are somewhat different for each melt treatment process as a result of the difference in their

total shrinkage. Table 4.2 summarises the sample weights, their standard deviations, and their corresponding total shrinkage for all of the various melt treatment processes studied.

Table 4.2 The average sample weight and the total shrinkage of various melt treated alloys.

Melt Treatment Processes	Avg. Sample Weight (g.)	Total Shrinkage (ml.)	Standard Deviation of Sample Weight
Untreated	1185.4	36.1	9.3
Grain refined 2.5Ti-2.5B	1200.3	30.4	7.8
Grain refined 5Ti-1B	1194.9	31.6	4.8
Grain refined 2.5Ti-2.5B and Modified	1209.7	26.9	10.1
Grain refined 5Ti-1B and Modified	1218.6	23.6	7.6
Modified	1228.4	19.9	4.8

The distributions of the two types of macroshrinkage (piping, and slumping and contraction) and microporosity for the three hydrogen levels in various melt treated alloys are illustrated in Fig. 4.7. For untreated alloy, Fig. 4.7a., as microporosity (solid bar) increases, slumping volume (open bar) is reduced notably whereas pipe volume (grey bar) slightly reduces as hydrogen increases. However, when modification is applied, the increasing volume of microporosity has significantly replaced the slumping volume as shown in Fig. 4.7b. Grain refinement, Fig. 4.7c. leads to effects similar to those seen in the untreated alloy where the effect of grain refinement and modification in combination, Fig. 4.7d., is between the effect of grain refinement or modification when used alone. The distributions of these shrinkages for all treatments are summarized in Appendix 4.1.

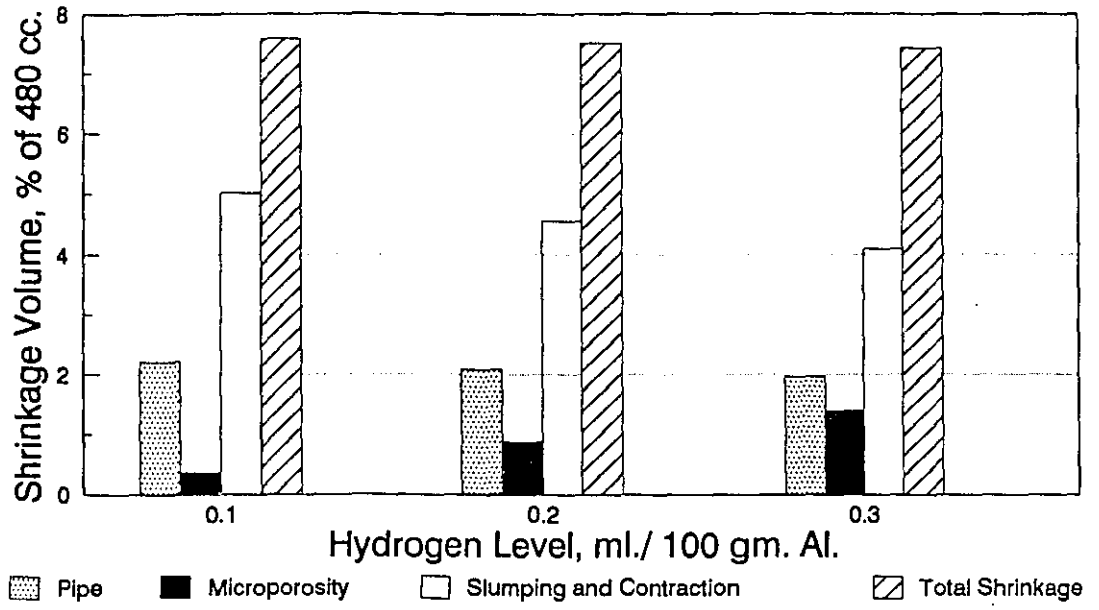

Fig. 4.7A. Untreated alloy.

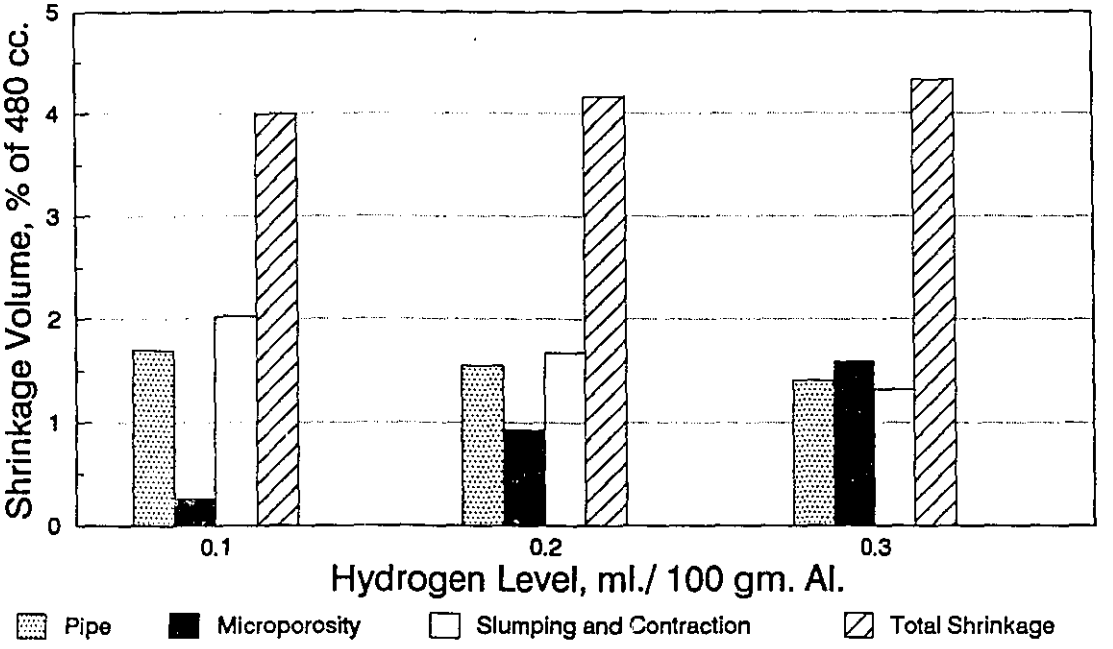

Fig. 4.7B. Modified alloy.

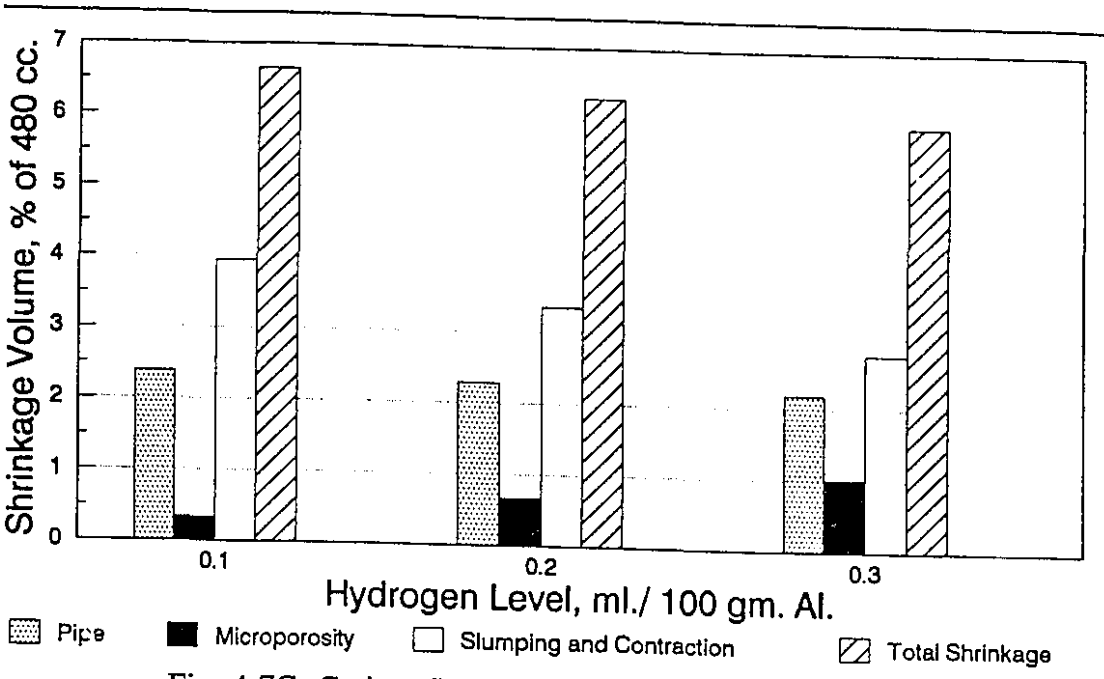

Fig. 4.7C. Grain refined alloy with 2.5Ti-2.5B master alloy.

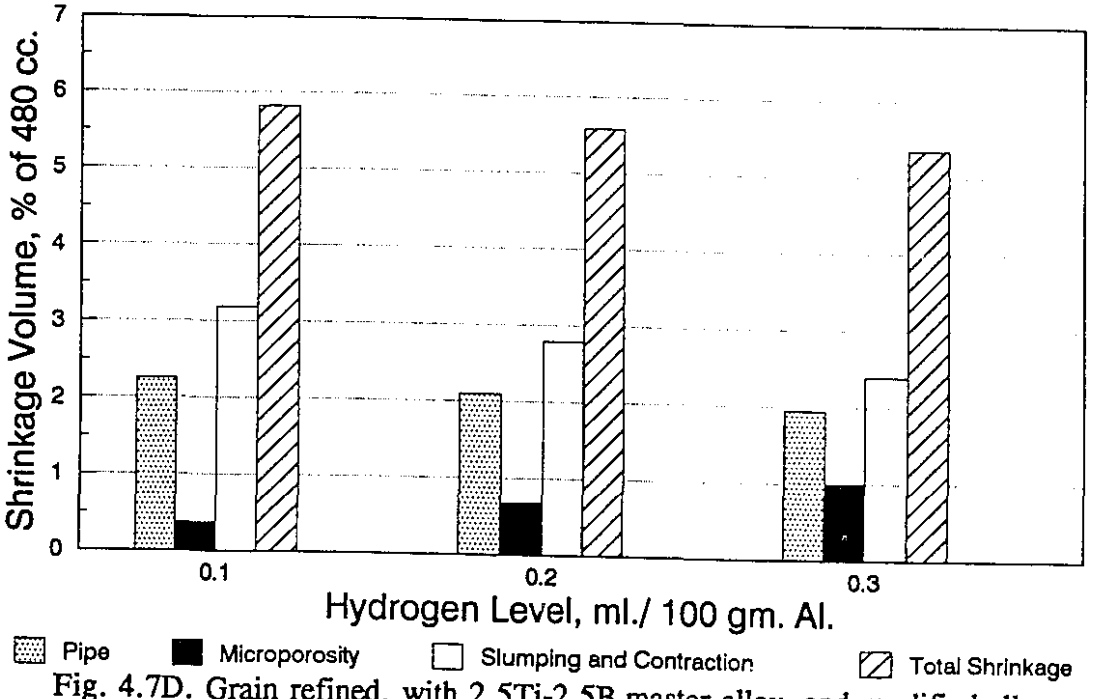

Fig. 4.7D. Grain refined, with 2.5Ti-2.5B master alloy, and modified alloy.

Figure 4.7 The distribution between microporosity and macroporosity (pipe, and slumping and contraction volume) for various melt treatments.

4.5 Discussion.

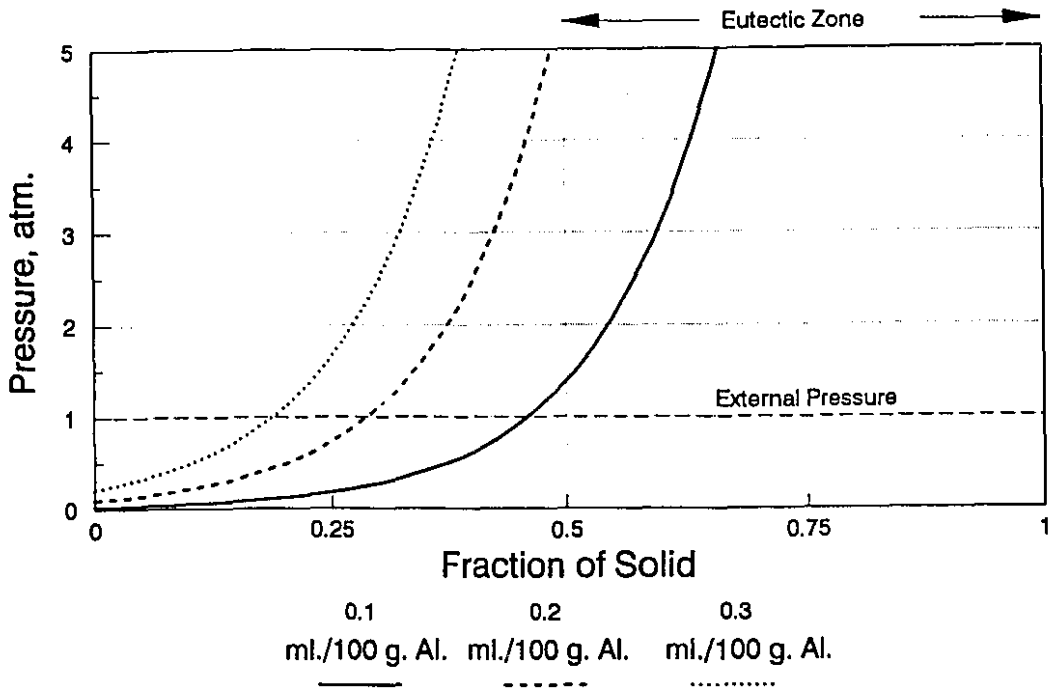

Figure 4.8 The accumulation of the internal gas pressure, P_g, of the melt containing different amounts of hydrogen as solidification proceeds.

The effects of melt treatment on microporosity are similar to those reported in previous work [4-7,34,44-45]. The dissolved hydrogen showed a strong effect on porosity followed by modification and grain refinement. The hydrogen dissolved in the melt helps to raise the internal gas pressure, P_g. The higher the gas content, the faster P_g can overcome the external pressure, resulting in a greater possibility to form gas bubbles. This effect can be illustrated in Fig. 4.8. P_g was calculated based on the initial hydrogen content and the gas solubility employing equations 2.3-2.6. The fraction of solid is calculated using the Scheil equation with the equilibrium partition ratio, k, of 0.131 for Si and 0.069 [46] for hydrogen dissolved in the melt. More details on the calculation and the computer program are given in Appendix 4.2. It is clearly seen that P_g in a melt which contains a high gas content exceeds the external pressure (solid line) faster than at lower hydrogen concentrations. P_g also grows as solidification proceeds and is much

higher at a given fraction of solid in the high gas content melt than in lower ones. This effect will help reduce the difficulty during the nucleation process of the gas bubble. The gas bubble thus forms faster and more readily in the high gas content melt than in the lower one. On the other hand, at low hydrogen content, P_g needs a considerable time to reach the external pressure. As shown in Fig. 4.8, P_g of the melt containing hydrogen at 0.1 ml./100 g. Al.(solid line) reaches the external pressure only at relatively high fraction of solid.

After P_g exceeds the external pressure, the formation of the bubble will depend on how easily the bubble can nucleate. The bubble can nucleate easily if there is a large number of available nucleation sites and lower surface energy. Modification may create these conditions and so results in higher porosity. Eutectic temperature suppression in modified alloys results in a longer mushy zone, as well as a longer solidification time. Shrinkage porosity is easily formed in this case. Longer solidification time will allow more hydrogen to diffuse to the site, thus enhancing the bubble growth. Modification may also introduce inclusions into the melt. These inclusions will serve as nucleation sites and also block fluid flow in the interdendrtic region, both of which will enhance porosity formation.

Grain refinement was found to reduce microporosity, which indicates that grain refinement hinders nucleation of the gas bubble or enhances feeding. Nucleation can be reduced by eliminating the nucleation sites or increasing the surface energy. There is no direct evidence that either of these occur; however, smaller crystals should exhibit better mass feeding than larger ones, simply because smaller crystals are more closely packed. This aids feeding and so results in less porosity.

Grain refinement, when applied with modification, helps to reduce porosity. However, the longer mushy zone and solidification time associated with modification causes more porosity to occur than if grain refining is used alone.

The total shrinkage difference between various melt treatments can be well explained by differences in liquid density as affected by the melt treatment processes. For a given casting volume, denser liquid will yield less shrinkage. Upon solidification, the

total shrinkage, which is defined as the difference between the volume of liquid and the volume of pore free solid of the same mass, can be calculated. Assuming that liquid metal completely fills the Tatur mold which is 480 cc., the liquid densities of various melt treated alloys can be calculated from their weight and volume as shown in Table 4.3. It is clearly seen that liquid densities of Sr-alloyed samples are higher than non Sr-alloyed ones. From known theoretical solid densities, total shrinkage can be calculated as also shown in Table 4.3. The calculated total shrinkages are then compared with the measured values, and an excellent correlation is found.

Table 4.3 Calculated total shrinkage from the liquid density compared to the measured values.

Melt Treatment Processes	Sample Weight (g.)	Calculated Solid Density (g./cc.)	Calculated Liquid Density (g./cc.)	Calculated Total Shrinkage (ml.)	Measured Total Shrinkage (ml.)
Untreated	1185.4	2.670	2.47	36.0	36.1
Grain refined 2.5Ti-2.5B	1200.3	2.670	2.50	30.4	30.4
Grain refined 5Ti-1B	1194.9	2.671	2.49	32.6	31.6
Grain refined 2.5Ti-2.5B and Modified	1209.7	2.670	2.52	26.9	26.9
Grain refined 5Ti-1B and Modified	1218.6	2.671	2.54	23.8	23.6
Modified	1228.4	2.670	2.56	19.9	19.9

One might argue that the differences in sample weight, which control the total shrinkage, may be due to feeding, since liquid metal was hand-poured at a slow rate. The heavier samples may have better liquid feeding than the lighter ones. If this is true, the well-fed sample should have a higher density than the poorly fed sample. However, this effect is not found here, since the density of modified alloy, which is heaviest, is lower than untreated alloy which is lightest. Moreover, the sample weights for each melt treatment are scattered in a certain range rather than randomly scattered which indicates that the sample weight is dependent upon melt treatment.

At particular hydrogen levels, the pipe volume was found to be higher for grain refined alloy. This can be explained by the effect of feeding mechanism and volumetric shrinkage, since pipe formation is dependent on these effects. Grain refined samples are better mass-fed than non grain refined ones. Moreover, grain refined liquid is less dense than modified, and shrinkage during solidification is then higher than in the samples that have denser liquid. Higher pipe volume is thus associated with grain refinement. In the case that mass feeding is the same, ie. untreated and modified, the pipe volume is then determined by the volumetric shrinkage. As mentioned before, modified alloy shows less volumetric shrinkage because of its liquid density, and the pipe volume is then found to be less than in the untreated case.

As the hydrogen level increases, pipe volume decreases. This is simply because microporosity replaces that volume. However, the reduction is not very sensitive to hydrogen level when compared to slumping and contraction.

Slumping and contraction volume, V_{sc}, is found to be sensitive to the hydrogen level. V_{sc} decreases notably as porosity increases. This indicates that porosity forms easily at the early stages and prevents the slumping effect. As expected, this is found to be true at high hydrogen levels. As solidification proceeds, a band of high hydrogen concentration is formed at the liquid/solid interface, enhancing porosity formation in this region, and compensating for shrinkage.

4.6 Summary.

In brief, the results and discussions presented in this chapter indicate the following:

i) Grain refinement, acting singly or in combination with modification, exerts a notable effect on porosity reduction particularly at high hydrogen levels (0.2-0.3 ml./100 g. Al.). This is because grain refinement induces mass feeding.

ii) There is no significant difference between the two types of grain refiners as

to their effects on the amount of porosity.

iii) There is a slight difference between the total shrinkage of the alloys treated by various melt treaments. Among these, Sr-alloyed samples have less shrinkage (about 4-5.5%) than non Sr-alloyed (6.5-7.5%). The cause of this effect may be due to the liquid density which may be affected by the melt treatment process.

iv) Pipe volume and slumping and contraction volume in Sr-alloyed samples were found to be less than those of non Sr-alloyed because of the lower volumetric shrinkage in the Sr-alloyed samples.

v) Microporosity formed in the melt displaces the volume of slumping and contraction more than the pipe volume.

Chapter 5

The Effects of Melt Treatments on the Impact Test

The mechanical properties of casting alloys are mostly affected by their microstructure, grain size and defects. The effects of these parameters have been studied extensively using the tensile test, but only rarely with the impact test. Previous work (14,36) has shown the significant effect of Si morphology on improving the impact strength of aluminum alloy. In this work, the effects of two other factors, porosity and grain size, have been studied and will be discussed in this chapter.

5.1. Porosity in Impact Test Specimens.

Fig. 5.1 shows the average volume fraction of porosity of the impact specimens as calculated from the density of the samples treated by various melt treatments. At the lowest hydrogen level (0.1 ml./100 g. Al.), melt treatment had no evident effect on the porosity level of the impact specimens. However, when higher hydrogen levels were present (0.2 and 0.3 ml./100 g. Al.), the effect of modification was to markedly increase the amount of porosity. This effect is similar to that found in the Tatur specimens. It is interesting to note that, in these impact specimens, there was no beneficial effect of grain refinement on porosity when the samples were modified. This behavior is different from that observed in the Tatur specimens and serves to underscore the complex nature of porosity formation in these alloys.

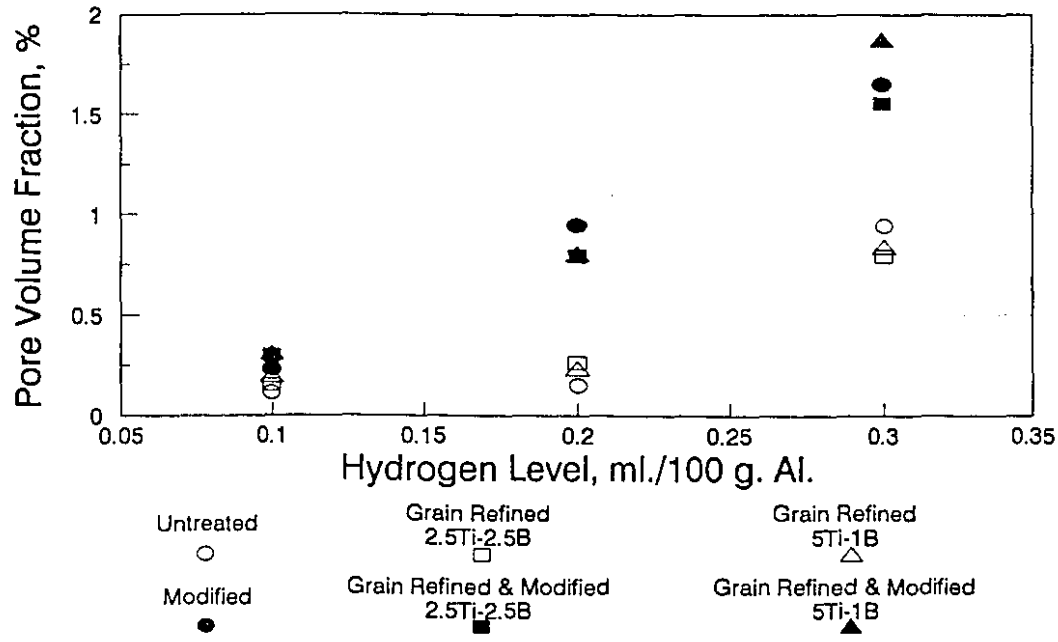

Figure 5.1 The average pore volume fraction of various melt treated alloys at different hydrogen levels.

5.2 Impact Strength.

Fig. 5.2 shows values of the impact strength as affected by the various melt treatments. Silicon morphology exerts a stronger influence on the impact strength than does porosity generated by modification. At low hydrogen levels, impact strengths in the alloys whose silicon phase is modified, represented by solid points, are improved by about 70 % from the untreated case. As hydrogen increases, the impact strength in the modified alloy is slightly impaired by porosity, but remains superior to that of the untreated alloy. At a normal hydrogen level,(0.2 ml./100 g. Al.), the impact strength of the modified alloy is reduced by 20 % because of porosity, but is still 60 % greater than in the untreated alloy. Even at the highest hydrogen level, the impact strength of modified alloy is greater than that of untreated alloy.

The work has been extended to study the relationship between the impact strength and the amount of porosity in each sample as shown in Fig. 5.3. There is a slight

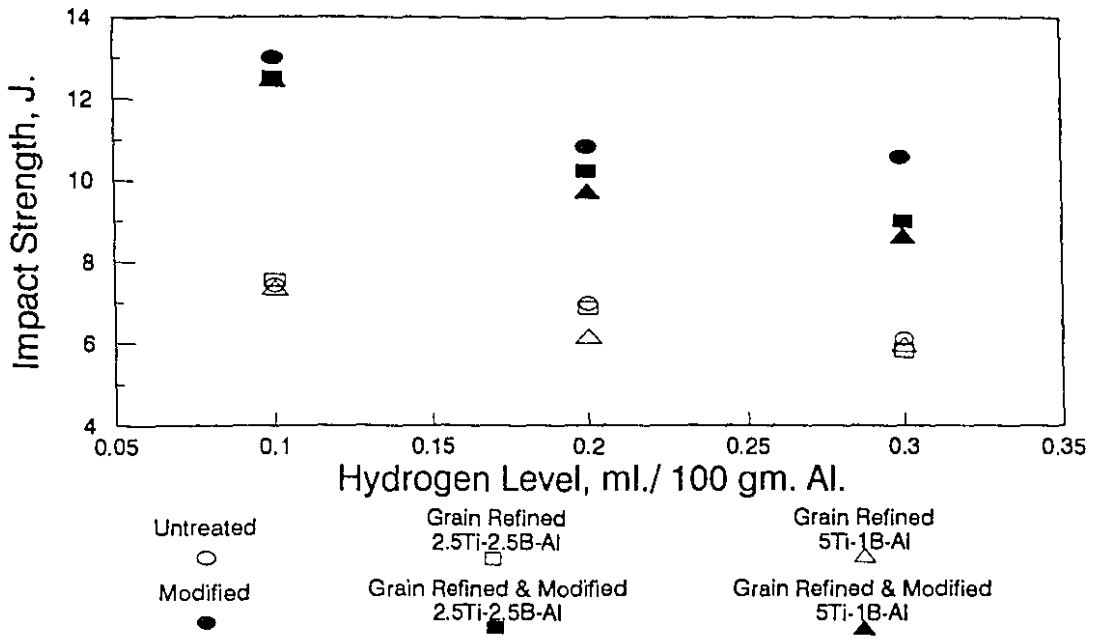

Figure 5.2 The average impact strength of various melt treated alloys at different hydrogen levels.

dependence of impact strength on porosity; however, the results must be separated into two groups in order to obtain the optimum confidence level. The first group is Sr-alloyed and the other is non Sr-alloyed. The relationship between impact strength and the pore volume fraction of the alloys in these two groups is summarized in Table 5.1. It should be noted that an error of ± 2.5 J. is present in this data.

Table 5.1 The relationship between impact strength and pore volume fraction of Sr-alloyed and non Sr-alloyed.

Impact Strength (J.) = b × Pore Volume Fraction (%) + a

	b	a	R^2
Sr-Alloyed	-2.2	12.8	0.28
non Sr-Alloyed	-1.4	7.3	0.23

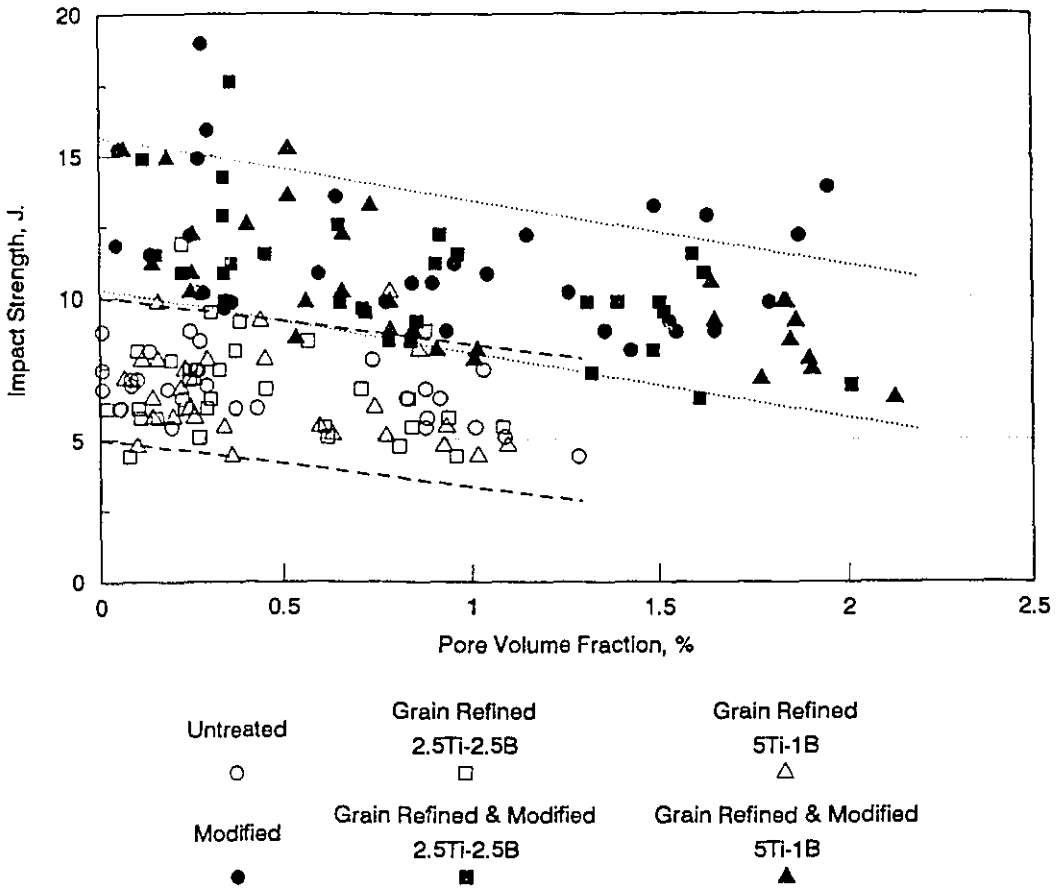

Figure 5.3 The relationship between pore volume fraction and the impact strength.

5.3 Crack Initiation and Propagation Energy.

The two significant energy values involved in the fracture of the impact specimens treated by various melt treatments are shown in Fig. 5.4. For a particular stack bar, the lower bar represents the energy required to initiate fracture, E_i, and the top bar represents the energy required to propagate fracture, E_p. The sum of these two bars is the total absorbed energy, or the impact strength of the alloy.

At a particular hydrogen level, the two energies in Sr-alloyed samples are higher than those of non Sr-alloyed samples. Both the crack initiation and propagation energy of the alloys whose silicon phase is acicular are about 40 % lower than those of the alloys with a fibrous silicon phase. The propagation energy in each melt treatment was

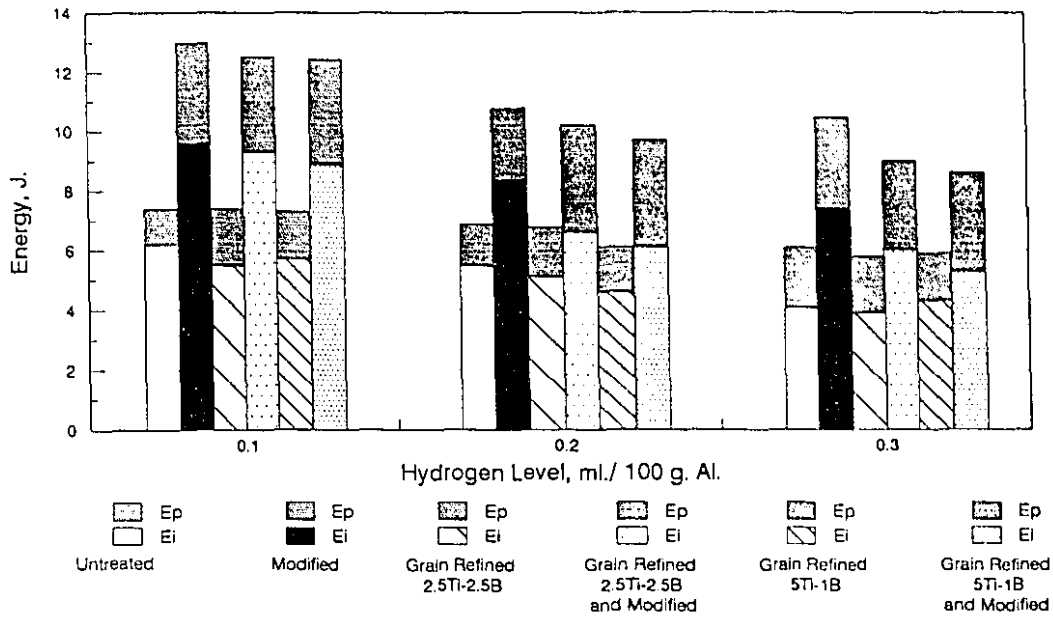

Figure 5.4 The average values of crack initiation energy, E_i, and crack propagation energy, E_p, in impact test specimens treated by various melt treatments.

found to be almost constant as the hydrogen level increased; however the crack initiation energy is dependent on the hydrogen level in a similar manner to the impact strength.

5.4 Discussion.

The fibrous form of the silicon phase clearly exerts a strong influence on the impact strength compared to the acicular form. This is simply because the sharp edge of the acicular silicon raises the stress concentration and results in easier cracking and propagation. On the other hand, Sr not only modifies the Si particle into the fiber form but also refines the size of this brittle phase which results in greatly improving the impact strength in this alloy.

In the presence of porosity, the impact strength is slightly reduced as porosity increases, because there is somewhat less mass to absorb the kinetic energy of the hammer. The variation of E_i as a function of hydrogen level is then understandable.

However, the propagation energy, E_p, was found to be independent of the hydrogen level. This indicates that porosity does not have a significant influence on propagation. On the other hand, silicon morphology did show a strong effect on crack propagation in this alloy since propagation energy of Sr-alloyed samples is about double that of non Sr-alloyed ones.

Grain refinement did not exert a significant effect on either porosity or impact strength in these samples. Grain refinement does not reduce porosity probably because of the relatively high cooling rate of the impact test mold which hinders the mass feeding. Another possibilty is that the size of the impact test specimens is too small, and this may inhibit mass feeding. The improved properties of fine-grain-sized castings are normally due to the finer distribution of microporosity and second phase particles. In this alloy, grain refinement apparently does not serve in these ways, and this results in no significant effect on the impact strength. The evidence for this is shown in Fig. 5.5 where the Si particles are compared for four cases of melt treatments which are untreated, grain refined, modified, and grain refined and modified. It is clearly shown that there is no difference in the size of these Si particles when the alloys are grain refined.

However, there is still more porosity in Sr-alloyed than non Sr-alloyed samples, similar to the effect found in the Tatur Test. Another interesting phenomenon found in this work is that porosity in modified alloy increases rapidly as the hydrogen level increases. This indicates that the factor that causes porosity in modified alloy must be a very strong function of hydrogen level.

Figs. 5.1 and 5.2 show the average values of porosity and the impact strength as a function of the hydrogen level in the melt. It is clearly shown that reducing the hydrogen in the melt to about 0.1 ml./100 g. Al. is the best way of decreasing the porosity problem. To obtain optimum ductility, a combination of modification and degassing to about 0.1 ml./100 g. Al. is recommended.

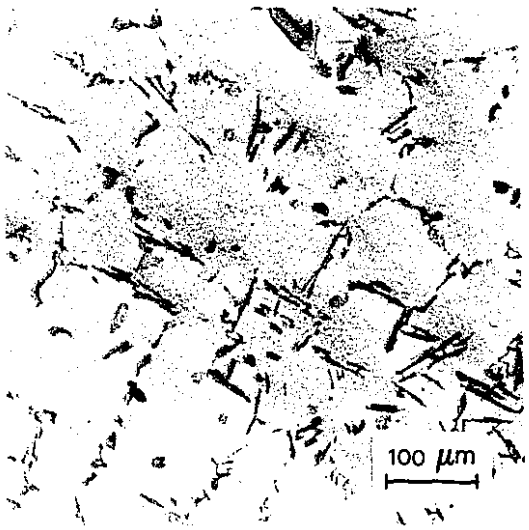

A. Untreated (grain size = 387 μm.)

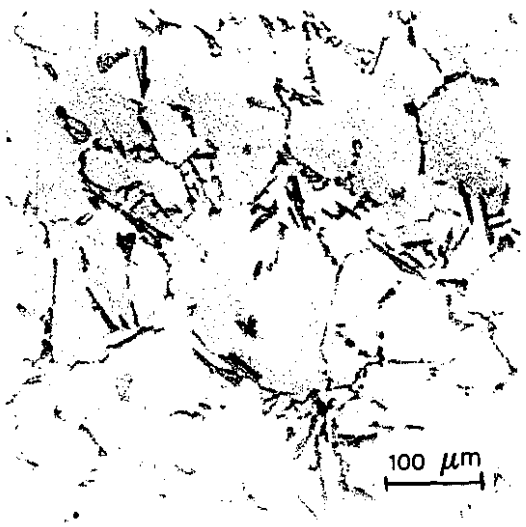

B. Grain refined with 2.5Ti-2.5B master alloy (grain size = 215 μm.)

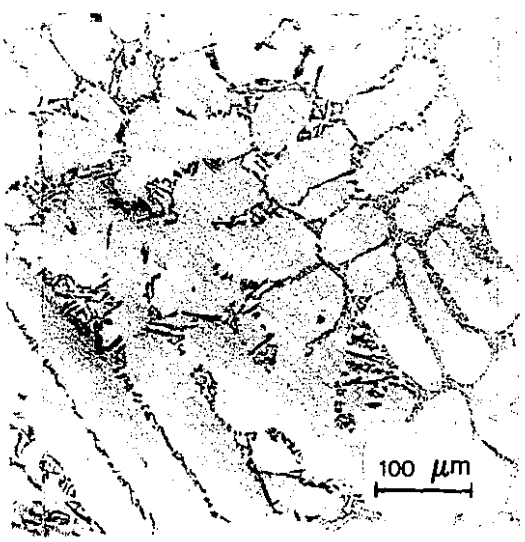

C. Modified (grain size = 351 μm.)

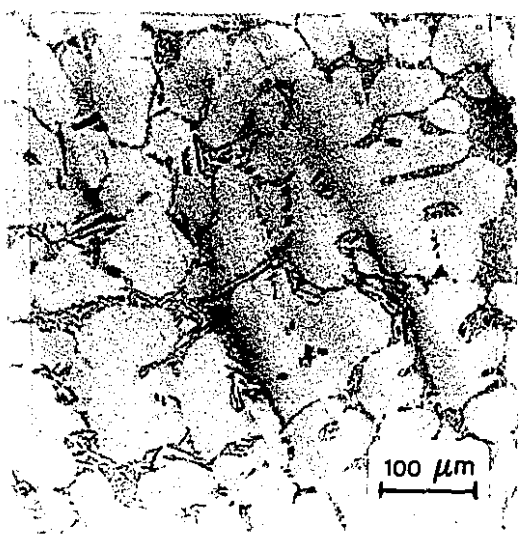

D. Grain refined with 2.5Ti-2.5B master alloy and modified (grain size = 215 μm.)

Figure 5.5 Comparison of the Si particles when grain refined to the original conditions of untreated and modified (all 125X).

5.5 Summary.

A summary of this chapter can be drawn as follows:

i) Among the three factors, Si morphology, porosity, and grain size, Si morphology has the strongest influence on the impact strength followed by the amount of porosity. These values can be related within the error range of ± 2.5 J.

ii) Grain refinement, acting singly or in combination with modification, does not improve the impact strength of A356 alloy.

iii) Grain refinement does not reduce porosity in this case probably because of high cooling rate which hinders the mass feeding.

iv) To obtain optimum ductility, a combination of modification and degassing to about 0.1 ml./100 g. Al. is recommended.

Chapter 6
Quantification of the Reduced Pressure Test

Quantification of the reduced pressure test can be used succesfully only when there is a good relationship between the sample density and the hydrogen level. The density-hydrogen relationship will be discussed here first followed by the effects of inclusions on this relationship. The third topic discussed here will be the vaildity of the crucible design. A discussion and summary of the results will complete the chapter.

6.1. Density and Hydrogen Relationship.

The effects of melt treatment on the relationship between the density of the reduced pressure samples and hydrogen in the melt are all similar. A typical result for the untreated alloy is shown in Fig. 6.1. Table 6.1. summarizes the effects of melt treatment on the slopes of the density versus hydrogen level curve. The coefficients of correlation of these curves are also listed in this table.

Densities in modified samples are the most sensitive to hydrogen in the melt, and this curve has the highest slope. The influence of hydrogen on the densities of grain refined samples is less, since the slopes of these curves are flatter than in the other cases.

A good linear relationship between density and a wide range of hydrogen in the melt exists in every melt treatment process. The coefficients of correlation of this relationship are reasonable and range from 0.77-0.96. The slopes of this relationship are slightly different, depending on the melt treatment process, as listed in Table 6.1. This implies that, at the same hydrogen level, there is less porosity in the grain refined alloy. From the slope of the curves, it is also shown that porosity in 2.5Ti-2.5B grain refined

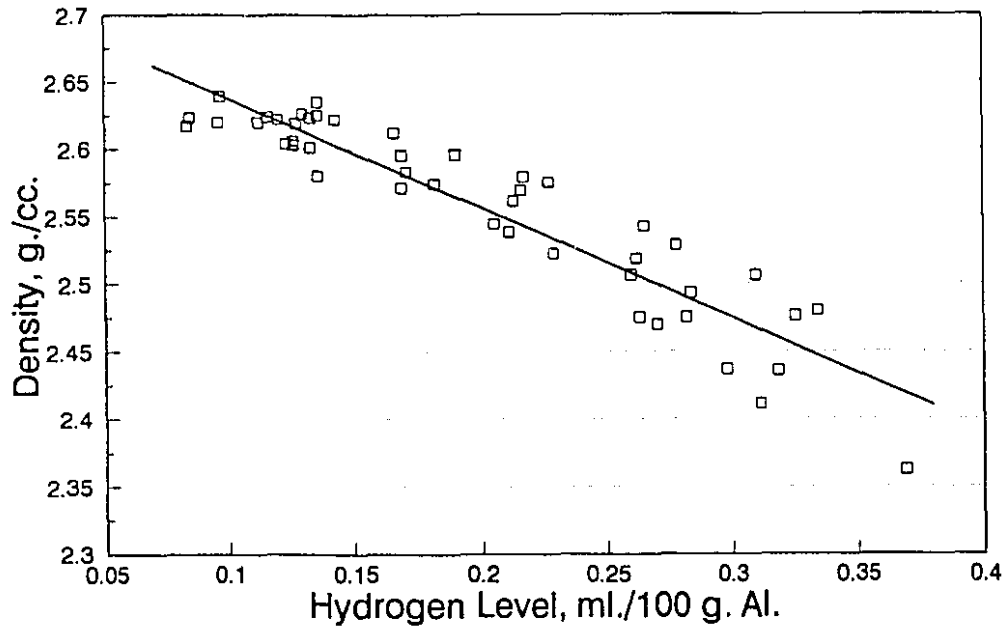

Figure 6.1 Sample density and hydrogen relationship of untreated alloys.

Table 6.1 The slopes and coefficients of correlation of density-hydrogen curves for various melt treatments.

Sample density = B × Hydrogen Level + A

Melt Treatment Processes	Slope(B)	Intercept(A)	R^2
Untreated	-0.81	2.72	0.87
Modified	-1.16	2.77	0.95
Grain Refined 2.5Ti-2.5B	-0.63	2.69	0.87
Modified and Grain Refined 2.5Ti-2.5B	-1.04	2.76	0.96
Grain Refined 5Ti-1B	-0.79	2.72	0.77
Modified and Grain Refined 5Ti-1B	-0.93	2.74	0.86

sample is less than that in 5Ti-1B sample. However, when grain refinement is applied in combination with modification, the amount of porosity generated by modification is slightly reduced, as indicated by the lower values of the coefficient B. The effects of the melt treatment on porosity in the reduced pressure test are similar to those found in the Tatur test where modification was found to increase porosity and grain refinement notably reduced the porosity.

6.2 The Effects of Inclusions.

As mentioned earlier in Chapter 2, the formation of gas porosity requires two important steps. The internal gas pressure must first exceed the external pressure before nucleation of the bubble can take place. Inclusions in the melt may then assist the gas formation process by reducing the energy required for nucleation, which is the second step. Thus a severe effect due to inclusions should be seen only at high hydrogen levels where the internal gas pressure may more readily exceed the external pressure. Samples with high contents of inclusions may form gas bubbles at an early stage of freezing. This can result in a lower density than that found in an inclusion-free sample. However, at low hydrogen levels, the sample requires a considerable time to accumulate the required internal gas pressure which will normally be achieved at almost the end of the solidification process. At this stage, the bubble formation may be induced by inclusions, but growth of the bubble is limited by the solidification time. Therefore, the variation of the gas bubble size should be small, and may not have a very significant effect on the sample density.

The variation of the sample density can be studied by the residual plot as shown in Fig. 6.2. The difference between the observed sample density and the predicted sample density (obtained from regression analysis), ΔD, is plotted versus hydrogen level. The zero line is the theoretical line on which all the points should fall. It is clearly shown that there is a trend that the variation of the sample density, ΔD, increases as hydrogen level

increases. Assuming that ΔD is caused solely by inclusions, its effect is significant only at the higher hydrogen levels.

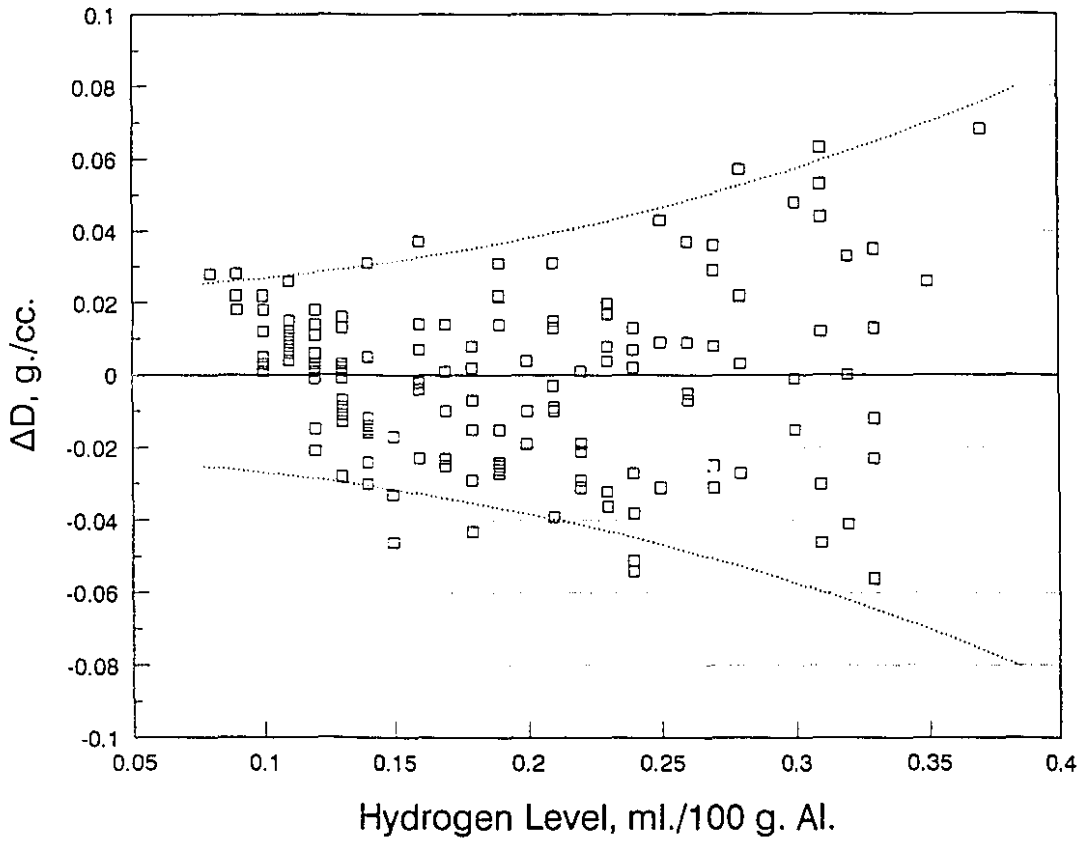

Figure 6.2 The residual plot of the sample density at different hydrogen levels.

However, at low hydrogen, shrinkage porosity is more important than gas porosity. ΔD in this region is, therefore, controlled by shrinkage porosity. A sample crucible design that yields less shrinkage may yield a smaller ΔD than one which results in high shrinkage porosity in the sample.

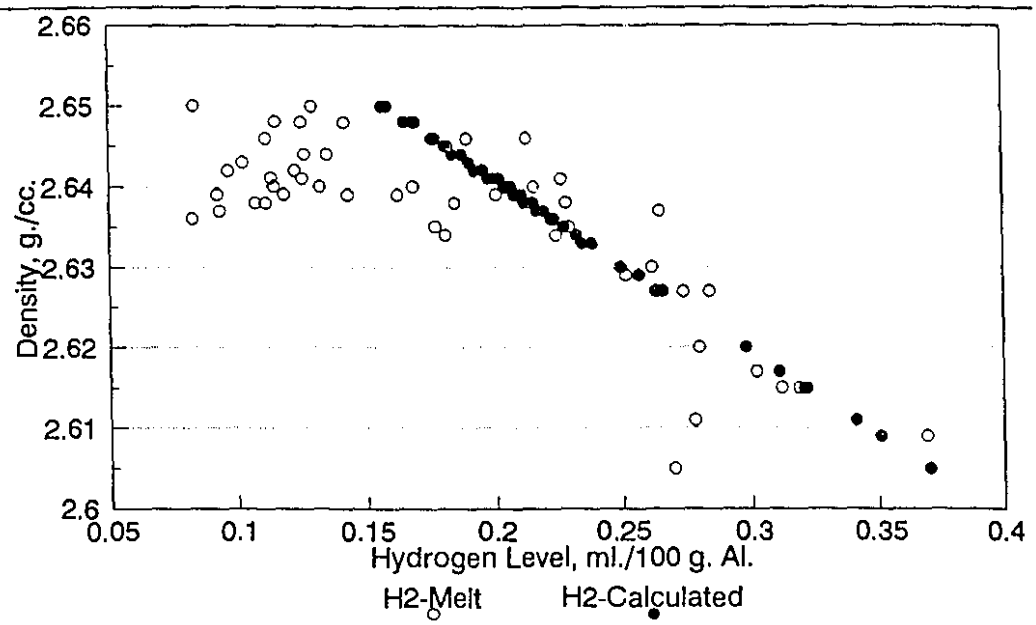

A. non Sr-alloyed.

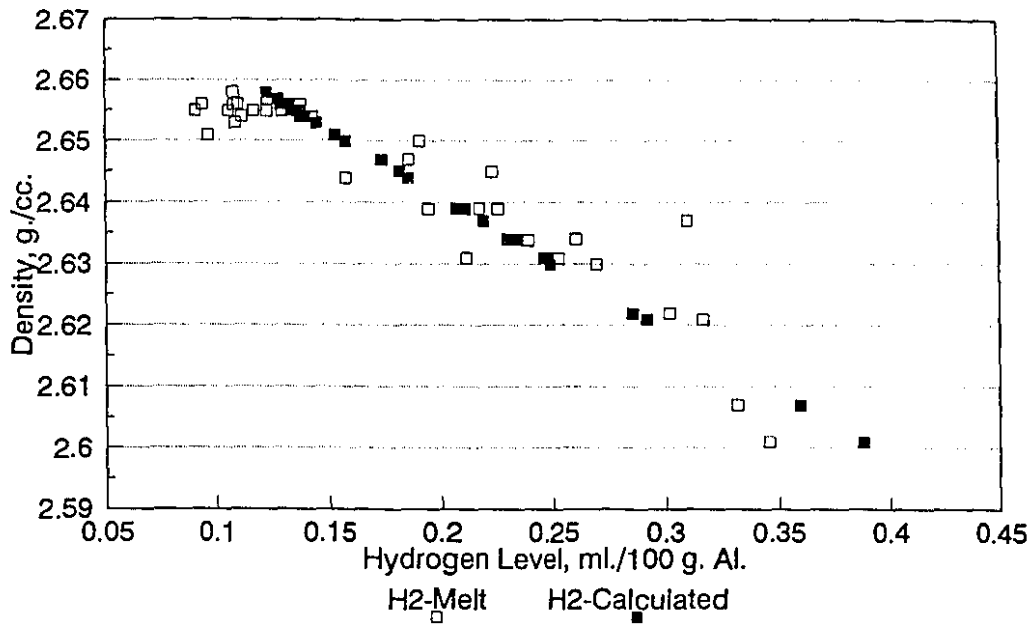

B. Sr-alloyed.

Figure 6.3 Calculated hydrogen level from density of atmospherically solidified sample.

6.3 Validity of the Crucible Design.

To obtain a reliable quantification of the test, the crucible must be well designed so that an accurate hydrogen level $[H_C]_A$ can be calculated from the atmospheric sample. The validity of the sample design used in this work can be studied by matching the $[H_C]_A$ to the true hydrogen. It was found that more accurate $[H_C]_A$ was obtained in Sr-modified samples than in non Sr-modified samples. These results are shown in Fig. 6.3. It is evident that over calculation is found at low hydrogen level for non Sr-alloyed (Fig. 6.3 a.), while Sr-alloyed yields better correlation (Fig. 6.3 b.). This indicates that, at low hydrogen levels, there is an unreasonable amount of porosity in atmospheric samples of non Sr-treated alloy. This effect is clearly seen by the plot of the atmospheric sample densities for the alloys of various melt treatments versus hydrogen levels as shown in Fig. 6.4. The density of non Sr-alloyed (open points) are consistently lower than those of Sr-alloyed samples (solid points), especially at around 0.1 ml./100 g. Al. The crucible used in this work is apparently more suitable for Sr-modified alloy.

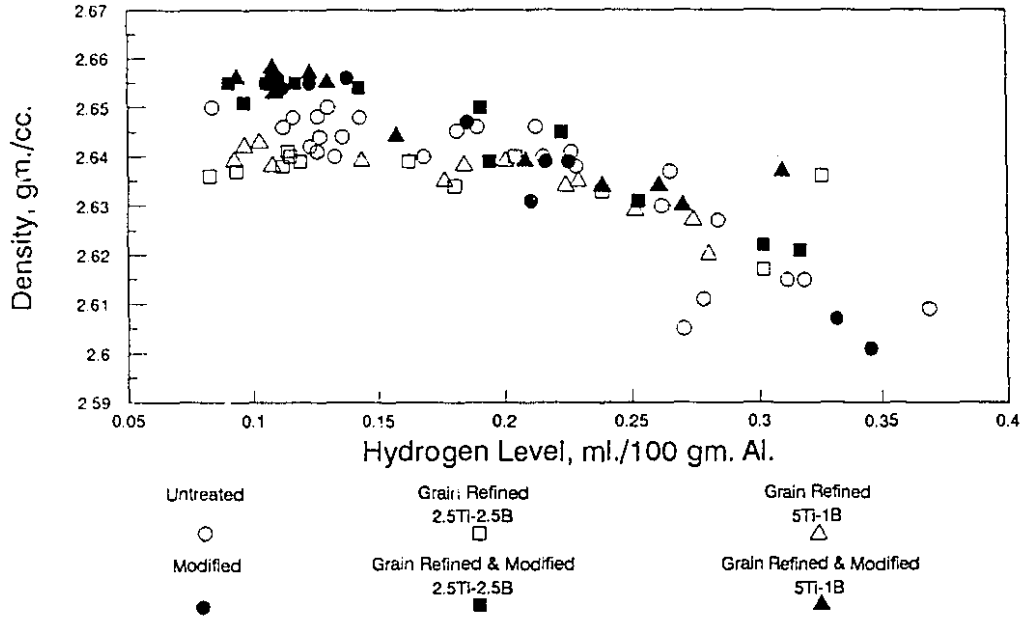

Figure 6.4 Atmospheric sample density for various melt treatments.

6.4 Correction Factor.

The amount of hydrogen in the melt can be calculated from the sample density. A typical result is shown in Fig. 6.5. The amount of hydrogen calculated from the sample density (triangle) is plotted and compared to the true hydrogen measured by Telegas (squares) of the untreated alloy. It is obvious that the calculated hydrogen is much less than the true hydrogen. A similar behavior was also found in all other melt treatment procedures as seen in Fig. 6.7.

A major aspect of this work was to deduce ways to correct this calculated hydrogen to the true hydrogen by applying some correction factor. A first step was to study the nature of the correction factor previously described (Eq. 1.1). A typical variation of this correction factor over a range of hydrogen levels is shown in Fig. 6.6. A similar behavior can be found in Appendix 6.1.

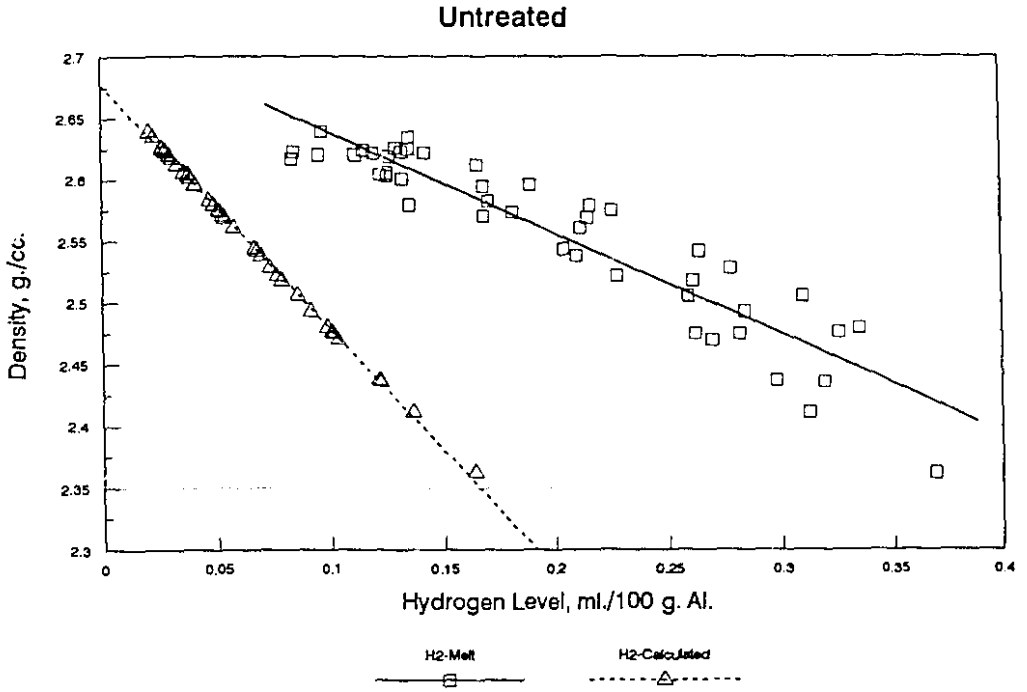

Figure 6.5 Calculated hydrogen (Δ) obtained from the sample density compared to the melt hydrogen (□).

These correction factors were found to be dependent on hydrogen level. The factor lies in the range 6-7 at lower hydrogen concentrations, and falls off exponentially to 2-3 in the range of 0.15-0.3 ml./100 g.Al. From a curve fit calculation, the correction factor will fall to unity at about 0.4-0.5 ml./100 g. Al. of hydrogen content.

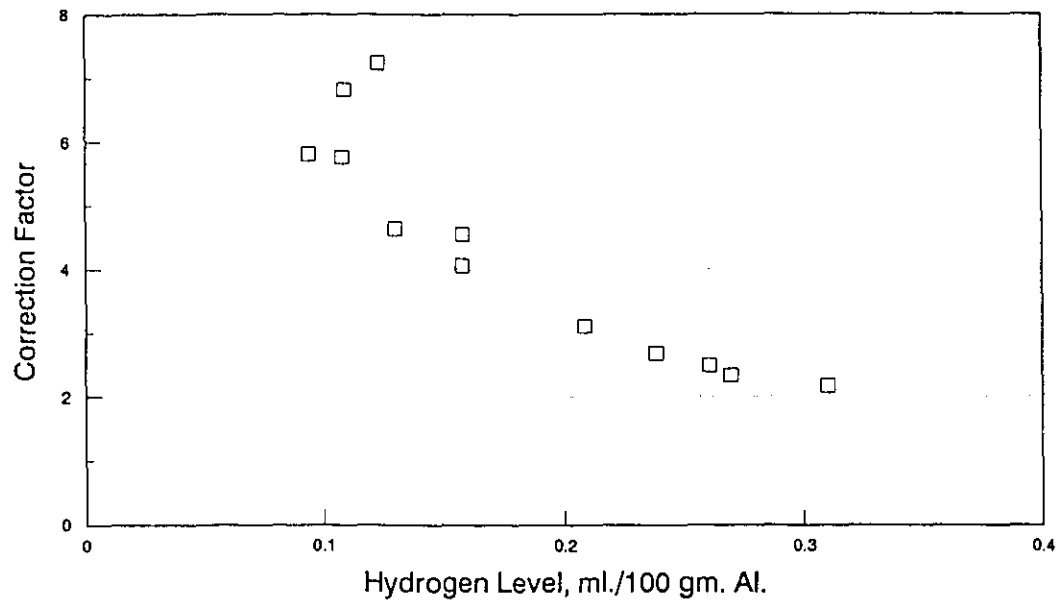

Figure 6.6 The variation of correction factor as a function of hydrogen level.

This non constancy of the correction factor complicates the quantification of the test. Three approaches were proposed to calculate a true hydrogen from the calculated hydrogen or the density of reduced pressure samples. In the simplest, a constant correction factor, an average of the factor taken from a hydrogen range of 0.15-0.3 ml./100 g. Al., was used. This approach is justified on the basis that the correction factor is not a strong function of the hydrogen level within this range. The calculated melt hydrogen can then be determined by the equation:

$$H_{corr} = C.F. \times [H_C]_R \qquad (6.1)$$

where

H_{corr} = corrected hydrogen level

C.F. = constant correction factor

$[H_C]_R$ = calculated hydrogen from the reduced pressure sample

This approach yields a relationship between density and corrected hydrogen as follows:

$$\rho = B \times H_{corr} + A$$

where

ρ = density of reduced pressure test sample (g. cm^{-3})

H_{corr} = corrected hydrogen level (ml./ 100 g. Al.)

A and B are constants.

Table 6.2 Linear Regression characteristics of corrected density-hydrogen relationship.

Sample density = B × Hydrogen level + A

Melt Treatment Processes	Slope (B)	Intercept (A)	Correction Factor
Untreated	-0.58	2.68	3.40
Modified	-0.58	2.68	3.34
Grain Refined 2.5Ti-2.5B	-0.55	2.68	3.74
Grain Refined 5Ti-1B	0.67	2.68	3.01
Modified and Grain Refined 2.5Ti-2.5B	-0.69	2.68	2.87
Modified and Grain Refined 5Ti-1B	-0.70	2.68	2.98

The linear regression characteristics of this equation are given in Table 6.2 for all of the melt treatment processes used.

Using this method all of the calculated hydrogen values from the reduced pressure samples were corrected to obtain the melt hydrogen. They are plotted versus true Telegas hydrogen for all of the melt treatments in Fig. 6.7.

The results obtained are reasonably good in the intermediate range of hydrogen, but there is a tendency to seriously overestimate the true hydrogen when it approaches a high level (eg. 0.35 ml./100 g. Al.). A slight underestimation of the true hydrogen is also found in the low hydrogen range (<0.1 ml./100 g. Al.). This is due to the fact that the correction factor is not in reality constant.

Fig. 6.7A. Untreated

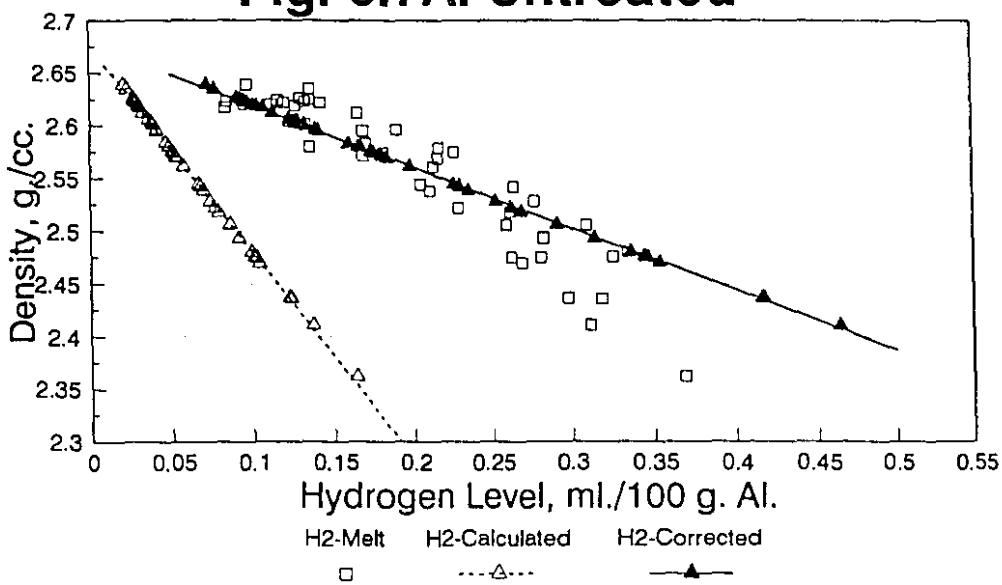

Fig. 6.7B. Modified*

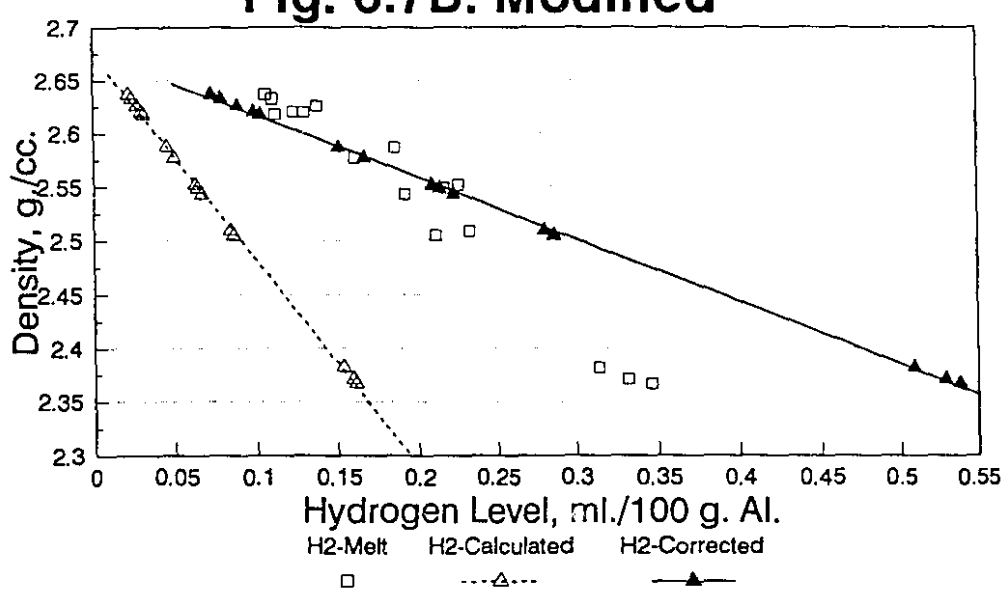

* with 90Sr-10Al modifier @ 0.02 wt. %

Fig. 6.7C Grain Refined*

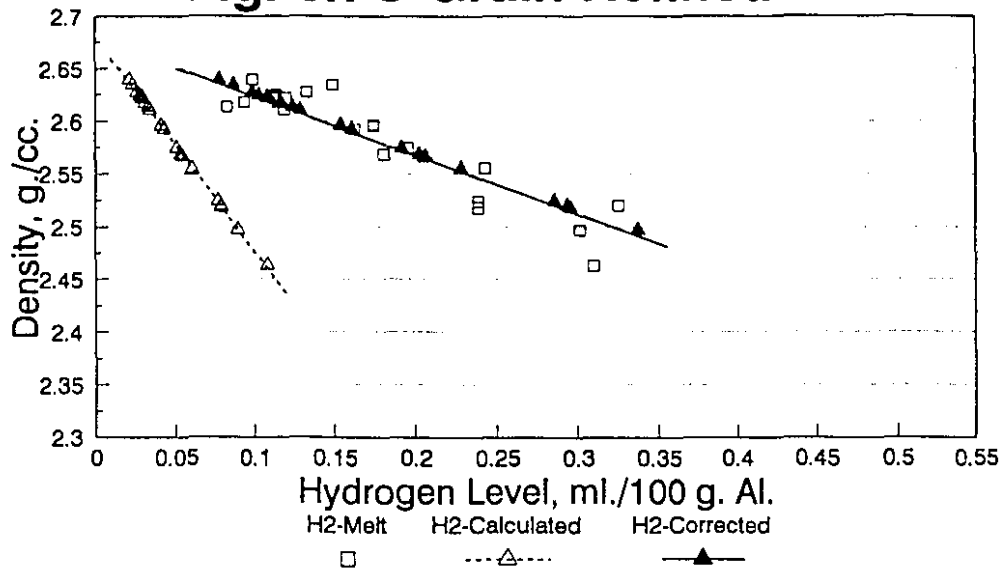

*with 2.5Ti-2.5B-Al grain refiner @ 0.17 wt.% Ti

Fig. 6.7D Grain Refined* and Modified*

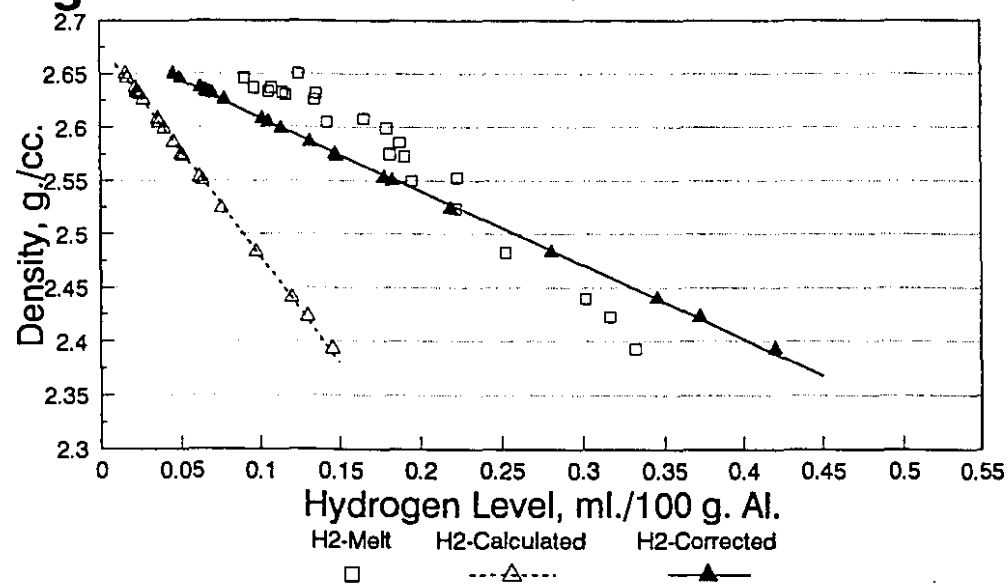

*with 2.5Ti-2.5B-Al grain refiner @ 0.17 wt.% Ti
*with 90Sr-10Al modifier @ 0.02 wt.% Sr

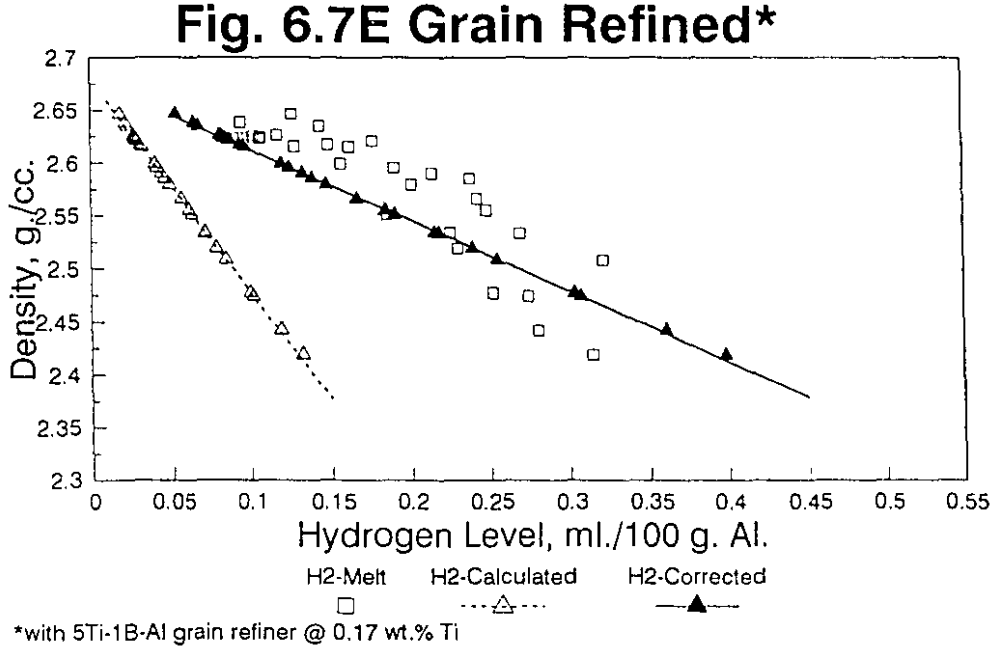

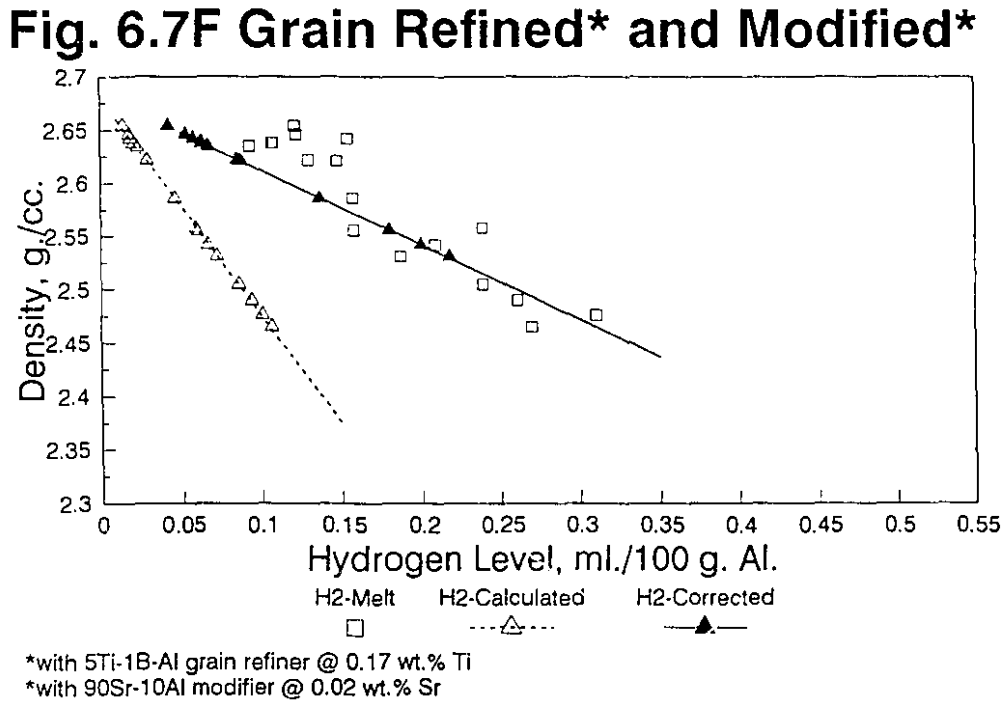

Figure 6.7 Corrected hydrogen (▲) calculated from a constant correction factor compared to the melt hydrogen (□) for various melt treatments.

To minimize this error, in a second approach, a non-constant correction factor was determined from the experimentally determined relationship of the correction factor to the calculated hydrogen from the reduced pressure sample, $[H_C]_R$, as follows:

$$C.F. = a \times \exp (b \times [H_C]_R) \quad (6.2)$$

where

$[H_C]_R$ = calculated hydrogen from reduced pressure sample (ml./100 g. Al.)

a and b are constants.

The corrected hydrogen is then obtained from the equation :

$$H_{corr} = C.F. \times [H_C]_R \quad (6.3)$$

Since there is little difference in the density-hydrogen relationship for all of the various melt treatment processes, it was found possible to use one correction factor equation for all of the data. The problem is to find the proper correction factor equation that yields the most accurate corrected hydrogen level. As mentioned earlier, the accuracy of the correction factor technique is based on the accuracy of the calculated hydrogen from the density of the atmospheric sample, $[H_C]_A$. Among all of the melt treatments used, it was found that $[H_C]_A$ in the modified alloy correlated best with measured melt hydrogen as shown in Fig. 6.8. The correction factor equation obtained from modification data was then selected. With minor modification to yield optimum accuracy, the correction factor equation was found to be :

$$C.F. = 5.5 \exp (-6 \times [H_C]_R) \quad (6.4)$$

This factor, when applied to calculated hydrogen, yields corrected hydrogen as shown in Fig. 6.9.

An excellent agreement with true hydrogen is obtained for all melt treatments over the entire hydrogen range. The superiority of this approach over the constant correction factor is evident.

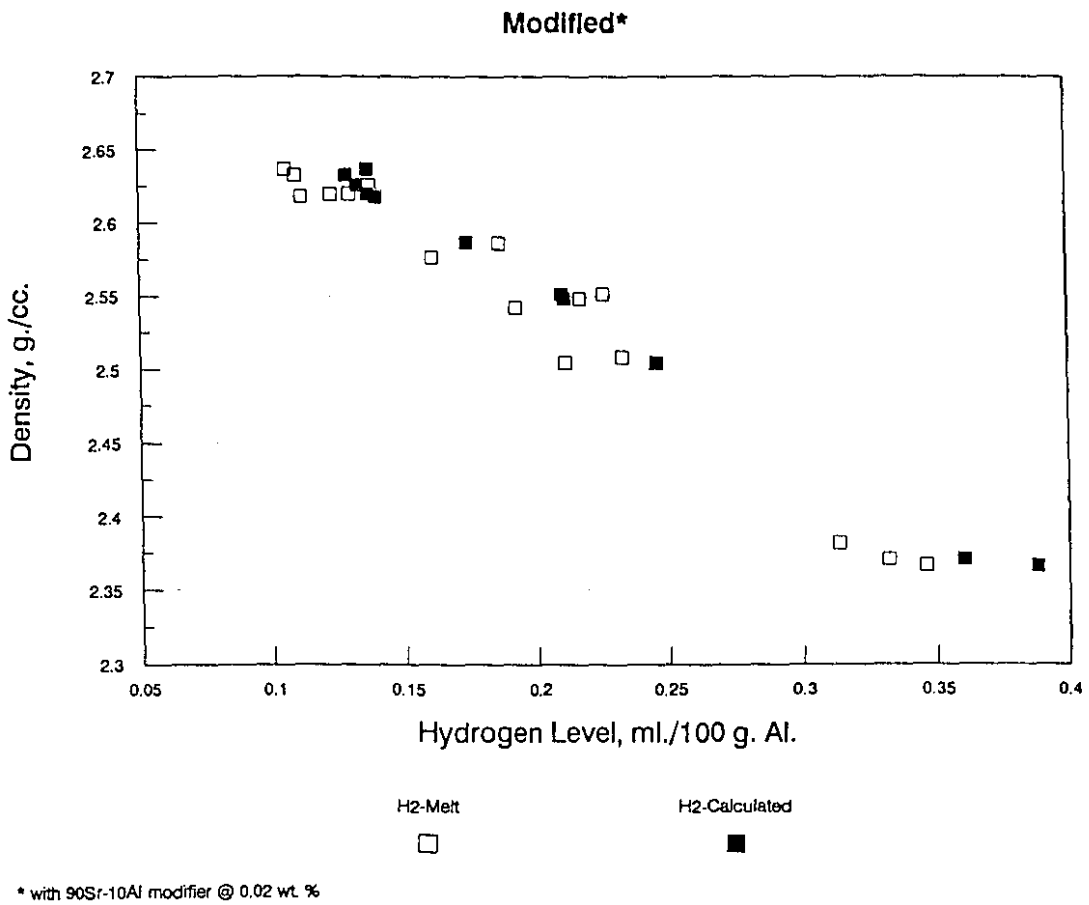

Figure 6.8 Calculated hydrogen level (■) from atmospheric sample density of modified alloy compared to the melt hydrogen level (□).

Fig. 6.9A Untreated

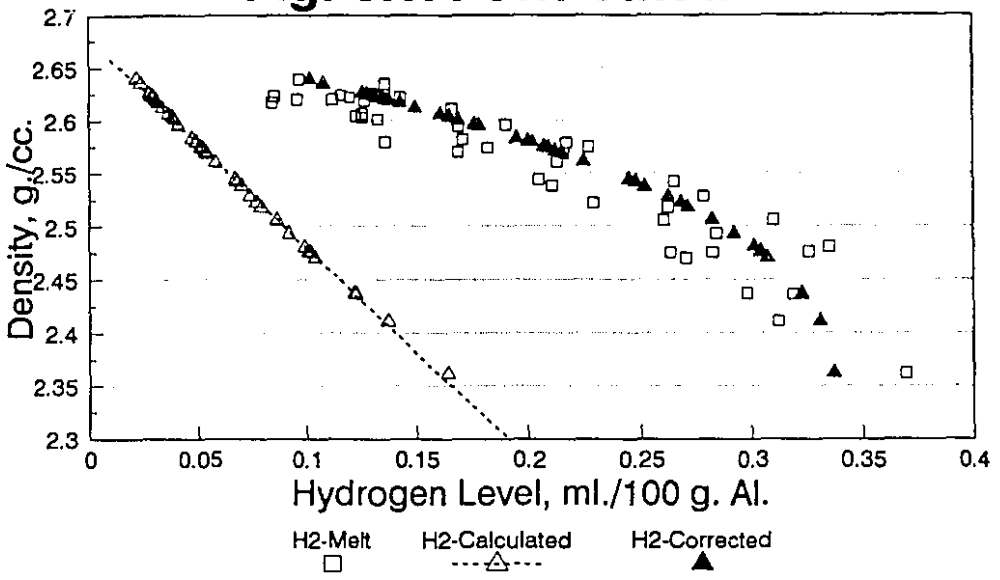

Fig. 6.9B Modified*

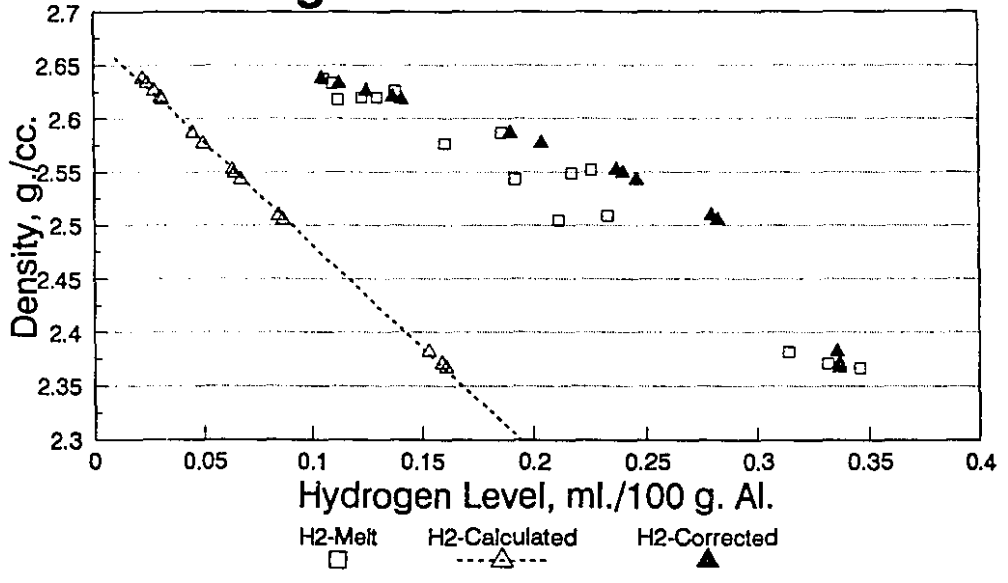

*with 90Sr-10Al modifier @ 0.02 wt. % Sr

Fig. 6.9C Grain Refined*

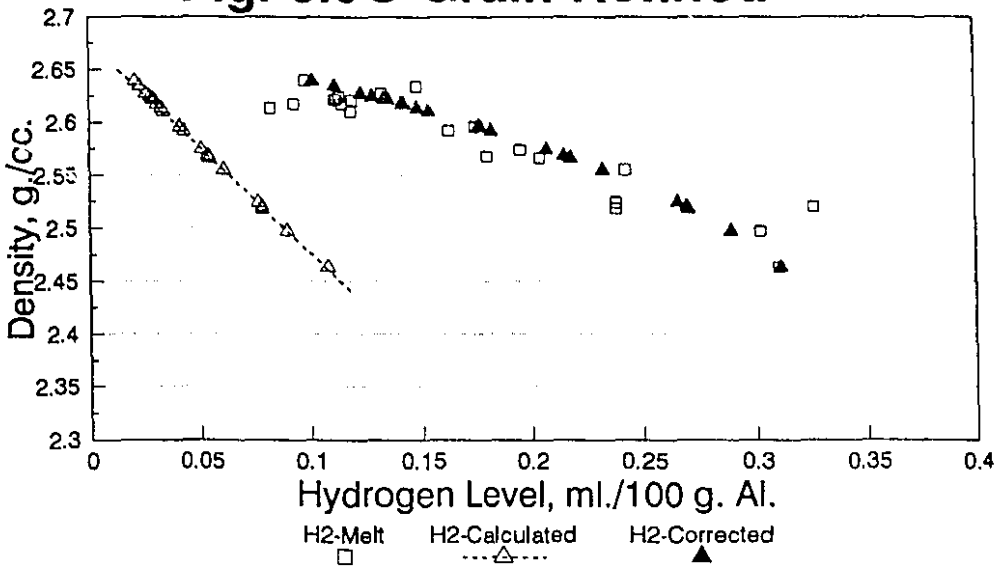

*with 2.5Ti-2.5B-Al grain refiner @ 0.17 wt.% Ti

Fig. 6.9D Grain Refined* and Modified*

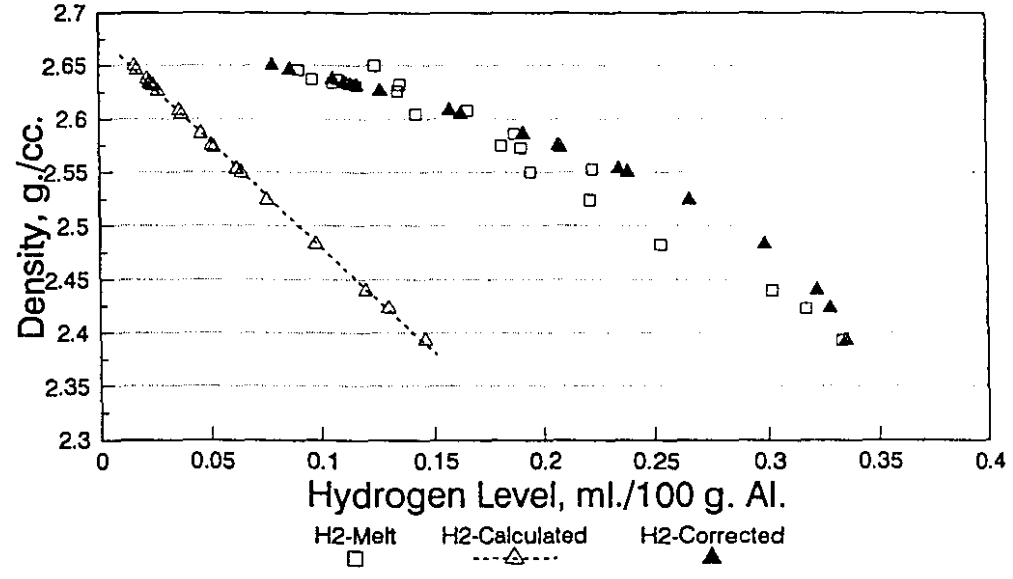

*with 2.5Ti-2.5B-Al grain refiner @ 0.17 wt.% Ti
*with 90Sr-10Al modifier @ 0.02 wt.% Sr

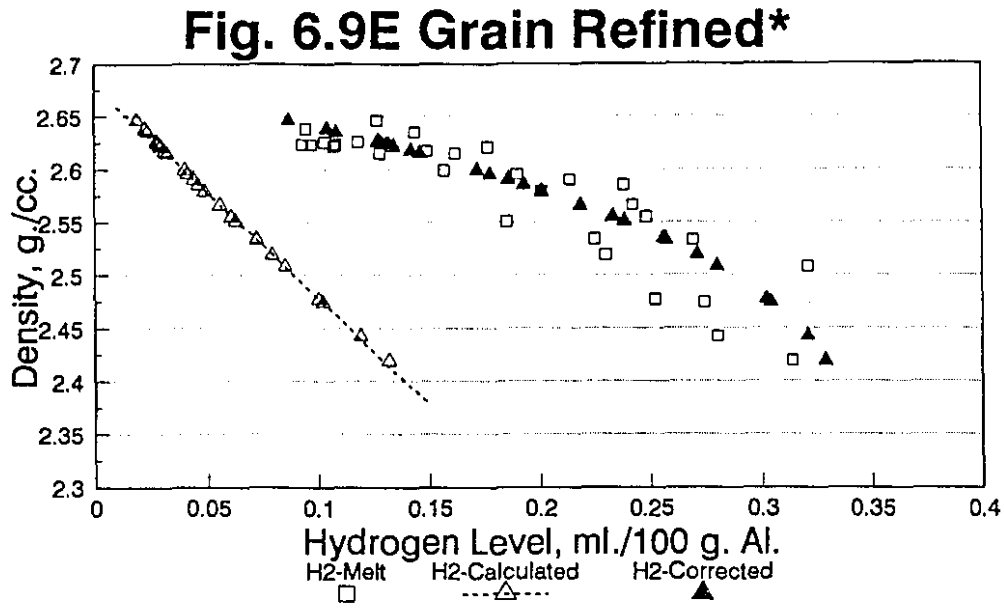

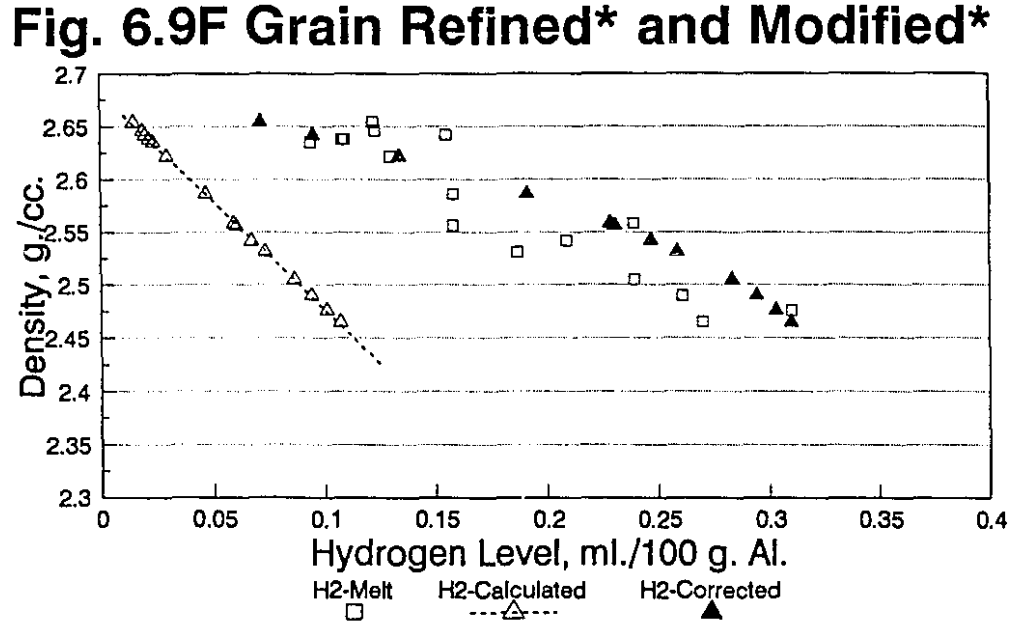

Figure 6.9 Corrected hydrogen (▲) calculated from the hydrogen dependent correction factor for various melt treatments compared to the melt hydrogen (□).

The disadvantage of the first two approaches is the complication due to inaccuracy of the $[H_C]_A$. To eliminate this effect, a third approach was used which considered only two parameters; the calculated hydrogen from the reduced pressure sample, $[H_C]_R$, and the true melt hydrogen. Since it was found that $[H_C]_R$ is less than the actual hydrogen, the difference between these two values may be presumed to be gas loss to the pumping system. The amount of gas loss, ΔH, was studied as a function of $[H_C]_R$ calculated from all of the samples treated from various melt treatments. This yields the following relationship:

$$\Delta H = 0.497 \times [H_C]_R^{0.452} \tag{6.5}$$

where ΔH = the amount of gas loss, ml./100 g. Al.
Once the amount of gas loss is known from the above relation,
one can calculate the true hydrogen by the relation:

$$H_{corr} = [H_C]_R + \Delta H \tag{6.6}$$

The corrected hydrogen levels were plotted versus the true hydrogen and the results are shown in Fig. 6.10. An excellent agreement with true hydrogen is obtained for all melt treatments over the entire hydrogen range. It is clear that quantification of the reduced pressure test is possible, at least for the alloy used in these experiments.

Fig. 6.10A Untreated

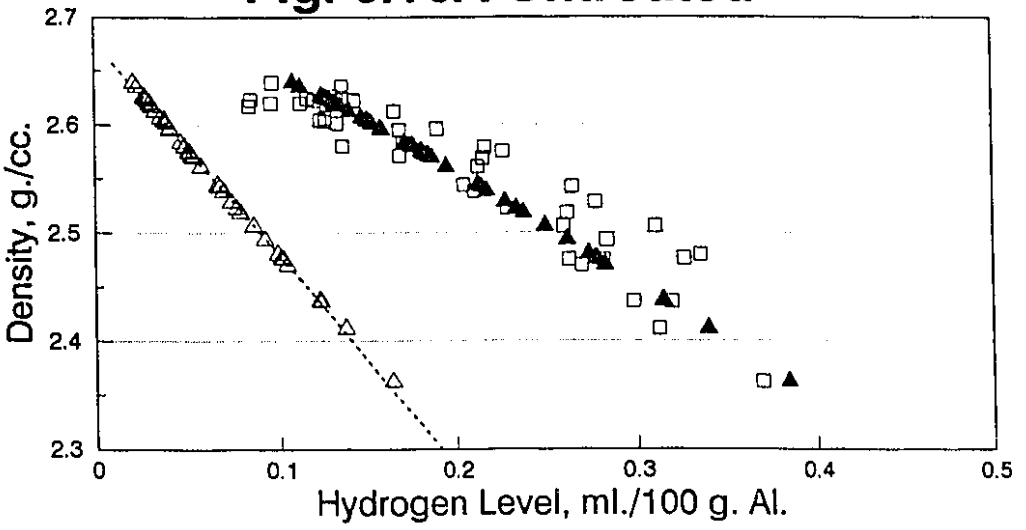

Fig. 6.10B Modified*

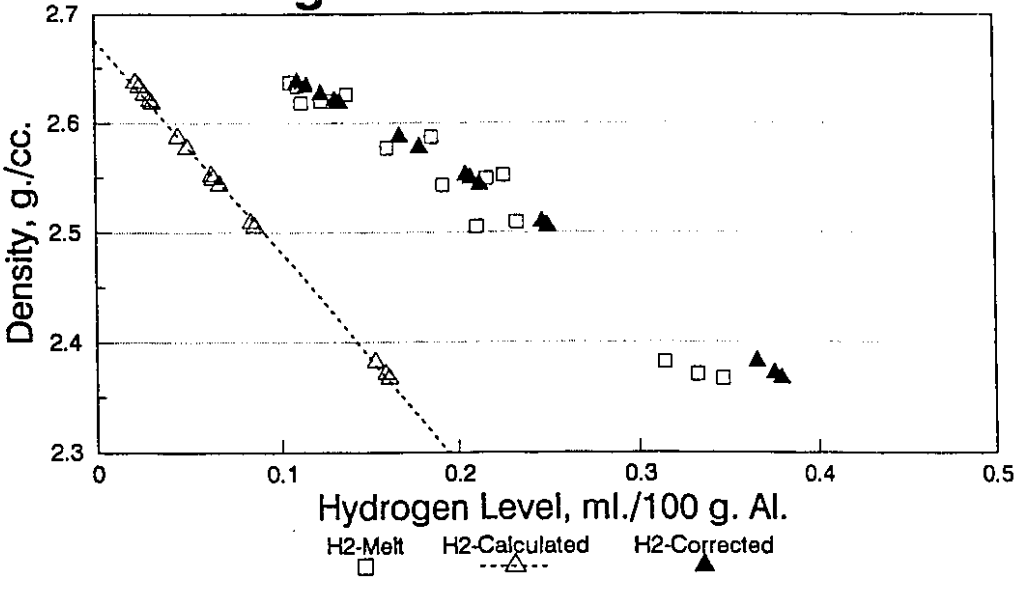

* with 90Sr-10Al modifier @ 0.02 wt.% Sr

Fig. 6.10C Grain Refined*

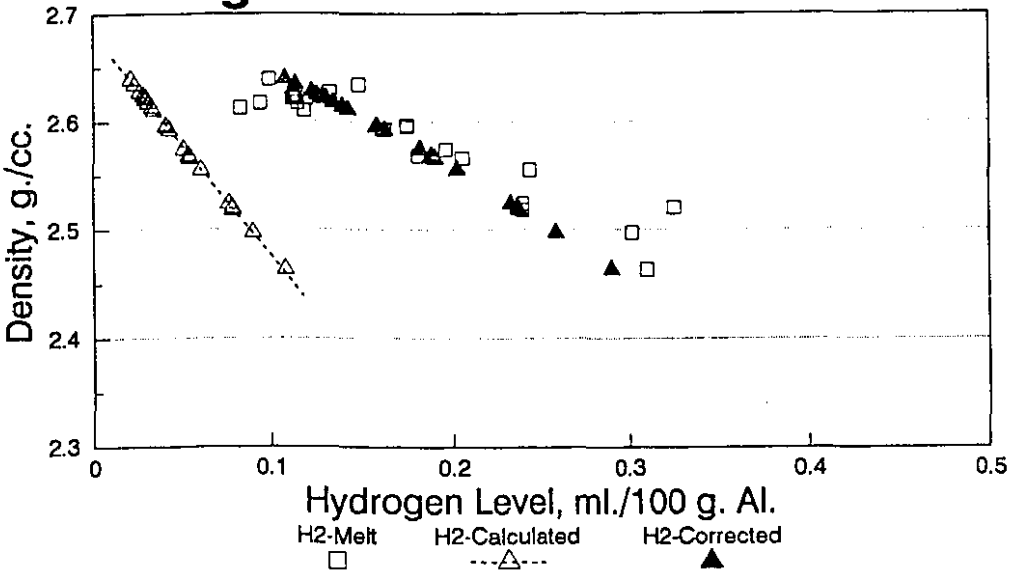

*with 2.5Ti-2.5B-Al grain refiner @ 0.17 wt.% Ti

Fig. 6.10D Grain Refined* and Modified*

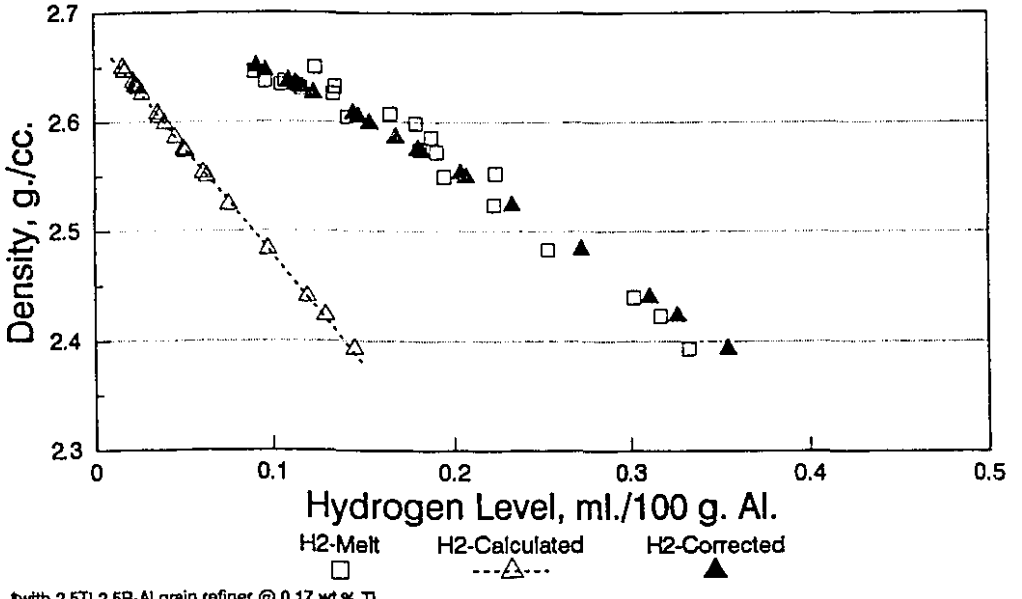

*with 2.5Ti-2.5B-Al grain refiner @ 0.17 wt.% Ti
* with 90Sr-10Al modifier @ 0.02 wt.% Sr

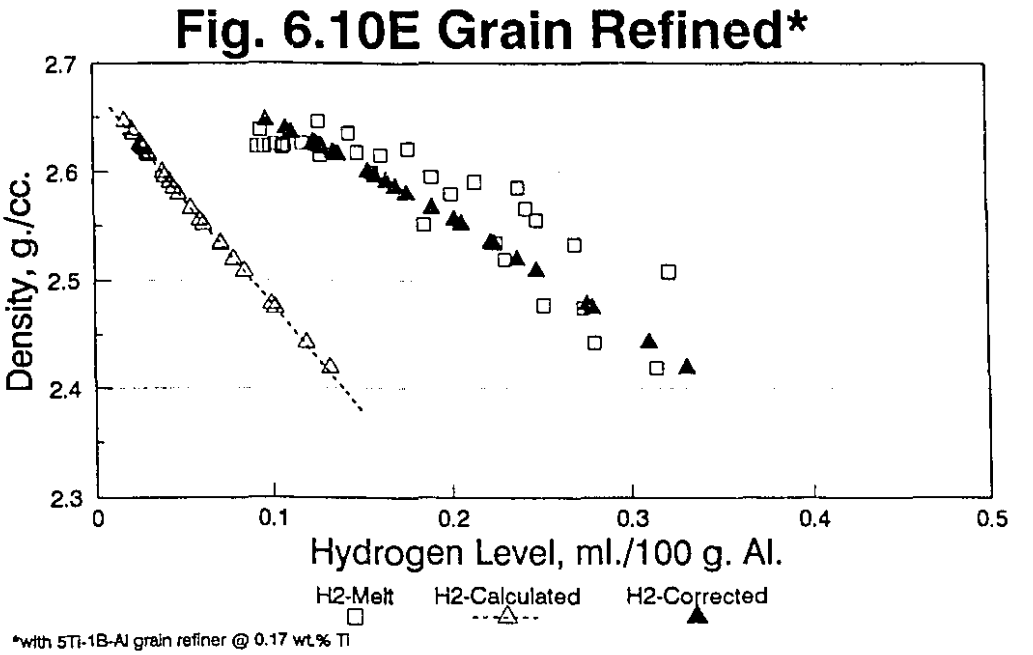

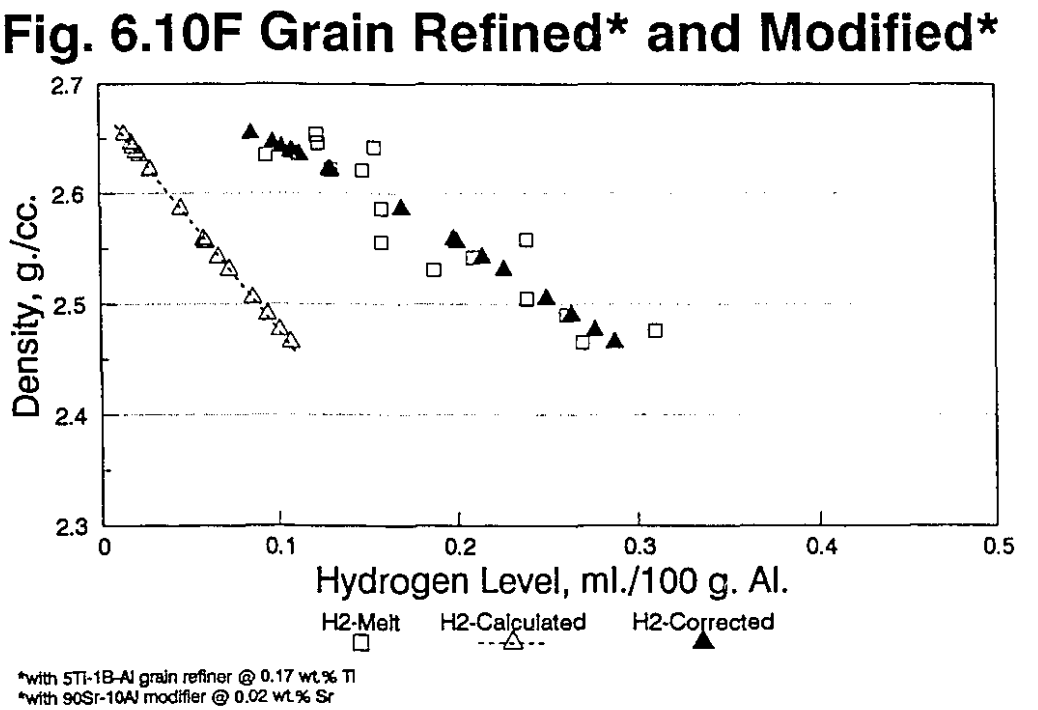

Figure 6.10 Corrected hydrogen (▲) calculated from the gas loss concept for various melt treatments compared to the melt hydrogen (□).

The work has been extended to study the error due to the calculation by each of these three approaches as a function of the reduced pressure test sample density. The errors which are the difference between the true hydrogen and predicted hydrogen level at a particular sample density are summarized in Fig. 6.11. A positive value of the error indicates over calculation, while a negative value shows under calculation. The zero line represents the true hydrogen level at which the predicted value should fall.

Fig. 6.11 a. is an error plot of calculations from the constant correction factor approach. Underestimation of the predicted value is found at high density, whereas over calculation is found at low density. This is simply because of the constant nature of the correction factor. The error in this case was found to be in the range of ± 0.1 ml./100 g. Al.

The error of the hydrogen dependent correction factor approach is slightly less than the previous one, Fig. 6.11 b. There is a tendency to over calculation at the intermediate range of the sample density, particularly for the Sr-alloyed samples. This is mainly because of the exponential correlation between the correction factor and calculated hydrogen, $[H_C]_R$. The correlation between sample density and $[H_C]_R$ is a straight line. The correction factor when applied to $[H_C]_R$ will give an exponential relationship between H_{corr} and the sample density. These H_{corr} values do not match well with the true hydrogen which has a linear relationship with the sample density resulting in an error. However, the error was found to be in the range of ± 0.05 ml./100 g. Al.

The error in the gas loss concept was also found to be in the range of ± 0.05 ml./100 g. Al. as shown in Fig. 6.11 c. With this technique, there is no positive or negative bias to the error.

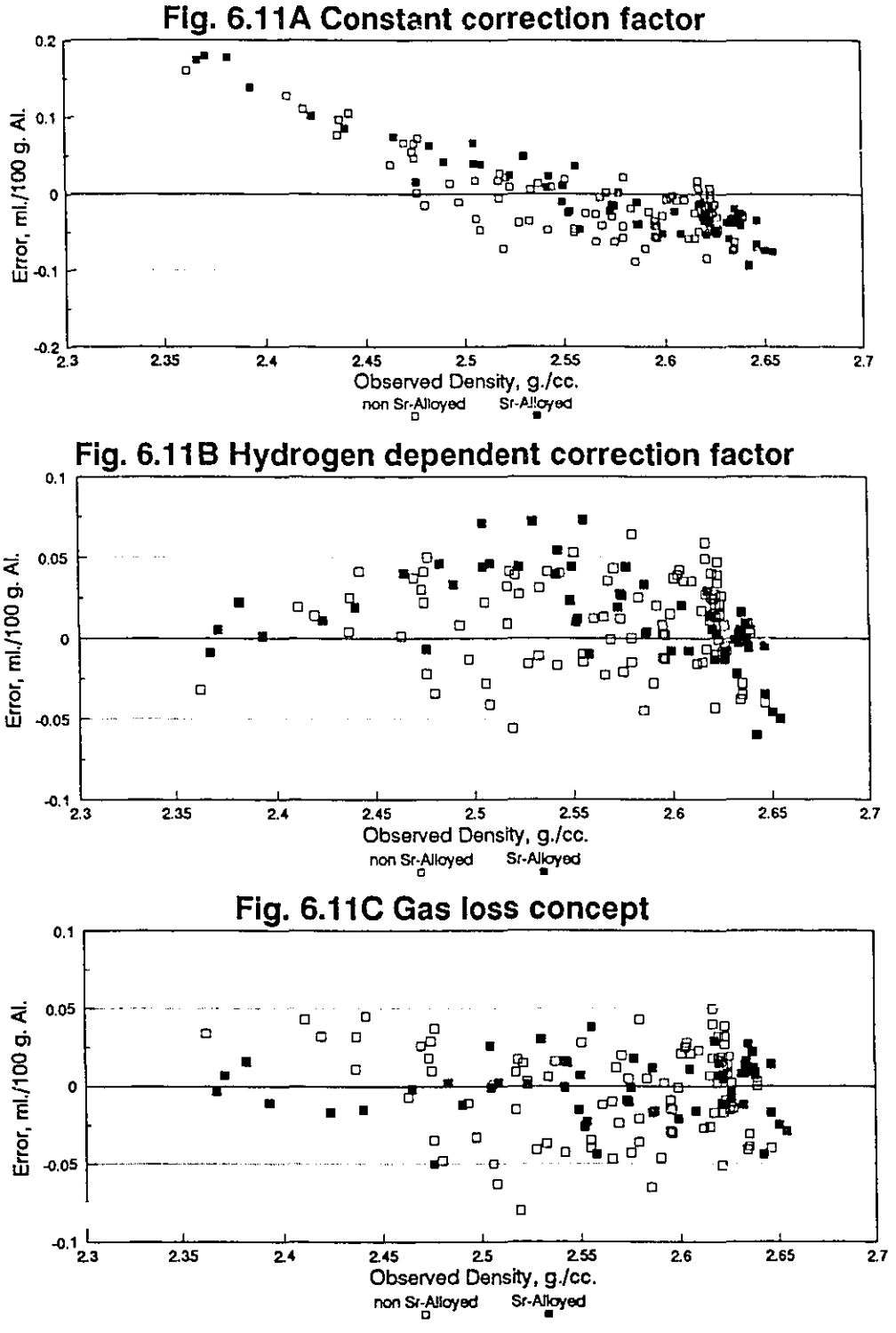

Figure 6.11 The error plot of the samples calculated by the three methods.

6.5 Discussion.

The solidification pattern of the melt in the crucible is the key to explain all of the phenomena occuring in this test. Since the crucible used in this work had a very thin wall thickness, the heat flow which controls the solid/liquid interface location can dissipate in all directions and results in shell formation as shown in Fig. 6.12. The solidification patterns as obtained from the commercial solidification modeling software AFSolid™ are plotted at the fraction of solid where the internal gas pressure, P_g, of the melt containing different levels of hydrogen exceeds the assumed external pressure, P_{ex}. P_{ex} in this case is the pressure in the chamber (0.1 atm.) and the pressure due to surface energy (1.5×10^{-4} atm. at a bubble radius of 1 μm.). Fig. 6.12 a. shows the solidification pattern at which P_g of the melt containing 0.3 ml./100 g. Al. exceeds P_{ex} Figs. 6.12 b. and c. show similar effects for melts containing 0.2 and 0.1 ml./100 g. Al., respectively.

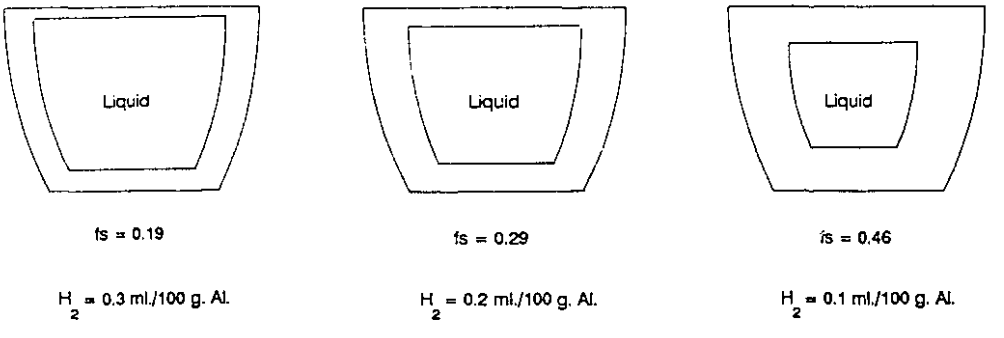

Figure 6.12 The solidification pattern in a crucible at the fraction of solid at which P_g in the melt exceeds the assumed P_{ex}.

In Fig. 6.12 a., gas bubbles can form easily since the semi-solid formed on top of the melt is very thin; however, at fs=0.46 in Fig. 6.12 c., a thick film of semi-solid forms on top of the melt. P_g of the melt containing 0.1 ml./100 g. Al. in this case may exceed the assumed P_{ex}, but the pressure may not be high enough to overcome the strength of the solid that forms the shell, resulting in difficulty of gas bubble formation. Porosity in this suituation is thus controlled by the shrinkage rather than by actual gas bubble formation.

Since shrinkage due to the phase change in a Sr-alloyed sample is presumed less than the non Sr-alloyed one because of the liquid density, less porosity will occur in the Sr-alloyed sample at low hydrogen levels. This effect results in the higher density of the Sr-alloyed samples at low hydrogen, as was previously shown in Fig. 6.4.

The shell formation also affects the sensitivity of the sample density to the hydrogen levels especially at hydrogen levels under 0.15 ml./100 g. Al.. The sample density is in the range of 2.55-2.65 g./cc. at the hydrogen level range of 0.07-0.15 ml./100 g. Al. This can be improved by redesign of the crucible to avoid shell formation and to keep the free surface liquid exposed to the reduced pressure as long as possible.

At relatively low hydrogen levels (<0.2 ml./100 g. Al.), the sample density is largely controlled by shrinkage due to the phase change. The variation of the sample density is then caused by the variation in the solidification pattern. At a given hydrogen level, the pattern that yields a thinner film of semi-solid on top of the melt will have more porosity than the one that has a thicker film. The variation of the pattern may be affected by such things as the amount of heat remaining in the plate underneath the crucible, or by other small variations in heat flow from one test to another.

The correction factor can be simplified to the ratio of pore volume of the atmospheric sample and the reduced pressure sample as shown in the equation:

$$C.F. = 10\times\frac{[V_P]_A}{[V_P]_R} \tag{6.7}$$

where,

$[V_P]_A$ = volume of pores in the atmospheric sample

$[V_P]_R$ = volume of pores in the reduced pressure sample

According to the Gas Law, $[V_P]_R$ must be ten times greater than $[V_P]_A$ since it is assumed that the pressure on top of the melt is one tenth of the atmospheric pressure. The ideal correction factor is unity, ie. $[V_P]_R = 10[V_P]_A$; however, gas loss and the shell formation effects result in $[V_P]_R$ being less than this ideal value which in turn increases the correction factor.

Quantification of the reduced pressure test can be improved by redesigning the crucible first. This can be done by modifying the crucible to meet these requirements:

i) minimize the shrinkage problem to ensure that porosity is due solely to gas.

ii) avoid shell formation and keep the free surface liquid exposed to the reduced pressure as long as possible in order to magnify the porosity size.

By doing this, the sensitivity of the sample density particularly at low hydrogen levels (<0.2 ml./100 g. Al) will be improved resulting in a more accurate test.

6.6 Summary.

A summary of the main points in this chapter is as follows:

i) An excellent linear relationship between density and hydrogen level in the reduced pressure test exists for all combinations of melt treatment.

ii) Inclusions may not have a significant effect on the quantification of the test particularly at low hydrogen level (below 0.2 ml./100 g. Al.)

iii) The crucible used in this study is valid only for Sr modified alloys where there is less shrinkage.

iv) Three methods of quantification of the hydrogen level are proposed leading to an error range of 0.05-0.1 ml./100 g. Al.

v) For future work, it is recommended to redesign the crucible and investigate the

reduced pressure that yields the optimum quantification of the reduced pressure test since the pressure effects the amount of gas loss which in turns influences the quantification of the test.

Chapter 7
Conclusions

7.1 Conclusions.

From the experimental results and discussion presented in the preceding chapters, the following major conclusions can be drawn:

1. Grain refinement, acting singly or in combination with modification, reduces microporosity by inducing mass feeding. However, this effect is more pronounced in a low cooling rate system.

2. There is a slight difference between the total shrinkage of the alloy treated by various type of melt treatments. Among these, Sr-alloyed samples have less shrinkage than non Sr-alloyed. The cause of this is probably because Sr increases the liquid density.

3. Pipe and slumping and contraction volume in Sr-alloyed samples were found to be less than those of non Sr-alloyed because of the lower volumetric shrinkage in the Sr-alloyed samples.

4. Microporosity displaces the slumping and contraction volume more than pipe volume.

5. The most important parameter that control the impact strength of the alloy is the Si morphology since the impact strength of Sr modified alloys was greatly improved when compared with other melt treated alloys.

6. An increased hydrogen level has a slight effect on reducing the impact strength of A356 alloy.

7. Grain refinement, acting singly or in combination with modification, does not

improve the impact strength of A356 alloy.

8. To obtain optimum impact strength, a combination of modification and degassing to about 0.1 ml. H_2/100 g. Al. is recommended.

9. An excellent linear relationship between density and hydrogen level in the reduced pressure test exists for all combinations of melt treatment processes.

10. It is possible to quantify the reduced pressure test by use of three quantification methods which are;

i) constant correction factor,

ii) hydrogen depedent correction factor, and

ii) gas loss concept.

These three methods predict the hydrogen level reasonably well within the error range of $\pm$0.05-0.1 ml./100 g. Al.

7.2 Recommendations for Future Work.

The author suggests further work based on the results of this thesis:

1. Investigation of the liquid density of modified alloy.

2. Study of the specific cooling rate and the casting size where mass feeding has no significant effect on reducing microporosity.

3. Redesigning of the reduced pressure test crucible to minimize shrinkage and to maximize the effect of reduced pressure upon porosity formation.

4. Investigation into the exact value of reduced pressure that yields the optimum quantification of the test particularly at low hydrogen levels.

5. Study of the amount of gas loss in the reduced pressure test as affected by various melt treatment processes.

6. Study of the effect of inclusions on the quantification of the reduced pressure test.

7. An extension of quantification of the reduced pressure test to various types of casting alloys.

References.

1. Hatch,J.E., editor, "*Aluminum, Properties and Physical Metallurgy*", ASM, Metals park,OH, 1984.

2. Isobe, T., Kubota, M., and Kitaoka, S., "*Castability of Aluminum Alloys*", Japanese J. of Cast Metals, V.47, 1974, pp. 345-355.

3. Rosenberg, R.A., Flemings, M.C., and Taylor, H.F., "*Nonferrous Binary Alloys Hot Tearing*", AFS Transactions, V.68, 1960, pp. 518-528.

4. Hurley, T.J., and Atkinson, R.G., "*Effects of Modification Practice in Aluminum A356 Alloys*", AFS Transactions, V.93, 1985, pp. 291-296.

5. Denton, J.R., and Spittle, J.A., "*Solidification and Susceptibility to Hydrogen Absorbtion of Al-Si Alloys Containing Strontium*", Materials Science and Technology, V.1, 1985, pp. 305-311.

6. Shahani, H., "*Effects of Hydrogen on the Shrinkage Porosity of Al-Cu and Al-Si Alloys*", Scand. J. of Metallurgy, V.14, 1985, pp. 306-312.

7. Argo, D., and Gruzleski, J.E., "*Porosity in Modified Aluminum Alloys Castings*", AFS Transactions, V.96, 1988, pp. 65-74.

8. Tsukuda, M., Suzuki, T., Fukui, I., and Harada, M., "*The Effect of Ti or Ti-B on Grain Size and Mechanical Properties of Al-7Si-0.3Mg Casting Alloy*", J. Japan Inst. Light Metals, V.29, pp. 437-444, 1979.

9. Vess, C., "*The Effect on Grain Size and Physical Properties of Various Ti/B Ratios*", Proc.Conf. "International Molten Metal Processing", AFS., Des Plaines, IL., 1986, pp. 101-147.

10. Wu, H.T., Wang, L.C., and Kung, S.K., "*Influence of Grain Refiner Master Alloy Additions on A356 Aluminum Alloy*", J. Chinese Foundryman's Assoc. V.29, 1981, pp. 10-18.

11. Purvis, A.L., and Pehlke, R.D., "*Processing, Structure, and Properties of Cast Al-Si alloy 319 Using the Lost Foam Evaporative Pattern Casting Process*", AFS Transactions, V.96, 1988, pp. 539-550.

12. Apelian, D., Sigworth, G.K., and Whaler, K.R., "*Assesment of Grain Refinement and Modification of Al-Si Foundry Alloys by Thermal Analysis*", AFS

Transactions, V.92, 1984, pp. 297-307.

13. Eady, J.A., Smith, D.M., "*The Effect of Porosity on the Tensile Properties of Aluminum Castings*", Materials Forum, V.9, 1986, pp. 217-223

14. Closset, B., "*Modification and Quality of Low Pressure Aluminum Castings*", AFS Transactions, V.96, 1988, pp. 249-260.

15. Rosenthal, H., and Lipson, S., "*Measurement of Gas in Molten Aluminum*", AFS Transactions, V.63, 1955, pp. 301-305.

16. Sulinski, H.V., and Lipson, S., "*Sample for Rapid Measurement of Gas in Aluminum*", AFS Transactions, V.67, 1959, pp. 56-64.

17. Rooy, E.L., and Fisher, E.F., "*Control of Aluminum Casting Quality by Vacuum Solidification Tests*", AFS Transactions, V.76, 1968, pp. 237-240.

18. Church, J.C., "*Qualitative Gas Testing for Production Control of Aluminum Castings Soundness*" AFS Transcaction, V. 78, 1970, pp. 277-280.

19. Brondyke, K.L., and Hess, P.D., "*Interpretation of Vacuum Gas Test Results for Aluminum Alloys*", TMS of AIME, V.230, 1964 (Dec.), pp. 1542-1546.

20. Hess, P.D., "*Measuring Hydrogen in Aluminum Alloys*", J. of Metals, V.25, 1973 (Oct.), pp. 46-50.

21. Mulazimoglu, M.H., Handiak, N., and Gruzleski, J,E., "*Some Observations on the Reduced Pressure Test and the Hydrogen Concentration of Modified A356 Alloys*", AFS Transactions, V.97, 1989, pp. 225-232.

22. Ransley, C.E., and Neufeld, H., "*The Solubility of Hydrogen in Liquid and Solid Aluminum*", J. of Inst. Metals., V.74, 1948, pp. 599-620.

23. Opie, W.R., and Grant, N.T., "*Hydrogen Solubility in Aluminum and Some Aluminum Alloys*", TMS of AIME, V.188, 1950 (Oct.), pp. 1237-1241.

24. Shahani, H., and Fredriksson, H., "*On the Mechanism of Precipitation of Pores in Melts*", Scand. J. Metallurgy, v. 14, 1985, pp. 316-320.

25. Charbonnier, J., Perrier, J.J., and Portalier, R., "*Recent Developments in Al-Si Alloys Having Guaranteed Structure Properties*", AFS Int. Cast Metals J., Dec. 1978, pp. 17-26.

26. Morimoto, H, Takamiya, H, Awano, Y., and Motoyuki, N., "*Effects of Si Content and Gas on Shrinkage Morphology of Hypoeutectoc Al-Si Alloys*", Japannese J. of Light Metals, V.19, 1988, pp. 216-221.

27. "*Copper-Base Alloys Foundry Practice*", 3rd Edtion, AFS, 1965

28. Piwonka, T.S. , and Flemings, M.C., "*Pore Formation in Solidification*", TMS. of AIME, V.236, 1966, pp. 1157-1165.

29. Hanna, M.D., Lu, S., and Hellawell, A., "*Modification in the Aluminum-Silicon System*", Met. Trans., V.20A., 1989, pp. 989-1000.

30. Drossel, G., Mai, R., Liesenberg, O., "*Influence of Treatment on the Density of Castings Made from Al-Si Alloy*", Giessereitechnik, V.27, 1981, pp. 167-180.

31. Sigworth, G.K., "*Fundamentals of Grain Refining in Aluminum Alloy Castings*", Proc. Conf. "International Molten Metal Processing", AFS., Des Plaines, IL., 1986, pp. 75-99.

32. Wang, L., Shivkumar, S., and Apelian, D., "*Modification and Grain Refinement in Lost Foam Castings*", Proc. Conf. "2nd International Molten Metal Processing", AFS., Orlando, Fl., 1989, pp. 5.1-5.20

33. Liu, C.Y., Murakami, K., and Okamoto, T., "*Effect of Capillarly Pressure on Interdendritic Liquid Flow*", Acta Metall., V.34, No.1, 1986, pp. 159-166.

34. Fang, Q.T., Granger, D.A., "*Porosity Formation in Modified and Unmodified A356 Alloy Castings*", AFS Transactions, V.97, 1989, pp. 989-1000.

35. Yeum, K., and Poirier, D.R., "*Predicting Microporosity in Aluminum Alloys*", Light Metals 1988, pp. 469-476.

36. Komatsu, N., Nakamura, M., and Yamamoto, Y., "*Relationship Between Si Crystallized form and Impact Strength of Al-Si Alloys-Observations of Impact Strength of Al-Si Alloys*", Japanese J. of Light Metals, V.43, 1989, pp. 398-408.

37. Ohira, G., and Kondic, V., "*Testing the Gas Content of Molten Metals*", Foundry Trade Journal, V.96, 1954, pp. 331-333.

38. Sigworth, G.K., and Engh, T.A., "*Chemical and Kinetic Factors Related to Hydrogen Removal from Aluminum*", Met. Trans., V.13B, 1982, pp. 447-460.

39. Sigworth, G.K., and Guzowski, M.M., "*Grain Refining of Hypoeutectic Al-Si Alloys*", AFS Transactions, V.93, 1985, pp. 907-912.

40. Apelian, D., and Cheng, J.J.A., "*Al-Si Processing Variables : Effect on Grain Refinement and Eutectic Modification*", AFS. Transactions, V.94, 1986, pp. 797-808.

41. Martin, J.-P., Tremblay, F., and Dubé, G., "*HyDRAL:A New and Simple Technique for In-Line Analysis of Hydrogen in Aluminum Alloys*", Light Metals 1989, pp. 903-912.

42. Kundle, D.E., and Willey, L.A., "*Theoretical Densities of Light Metals*", J. Materials, V.1, 1966, p. 226-230.

43. "*Lange's Handbook of Chemistry*", 13th Ed., McGraw-Hill Book Co., New York, 1985.

44. Entwistle, R., Gruzleski, J.E., and Thomas, P.M., "*Development of Porosity in Aluminum-base Alloys*", Proc. Conf. "Solidification and Casting of Metals", U. of Sheffield, July 18-21, 1977, p.345-352.

45. Fang, Q.T., Anyalebechi, P.N., and Granger, D.A., "*Measurement of Hydrogen Porosity in Unidirectionally Solidified Aluminum Alloys*", Light Metals 1988, pp. 477-486.

46. Poirier, D.R., Yeum, K., and Maples, A.L., "*A Thermodynamic Prediction for Microporosity Formation in Aluminum-Rich Al-Cu Alloys*", Met.Trans., 18A., 1987, pp. 1979-1987.

APPENDIX 4.1

SHRINKAGE DISTRIBUTION FOR VARIOUS MELT TREATMENTS

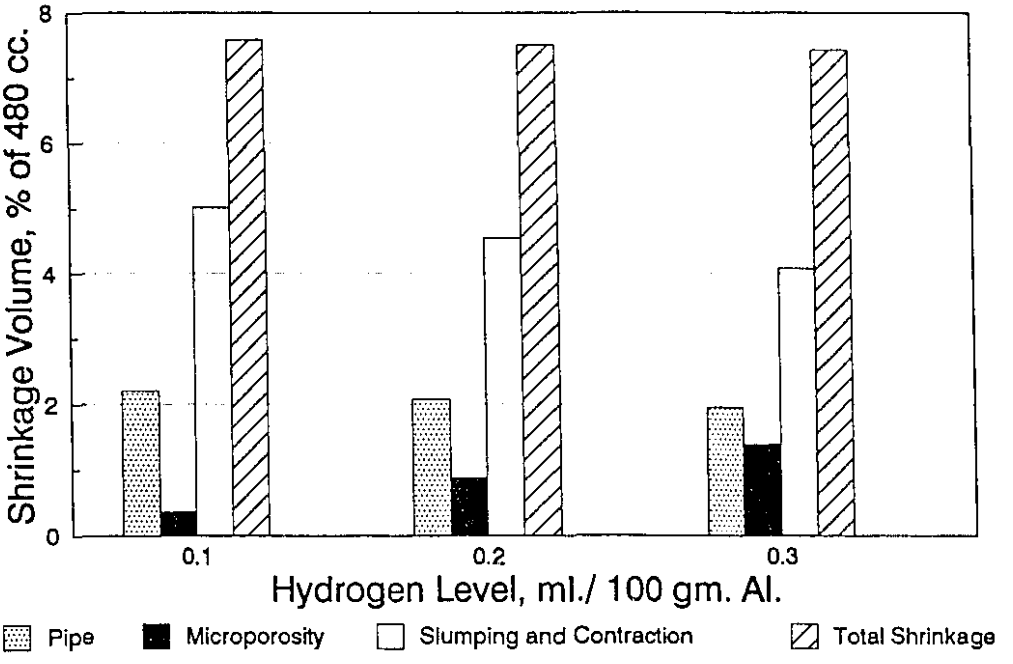

A. Untreated

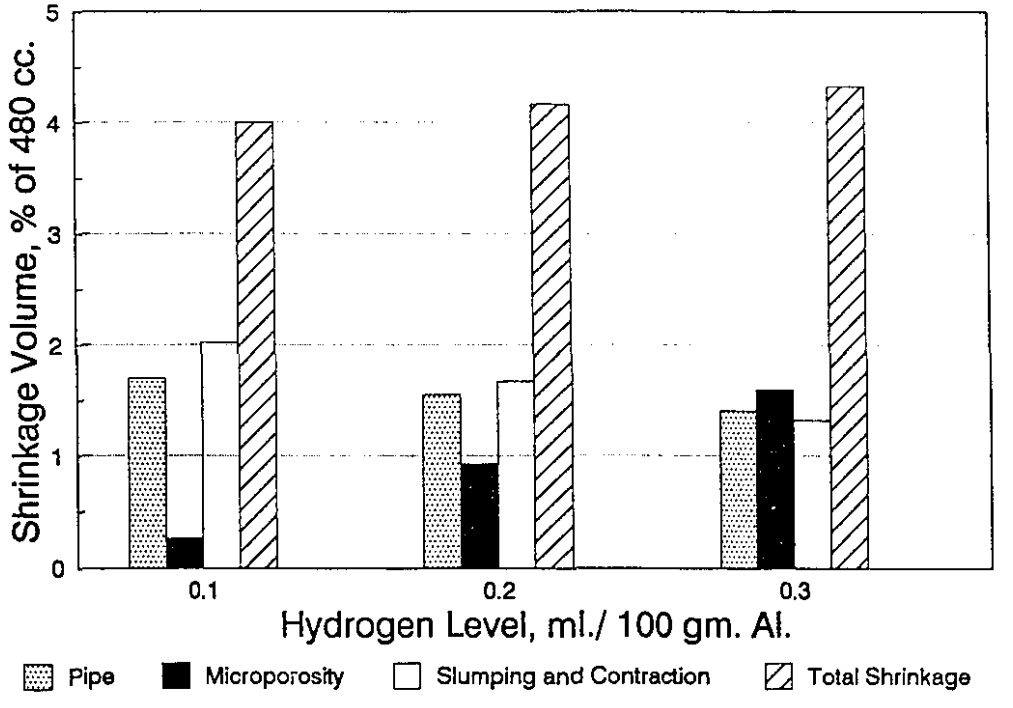

B. Modified

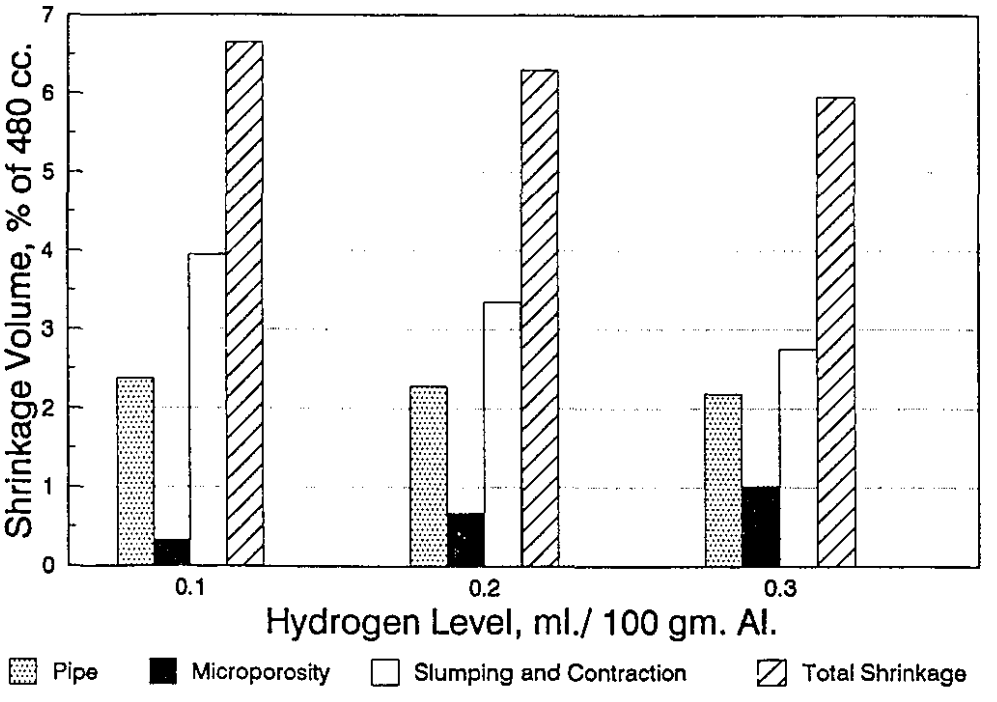

C. Grain refined with 2.5Ti-2.5B master alloy.

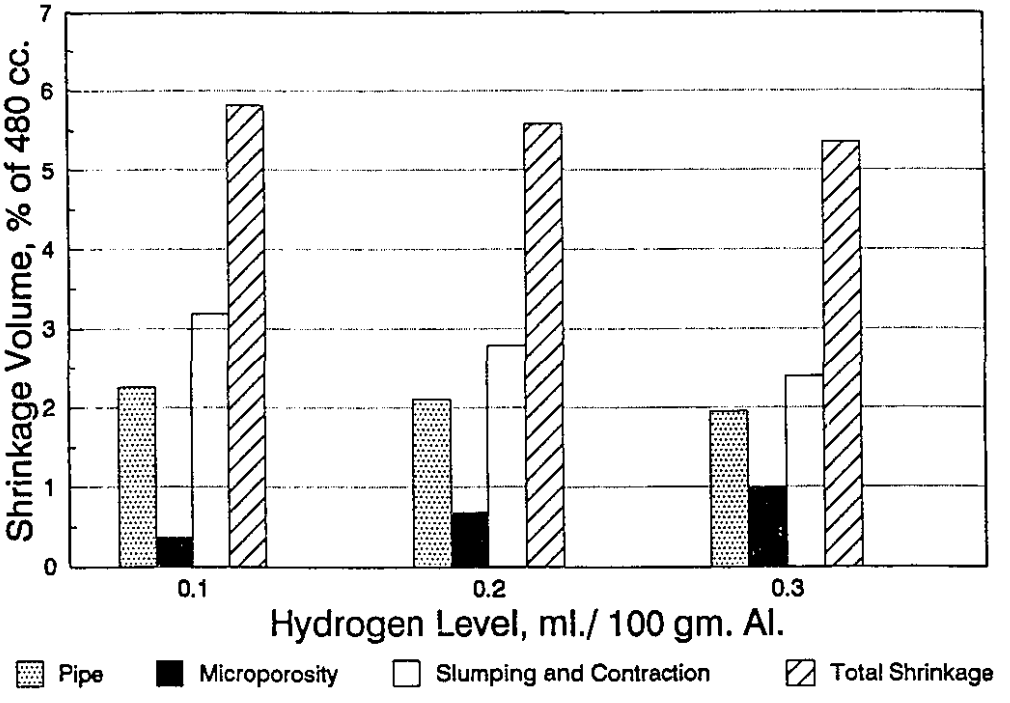

D. Grain refined, with 2.5Ti-2.5B, and Modified

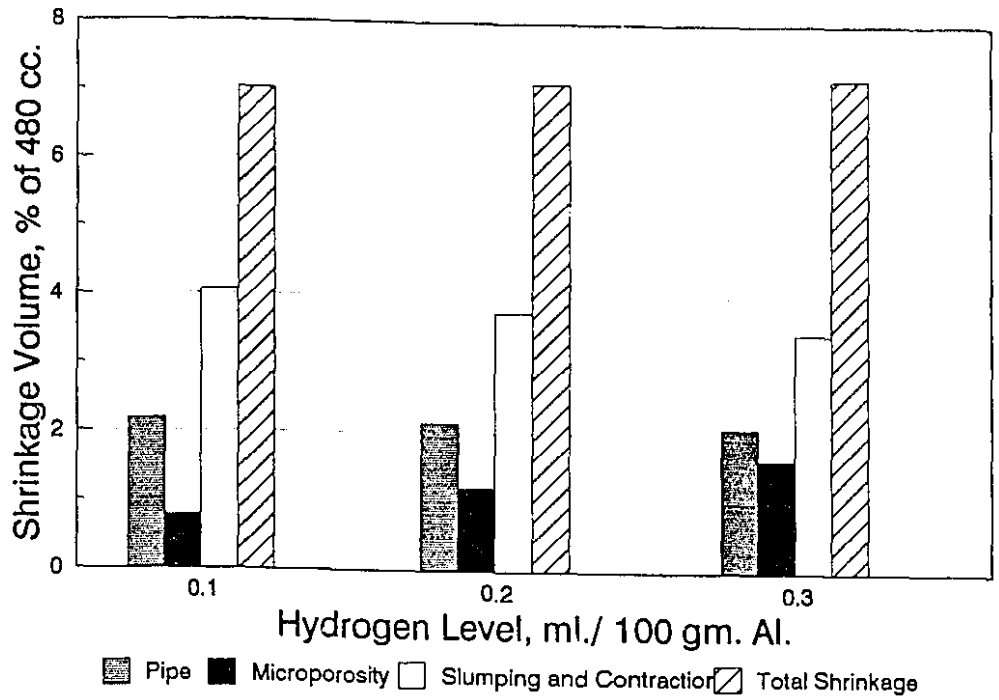

E. Grain refined with 5Ti-1B master alloy

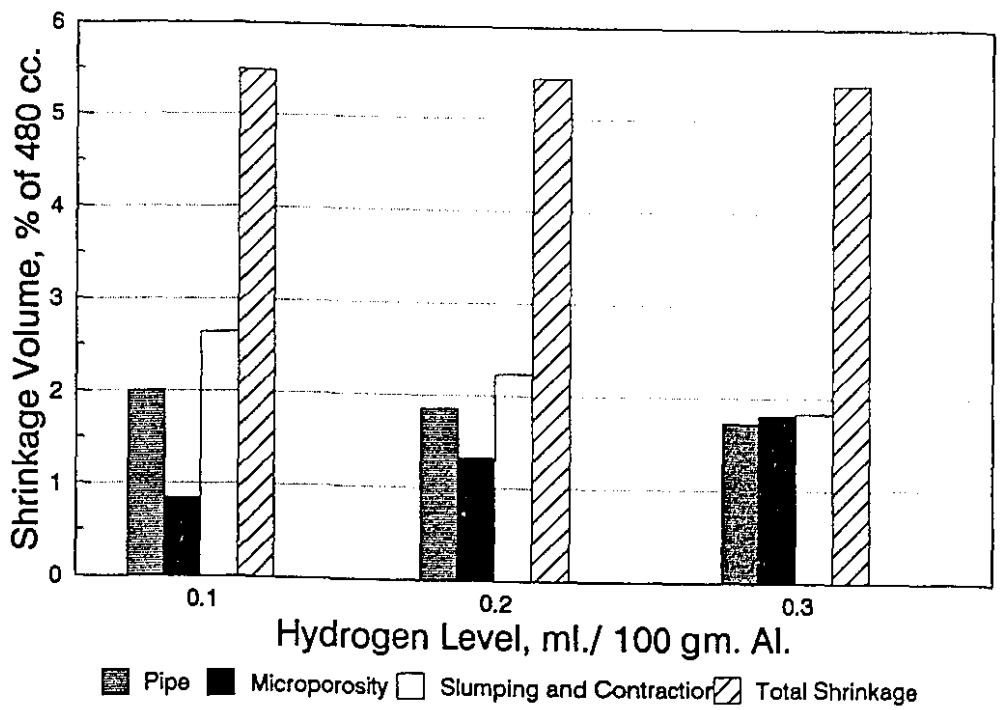

F. Grain refined, with 5Ti-1B master alloy, and Modified

APPENDIX 4.2

INTERNAL GAS PRESSURE CALCULATION

The internal gas pressure, P_g, can be calculated from Sievert's Law (equation 42.1) which assumes thermodynamic equilibrium between the molecular gas in the bubble and the diatomic hydrogen dissolved in the melt.

$$P_g = \left(\frac{C_H}{S}\right)^2 \qquad (42.1)$$

where,

P_g = equilibrium partial pressure of the dissolved gas,

C_H = amount of hydrogen dissolved in the melt,

S = solubility constant of the melt.

The gas pressure in the bubble can then be assumed to be equal to P_g from this equation.

The first factor that must be calculated is the amount of gas dissolved in the melt, C_H. As solidification proceeds, C_H increased due to the rejection of the solid phase and can be calculated by employing the Scheil equation. The value of equilibrium partition ratio for hydrogen, k_H, of 0.069 is used in this calculation. This approximate value is recommended by Poirier et al [46].

Another factor that controls the gas pressure is the solubility constant of the melt, S. The solubility of hydrogen relates to temperature and the amount of silicon in the melt as given in the equation:

$$\log_{10} S = -\frac{A}{T} + B \qquad (42.2)$$

where,

S = solubility constant of the melt,

A and B are parameters that depend on the concentration of silicon in the alloy.

Yeum and Poirier [35] have analyzed the values of A and B given by Opie and Grant [22] and expressed these values in terms of the concentrations of the alloy elements as:

$$A = a_0 + a_1 C_i^{\frac{1}{2}} + a_2 C_i + a_3 C_i^{\frac{3}{2}} \qquad (42.3)$$

and

$$B = b_0 + b_1 C_i^{\frac{1}{2}} + b_2 C_i + b_3 C_i^{\frac{3}{2}} \qquad (42.4)$$

where,

C_i = wt.% of silicon in the melt,

a_x and b_x are coefficients as shown in Table 42.1

Table 42.1 Coefficients for equations 42.3 and 42.4.

a0	2550
a1	-14.65
a2	203
a3	-47.86
b0	2.62
b1	-0.09268
b2	0.2271
b3	-0.05411

The concentration of silicon in the melt can be calculated by the Scheil equation and using the binary Al-Si phase diagram data as shown in Table 42.2.

Table 42.2 Data from the Al-Si binary phase diagram.

Melting point of Al (°C)	660
Eutectic temperature (°C)	577
Eutectic composition (wt.%)	12.6
Equilibrium partition ratio of Si	0.131

The computer program has been written to calculate the internal gas pressure and is shown in Table 42.3. The program is written in BASIC language by the commercial software QuickBASIC Version 4.5.

Table 42.3 Computer program used to calculate the internal gas pressure.

```
REM INTERNAL GAS PRESSURE PROGRAM
INPUT "H2 IN SYSTEM = ", Ch0
INPUT "output filename  ",f$
f$ = "a:" + f$ + ".prn"
REM constant used
        c0 = 7.0
        ksi = 0.131
        tm = 660+273
        te = 577+273
        kh = 0.069
        ml = -7.38
        ce = 12.6
        temp = 750+273
        fl = 1
```

```
        pressure = 1
        R = 0.000001
DO UNTIL fl < 0.05
        temp = temp
        IF temp < 610+273 and te < temp THEN
          fl = ((temp-tm)/(ml*c0))^(1/(ksi-1))
          ci = c0*fl^(ksi-1)
        ELSEIF temp <= te THEN
          fl = ((temp-tm)/(ml*c0))^(1/ksi/(ksi-1))
          ci = ce
        ELSE
          fl = 1
          ci = c0
        END IF
        A = 2550-14.65*ci^0.5+203*ci-47.86*ci^1.5
        B = 2.62-0.09268*ci^0.5+0.2271*ci-0.05411*ci^1.5
        s = 10^((-A/temp)+B)
        k = 8.923E-05*s
        Ch = Ch0*8.923E-05/(fl+(1-fl)*kh)
        Pg = ((Ch/k)^2)
        gamma = (864-(24.781*ci)+(2.7856*ci^2)-(0.11532*ci^3))*0.0000001/101325
        Pex = pressure + 2*gamma/R
        fs = 1 - fl
        OPEN f$ FOR APPEND AS #1
        PRINT #1, temp, fs, Pg, Pex
        CLOSE #1
        temp = temp - 5
LOOP
END
```

APPENDIX 6.1

CORRECTION FACTOR FOR VARIOUS MELT TREATMENTS

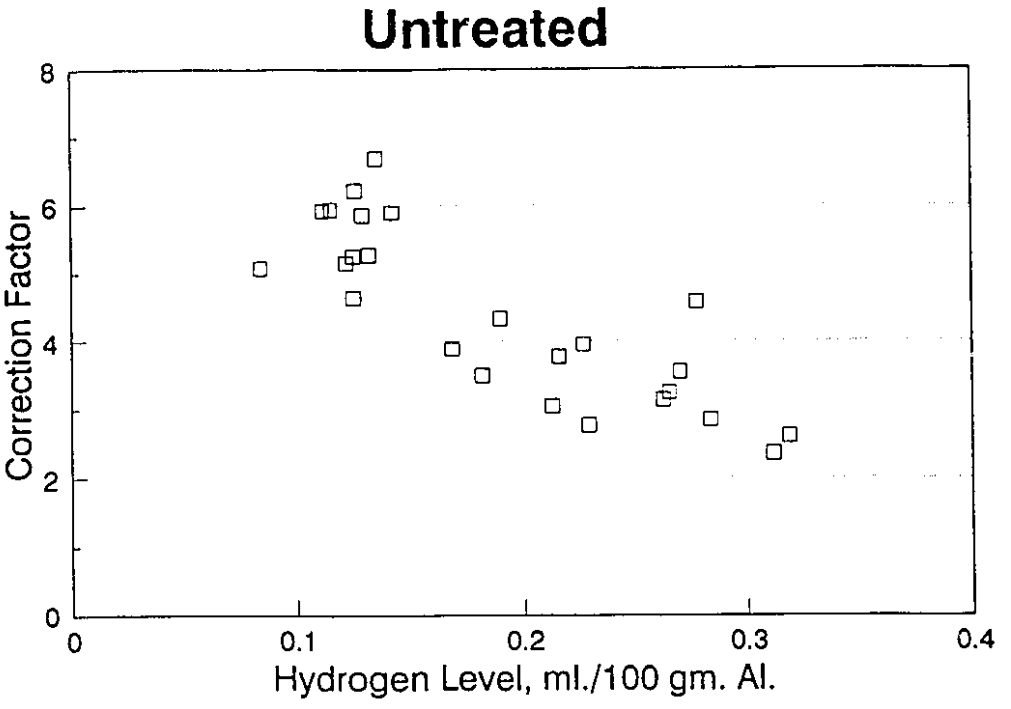

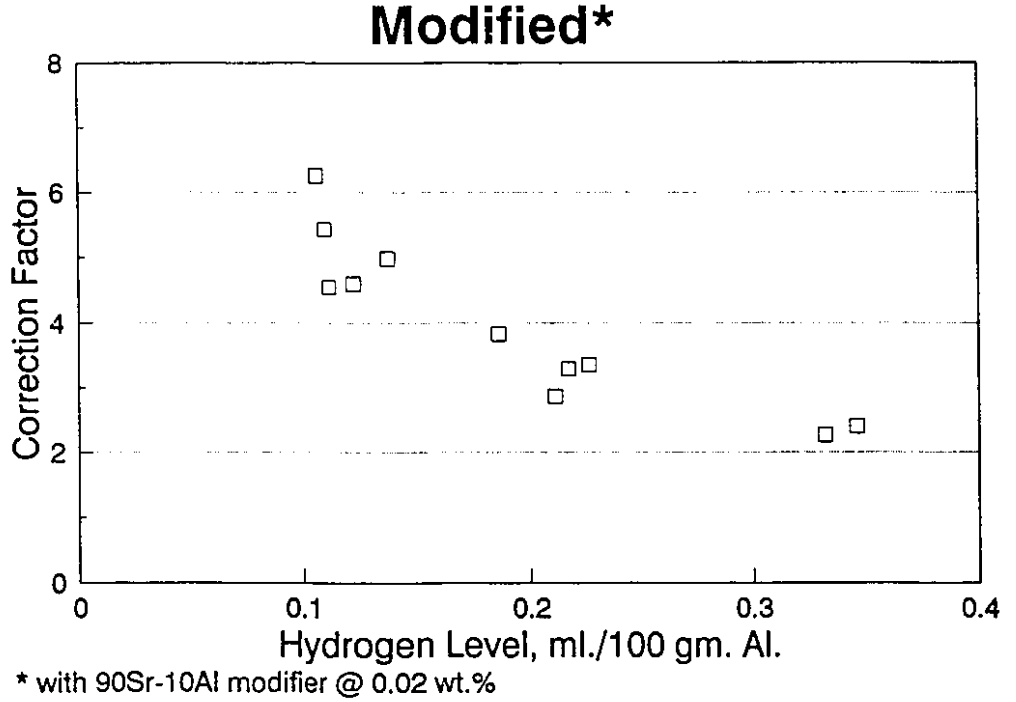

* with 90Sr-10Al modifier @ 0.02 wt.%

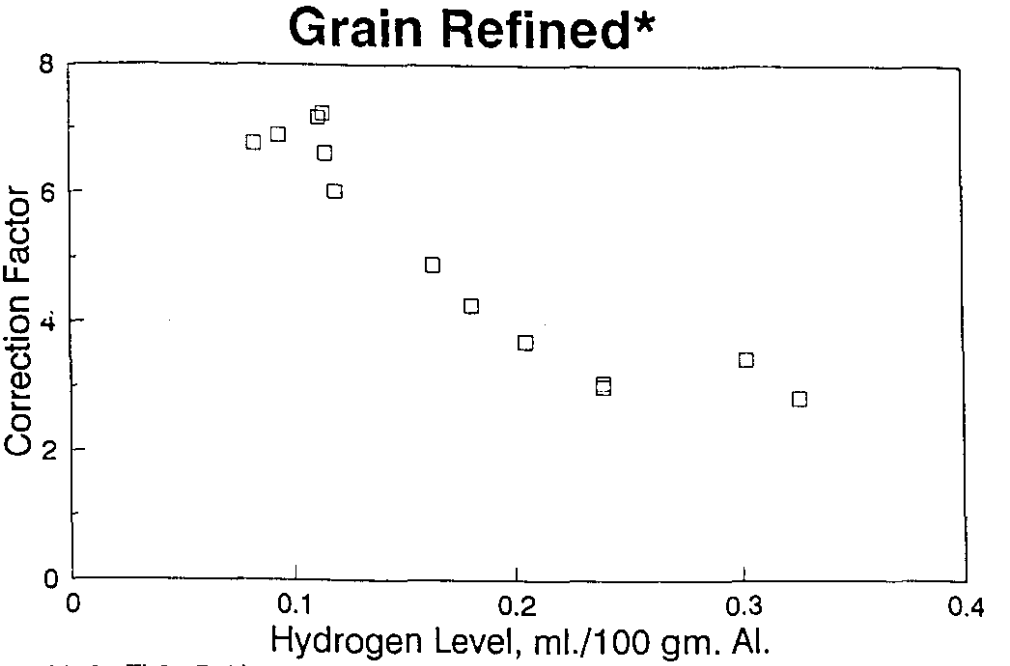

* with 2.5Ti-2.5B-Al grain refiner @ 0.17 wt.%

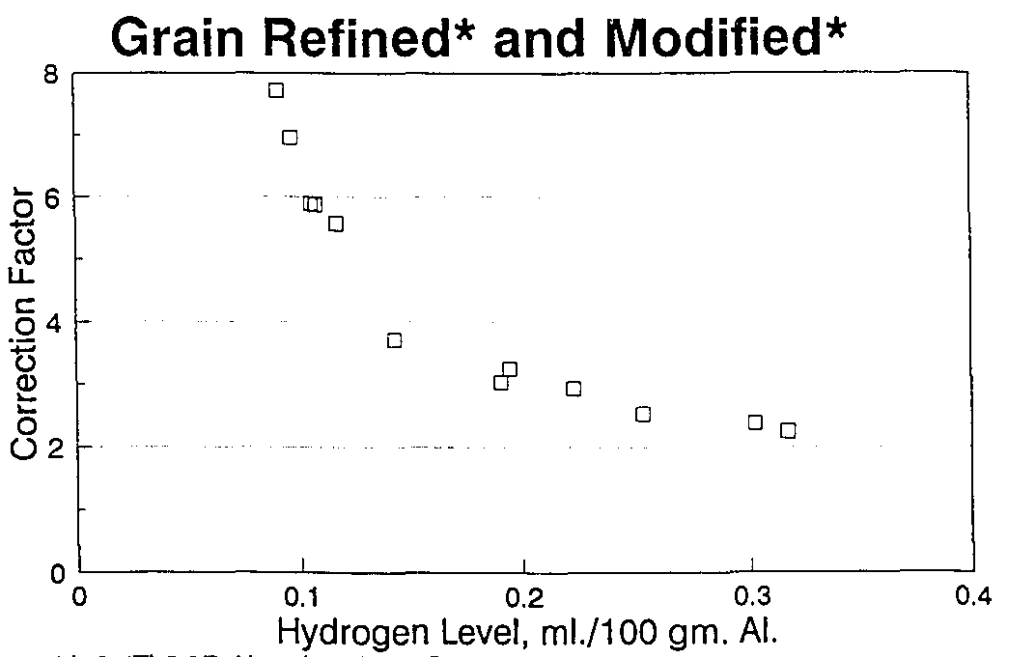

* with 2.5Ti-2.5B-Al grain refiner @ 0.17 wt.%
* with 90Sr-10Al modifier @ 0.02 wt.%

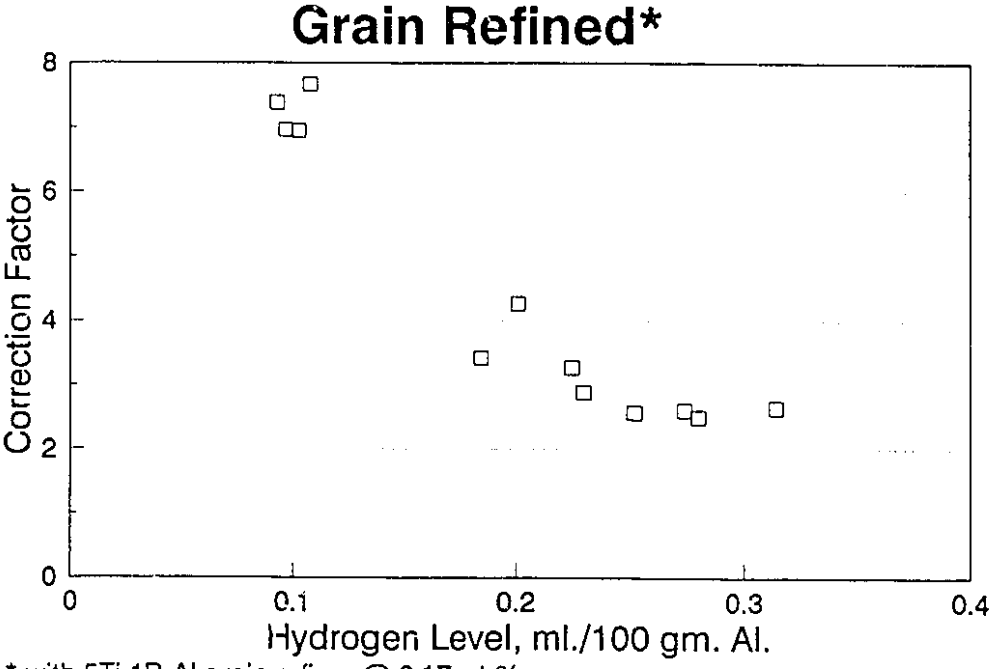

* with 5Ti-1B-Al grain refiner @ 0.17 wt.%

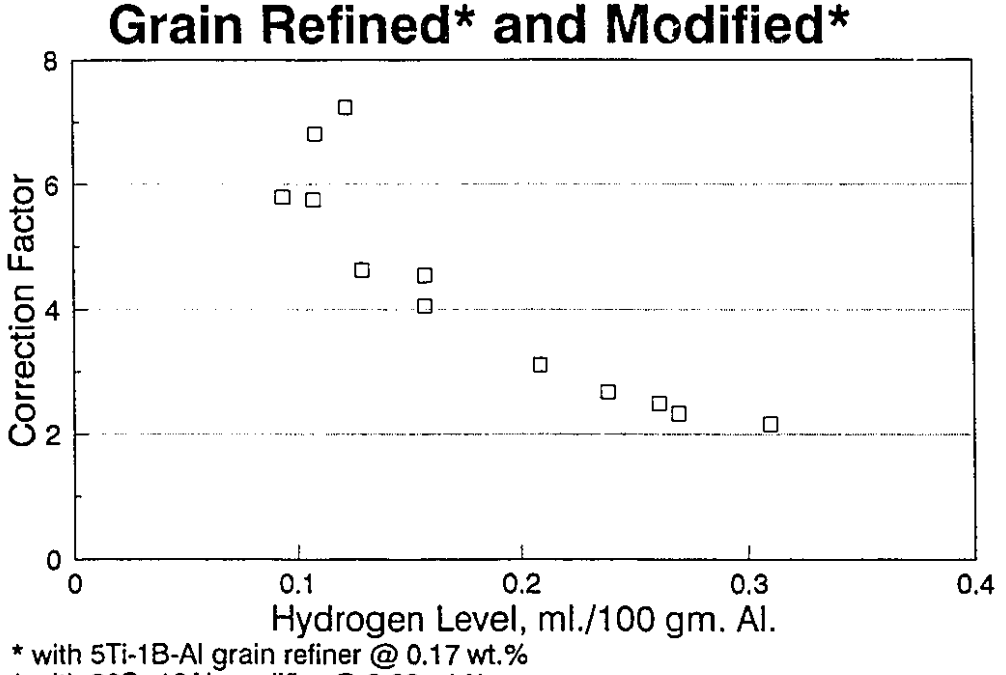

* with 5Ti-1B-Al grain refiner @ 0.17 wt.%
* with 90Sr-10Al modifier @ 0.02 wt.%